

3675
CONTRACTOR REPORT

PEARSON ET AL

SAND86-7177
Unlimited Release
UC-70

HYDROLOGY DOCUMENT NUMBER 603

Preliminary Design for a Sorbing Tracer Test in the Culebra Dolomite at the H-3 Hydropad at the Waste Isolation Pilot Plant (WIPP) Site

**F. J. Pearson, Jr., V. A. Kelley, J. F. Pickens
INTERA Technologies, Inc.
6850 Austin Center Blvd.
Suite 300
Austin, TX 78731**

Prepared by Sandia National Laboratories Albuquerque, New Mexico 87185
and Livermore, California 94550 for the United States Department of Energy
under Contract DE-AC04-76DP00789

Printed February 1987

Issued by Sandia National Laboratories, operated for the United States Department of Energy by Sandia Corporation.

NOTICE: This report was prepared as an account of work sponsored by an agency of the United States Government. Neither the United States Government nor any agency thereof, nor any of their employees, nor any of their contractors, subcontractors, or their employees, makes any warranty, express or implied, or assumes any legal liability or responsibility for the accuracy, completeness, or usefulness of any information, apparatus, product, or process disclosed, or represents that its use would not infringe privately owned rights. Reference herein to any specific commercial product, process, or service by trade name, trademark, manufacturer, or otherwise, does not necessarily constitute or imply its endorsement, recommendation, or favoring by the United States Government, any agency thereof or any of their contractors or subcontractors. The views and opinions expressed herein do not necessarily state or reflect those of the United States Government, any agency thereof or any of their contractors or subcontractors.

Printed in the United States of America
Available from
National Technical Information Service
U.S. Department of Commerce
5285 Port Royal Road
Springfield, VA 22161

NTIS price codes
Printed copy: A10
Microfiche copy: A01

SAND86-7177
Unlimited Release
Printed March 1987

Distribution
Category UC-70

PRELIMINARY DESIGN FOR A SORBING TRACER TEST
IN THE CULEBRA DOLOMITE AT THE H-3 HYDROPAD
AT THE WASTE ISOLATION PILOT PLANT (WIPP) SITE

Prepared for

SANDIA NATIONAL LABORATORIES
ORGANIZATION 6331
ALBUQUERQUE, NEW MEXICO

by

F.J. Pearson, Jr., V.A. Kelley, J.F. Pickens
INTERA Technologies, Inc.
6850 Austin Center Blvd.
Suite 300
Austin, Texas 78731
(512) 346-2000

December 18, 1986

ABSTRACT

The use of sorbing tracers in a field hydrologic test is a method of estimating the nuclide transport characteristics at one location in the Culebra dolomite at the Waste Isolation Pilot Plant (WIPP) site. The Culebra is considered to be the principal continuous pathway from the site in the event of a breach of the planned nuclear-waste repository. To prepare for such a tracer test, data evaluation and design calculations are necessary to estimate the principal parameters governing solute transport and the quantity and geochemical character of potential tracers. The following report represents the first step in preparing for a sorbing tracer test, namely a preliminary analysis which considers: (a) the selection of the best location for the first test at the WIPP site; (b) an evaluation of a conservative tracer test at the recommended site to provide estimates of the physical solute-transport parameters; (c) a hydrogeochemical and mineralogic characterization of the Culebra dolomite; (d) the rationale and recipe for the tracer-injection solution; (e) the compilation of a list of potential sorbing and conservative tracers; and (f) the identification of other needs before fielding the sorbing tracer test. The appendix to this report contains the thermodynamic data base used to support the geochemical model (PHREEQE) used in this study.

The Culebra dolomite at the H-3 hydropad is the recommended site for conducting a sorbing tracer test because: (a) the site has been well-characterized hydraulically in a number of multi-well interference tests; (b) a convergent-flow conservative tracer test has been conducted at the H-3 hydropad, and analysed to yield estimates of the physical solute-transport parameters (this test identified the role played by fractures in dominating solute-transport behavior at the hydropad scale); (c) a number of high-quality ground-water samples have been collected from the Culebra at the H-3 site and they have provided analyses with which to assemble a well-understood geochemical characterization; (d) the H-3 site is located down-gradient from the repository site on a probable ground-water flow path under natural gradients; and (e) the H-3 site has appropriate

hydraulic characteristics to allow the use of sorbing tracers with a wide range of partition coefficients and provide breakthrough in the allowable tracer-test operational period, assumed to be two to five years. The combination of relatively high transmissivity, extensive geologic and geochemical characterization, and down-gradient location make H-3 the optimum location for conducting the first sorbing tracer test at the WIPP site. In order to bracket geochemical variability and to test transport under different hydraulic conditions, it may prove desirable to conduct a second experiment at a location where Culebra brines are more concentrated. However, this second experiment is not considered further in this report.

The H-3 hydropad complex consists of three wells arranged in an equilateral triangle with approximate 30 m sides. Each well is completed either open-hole or through perforated casing to the Culebra, which is about seven meters in thickness. Interpretation of a convergent-flow tracer test, performed at the H-3 hydropad in 1984 using two conservative organic tracers, meta-trifluoromethylbenzoate (m-TFMB) and pentafluorobenzoate (PFB), has yielded the following physical solute-transport characteristics: longitudinal dispersivity of 1.5 to 3 m, a fracture porosity of 1.9×10^{-3} , and effective matrix-block sizes ranging from 0.25 to 2.0 m. During this test, H-3b3 was the pumping well and tracers were introduced into wells H-3b1 and H-3b2. Using the above estimates, coupled with a laboratory-measured matrix porosity of 0.2, estimated tortuosities of 0.15 to 0.45, and free-water diffusion coefficients of 7.4×10^{-6} cm²/s (m-TFMB) and 7.2×10^{-6} cm²/s (PFB), the breakthrough curves for the two tracers were simulated using the flow and solute-transport code SWIFT II.

Design simulations for the sorbing tracer test were conducted assuming an injection of one kilogram of generic tracer and applying a range of partition coefficients of 0.1 to 50.0 ml/g for the flow path with the higher transport rate (H-3b1 to H-3b3) and 0.1 to 10.0 ml/g for the flow path with the lower transport rate (H-3b2 to H-3b3) at the H-3 hydropad. The results of these simulations were utilized to assist in the selection of sorbing tracers that would break through within the two- to five-year period planned for the test.

Analyses of ground water and core samples from the Culebra at the H-3 hydropad indicate that the water samples are reasonably consistent and represent Culebra formation water. The Culebra is a gypsiferous dolomite with minor amounts of halite bounded by claystones. The water chemistry is controlled by the mineralogy of the formation. Thermodynamic equilibrium calculations indicate that the water is in equilibrium with calcite, dolomite, gypsum, and celestite and has a pH of 7.3 to 7.4. The calculations also suggest that the water is in near-equilibrium with goethite and uraninite with an Eh of 0.05 to -0.15 volts.

Geochemical analysis of the Culebra formation water led to the development of a recipe for the solution into which the tracer will be mixed prior to injection. The composition of the tracer solution is such that it should mimic the properties of the natural formation water and neither alter the chemistry of the matrix or formation water of the Culebra, nor cause the tracer to precipitate or to become unstable under the existing redox conditions in the Culebra.

In considering sorbing and conservative tracers for the planned test at H-3, it was necessary to consider geochemical constraints on the injected tracers. The tracers must be able to be injected at concentrations low enough to not significantly alter the injection fluid or to provoke any reaction which could cause precipitation of the tracer before or during injection. The concentration should be high enough to define the breakthrough curve while being relatively easy to analyze. The sorbing and conservative tracers should be compatible. Radionuclide tracers are considered to be the most appropriate tracers because they require low mass input, while still being extremely sensitive to detection, and they should mimic the transport characteristics of the projected waste inventory.

Radionuclide tracers most suitable for use as a sorbing tracer are either fission-products or actinides. Nuclides of nickel, cobalt, strontium, uranium, neptunium and plutonium were reviewed for suitability as possible sorbing tracers because they have partition coefficients low

enough to achieve breakthrough in a two- to five-year test, and they are elements with long-lived nuclides in the projected WIPP waste inventory. Based on their half-lives, the nuclides ^{63}Ni , ^{58}Co , ^{60}Co , ^{85}Sr , ^{89}Sr , ^{90}Sr , ^{232}U , ^{235}Np , ^{236}Pu , and ^{241}Pu are recommended for further consideration. One important consideration will be the presence of certain fission-products, such as ^{90}Sr , in the probable waste inventory, and whether objections might be raised over the use of such nuclides for testing. In order to provide data for interpretation of the physical solute-transport parameters along the flow paths between the wells (also, to provide a comparison to parameters from the previously-conducted conservative tracer test), conservative tracers should accompany the selected sorbing tracers. The most likely candidates are ^3H (tritium), ^{82}Br , and ^{131}I .

Prior to fielding a sorbing tracer test, a final detailed design report will be completed. This report will describe final tracer selection, detailed design calculations, site preparation, instrumentation requirements, staffing requirements, review of safety, health, and regulatory requirements and procedures, and determination of the optimum operational conditions for the test.

TABLE OF CONTENTS

ABSTRACT	ii
LIST OF FIGURES	viii
LIST OF TABLES	x
1.0 INTRODUCTION	1-1
1.1 Purpose and Contents of This Report	1-1
1.2 Solute-Transport Processes	1-3
2.0 SELECTION OF SITE FOR THE SORBING TRACER TEST	2-1
2.1 Criteria	2-1
2.2 Hydraulic Characterizations	2-2
2.3 Solute-Transport Characterizations	2-3
2.4 Geochemical Characterization	2-4
2.5 Potential Flow Paths From Repository	2-5
2.6 Tracer-Test Operational Period	2-6
2.7 Extrapolation of Tracer-Test Results to a Larger Scale ...	2-7
2.8 Summary and Recommendations	2-8
3.0 SOLUTE TRANSPORT IN THE CULEBRA AT THE H-3 HYDROPAD	3-1
3.1 Physical Characterization at the H-3 Hydropad	3-1
3.1.1 Geology	3-1
3.1.2 Well Configurations	3-2
3.1.3 Hydrogeology	3-3
3.2 Physical Transport Characteristics From the Conservative Tracer Test at the H-3 Hydropad	3-4
3.2.1 Tracer-Test History	3-5
3.2.2 Interpretation Approach	3-6
3.2.3 Simulation Model	3-9
3.2.4 Model Input Parameters	3-10
3.2.5 Analysis of Tracer-Breakthrough Curves	3-17
3.3 Design Calculations for Sorbing Tracer Test	3-20
4.0 GEOCHEMICAL CONTROLS ON THE TRANSPORT IN THE CULEBRA AT THE H-3 HYDROPAD	4-1

TABLE OF CONTENTS

(continued)

4.1	Formation Water Chemistry	4-3
4.2	Identity and Distribution of Solid Phases	4-5
4.3	Characterization of Geochemical Environment	4-6
4.3.1	Geochemical Modeling	4-6
4.3.2	Formation-Water Interactions	4-8
4.3.2.1	Saturation Index Calculations	4-9
4.3.2.2	Redox Controls.....	4-13
4.4	Summary	4-16
5.0	PRELIMINARY DESIGN OF TRACER-TEST SOLUTION	5-1
5.1	Injection-Fluid Matrix Composition	5-1
5.1.1	Design Constraints	5-2
5.1.2	Constraints on Tracer-Injection Procedures	5-4
5.1.3	Preparation and Handling of Injection Matrix Fluid ...	5-6
5.2	Tracers and Tracer Concentrations	5-8
5.2.1	Constraints on Tracer Concentrations	5-11
5.2.2	Sorbing Tracer Selection	5-12
5.2.2.1	Projected Waste Elements	5-12
5.2.2.2	Partition Coefficients	5-14
5.2.2.3	Tracer Nuclides	5-20
5.2.3	Conservative Tracer Selection	5-27
6.0	FURTHER REQUIREMENTS BEFORE FIELDING TEST	6-1
7.0	SUMMARY AND CONCLUSIONS	7-1
8.0	REFERENCES	8-1

FIGURES

TABLES

APPENDIX: Thermochemical Data Base

LIST OF FIGURES

- Figure 1.1 Schematic Diagram Illustrating Solute Transport Processes in Fractured Media: (a) Regional Scale, (b) Fracture Sets, and (c) Single Fracture.
- Figure 2.1 Site Locations for the Waste Isolation Pilot Plant Showing the Observation-Well Network for Regional Hydrogeologic Characterization Studies.
- Figure 3.1 Results of Core Examination of Culebra Dolomite from Borehole H-3b2.
- Figure 3.2 Results of Core Examination of Culebra Dolomite from Borehole H-3b3.
- Figure 3.3 Plan View of Wells at the H-3 Hydropad Showing Distances Between Wells at Ground Surface and Culebra Depth.
- Figure 3.4 Well Construction Details for the H-3 Hydropad
- Figure 3.5a Observed Tracer Concentration for PFB and m-TFMB Expressed as (a) Micrograms per Liter.
- Figure 3.5b Observed Tracer Concentrations for PFB and m-TFMB Expressed as (b) Mass per Unit Mass.
- Figure 3.6 Schematic Representation of the Modeled Region, (a) Cross Section, (b) Plan View.
- Figure 3.7a Observed and Simulated Breakthrough Curves for Tracer m-TFMB for (a) Assumed Tortuosity of 0.15.
- Figure 3.7b Observed and Simulated Breakthrough Curves for Tracer m-TFMB for (b) Assumed Tortuosity of 0.45.
- Figure 3.8a Observed and Simulated Breakthrough Curves for Tracer PFB for (a) Assumed Tortuosity of 0.15.
- Figure 3.8b Observed and Simulated Breakthrough Curves for Tracer PFB for (b) Assumed Tortuosity of 0.45.
- Figure 3.9a Simulated Breakthrough Curves at Pumping Well for a Range of Partition Coefficients for the (a) H-3b1 to H-3b3 Flow Path.

LIST OF FIGURES
(continued)

- Figure 3.9b Simulated Breakthrough Curves at Pumping Well for a Range of Partition Coefficients for the (b) H-3b2 to H-3b3 Flow Path.
- Figure 5.1 Calculated Peak-Concentration Arrival Times at Pumping Well for Various Assumed Partition Coefficients for the H-3b1 to H-3b3 Flow Path.
- Figure 5.2 Calculated Peak-Concentration Arrival Times at Pumping Wells for Various Assumed Partition Coefficients for the H-3b2 to H-3b3 Flow Path.
- Figure 5.3 Peak Concentration Versus Peak-Concentration Arrival Times for the H-3b2 to H-3b3 Flow Path.
- Figure 5.4 Peak Concentration Versus Peak-Concentration Arrival Times for the H-3b1 to H-3b3 Flow Path.

LIST OF TABLES

- Table 2.1 Relative Transport Rates Determined from the Conservative Tracer Tests.
- Table 2.2 Summary of Suitability of Multi-Well Hydropad Locations to Site Selection Criteria for the Sorbing Tracer Test.
- Table 3.1 Summary of Tracer Arrival Times and Mass Recoveries at the Pumping Well H-3b3.
- Table 3.2 Summary of Best-Fit Parameters for m-TFMB and PFB Breakthrough Curves at the H-3 Hydropad.
- Table 3.3 Parameters for the Design Calculations for the Sorbing Tracer Test.
- Table 3.4 Summary of Tracer Arrival Times and Peak Concentrations Calculated for a Range of Partition Coefficients.
- Table 4.1 Chemical Analyses of Water Samples from the Culebra at the H-3 Hydropad.
- Table 4.2 Whole-Rock Mineral Composition in Weight Percent, of Core Samples from H-3b2 and H-3b3.
- Table 4.3 Saturation Indices Calculated from Analyses of Water Samples from the Culebra at the H-3 Hydropad.
- Table 4.4 Oxidation Potentials Calculated from Equilibrium Between H-3 Culebra Waters and Redox-Sensitive Minerals.
- Table 5.1 Estimated Composition of Culebra Formation Fluid at the H-3 Hydropad.
- Table 5.2 Saturation Indices of Selected Minerals and Parameters of the Carbonate System Calculated for Culebra Formation Water at Two pH Values.
- Table 5.3 Masses of Salts to Produce One Liter of Water of the Type Found in the Culebra at the H-3 Hydropad.
- Table 5.4 Comparison Between Compositions of Culebra Formation Water at H-3 Hydropad and Artificial Formation Water from Table 5.3.

LIST OF TABLES
(continued)

- Table 5.5 Properties of Fission Product Nuclides of Possible Importance in Projected WIPP Waste Inventory.
- Table 5.6 Properties of Actinide Nuclides of Possible Importance in Projected WIPP Waste Inventory.
- Table 5.7 Composition of Waters Used for Measurements of Sorption Coefficients and Actinide Speciation with Culebra Core Material.
- Table 5.8 Distribution Coefficient (Kd) Values Measured on Culebra Core Material.
- Table 5.9 Speciation of Divalent Cations in H-3 Culebra Water.
- Table 5.10 Possible Sorbing Tracer Isotopes and Input Concentrations Required for Peak Concentrations of 100 pCi/l at Pumping Well if Breakthrough Peak is at Two Years.
- Table 5.11 Possible Conservative Tracer Isotopes with Input Concentrations Required for Peak Concentrations of 100 pCi/l at Pumping Well.

1.0 INTRODUCTION

1.1 Purpose and Contents of This Report

Conducting field tests using sorbing (reactive) tracers is one means of improving knowledge of the nuclide transport properties of the Culebra dolomite at the WIPP site. "Sorbing" in this context simply means a tracer which reacts with the aquifer and so is transported more slowly than a non-sorbing or conservative tracer. This report examines where and how such a test might be carried out at the WIPP site.

This introductory chapter includes a brief discussion of processes influencing the transport of substances in flowing ground water, with particular reference to the description of transport in a fractured porous medium. This discussion is intended to provide a perspective from which the remainder of the report can be viewed by those of varying scientific disciplines.

Within the WIPP site, there are a number of locations where potentially successful sorbing tracer tests could be carried out. Chapter 2 outlines criteria for selecting a site for such a test, and reviews potential locations within the WIPP site, leading to the recommendation of the H-3 hydro pad for the first test.

Both physical and chemical processes influence nuclide transport and must be considered in designing a sorbing tracer test. Chapter 3 describes the physical processes controlling transport at the H-3 hydro pad, based on interpretation of the results of a conservative tracer test performed at that location in 1984. With this interpretation of the physical processes, several test design calculations were performed. The results of these calculations are given in Chapter 3. These calculations provided bounding values for the chemical retardation parameters which should not be exceeded by potential tracers if breakthrough is to

be assured during the anticipated test period of approximately two to five years. The design calculations also provide the factors by which tracers would be diluted during the test. Both the maximum values of the retardation parameter and the dilution factors were required for selecting potential tracers and for defining the concentration of the tracer input solutions. Tracer selection and calculation of the input concentrations are described in Chapter 5.

Geochemical controls on transport of tracers at the H-3 hydropad are discussed in Chapter 4. An estimate of the chemistry of water in the Culebra was made using analyses of several water samples from wells at the hydropad. This was combined with information on the mineralogy of the aquifer from core analyses to suggest mineralogical controls on the water chemistry. This understanding was required to permit the design of a matrix solution in which to inject the tracer and which will not react with the aquifer and affect tracer transport. This understanding of water-rock interactions also permitted estimates of the extent to which potential tracers might be subject to chemical retardation.

Chapter 5 discusses the design of the tracer matrix solution and the selection of possible sorbing and conservative tracers. A recipe for the preparation of a solution closely similar to H-3 Culebra water is developed. This is the matrix solution in which tracers could be introduced with minimum disturbance to the aquifer and minimum likelihood that the injection of the tracer solution itself would bring about reactions causing retardation.

The second part of Chapter 5 describes the tracer selection procedure used and suggests a number of nuclides, which from the standpoint of transport processes alone, would be useful as sorbing and conservative tracers at the H-3 site. Only radioactive nuclides were examined, because highly sensitive analytical techniques are available for radio-nuclides and low total tracer masses are desirable to minimize potential

problems with tracer precipitation from the input solution. Regulatory and logistic problems associated with the use of radiotracers and the availability and cost of the radionuclides suggested were not examined in detail as part of this study, but should be given considerable attention as part of a final design study.

This study was intended to lead only to a preliminary design for a sorbing tracer test. In the course of the work, however, a number of questions arose which require resolution as part of later work leading to a final design. A number of these questions are given in Chapter 6.

Chapter 7 contains a summary of the entire report and of the major conclusions to be drawn from it. References to the literature cited in the report appear in Chapter 8.

In examining water-mineral reactions in the Culebra and evaluating the possible geochemical controls on tracer retardation, a thermodynamic data base was required. This data base is included in the Appendix.

1.2 Solute-Transport Processes

Before proceeding to the discussion of tracers suitable for use in performing the sorbing tracer test, it is useful to consider the important hydrogeologic parameters and processes that may be evaluated using laboratory or field experiments.

The investigation of the migration of solutes in fractured rock generally considers five basic processes, some of which are illustrated in Figure 1.1.

1. Solutes will be transported with ground water as it moves through a system of fractures in response to the hydraulic gradient. This transport process is known as advection.

2. In addition to the advective solute flux, there is an additional solute flux resulting from variations of water velocity across an individual fracture opening and also due to the interconnections and non-linearities of the fracture system. This additional flux is perceived on the macroscopic scale as an effective mixing. It is known as mechanical dispersion.
3. Mixing also occurs on the microscopic level due to the process of molecular diffusion. In a fractured medium with a porous matrix, molecular diffusion can take place both in the fluid-filled fractures and in water contained in the pores of the matrix. When solute diffuses into the matrix pores its movement along the fracture will be retarded with respect to the flux of water in the fracture since, in general, water flows more rapidly in fractures than through the matrix. In a fractured system, it is generally assumed that the matrix has the bulk of the storage capacity of the medium whereas the fractures represent the principal transport capability.
4. Transfer across phase boundaries due to adsorption, precipitation, ion-exchange or other geochemical processes will retard both advective and dispersive solute movement. These mechanisms can be considered together as the process of geochemical retardation.
5. Radioactive solutes decay to daughter isotopes which may be either radioactive or stable. The process of radioactive decay serves in some instances to limit migration of radioactive solutes, while in others, for instance where the daughter products are long-lived radioisotopes with different geochemical properties, radioactive decay can result in increased distance of radionuclide transport in a ground-water system.
6. For organic constituents, biodegradation can serve to eliminate the solute from the ground-water system.

The SWIFT II model was chosen both for the interpretation of a previously-conducted conservative tracer test and for the design calculations for a sorbing tracer test proposed for the H-3 hydropad. A comprehensive description of the theory and implementation of the SWIFT II model is presented in Reeves et al. (1986a). Two other documents related to the SWIFT II code have been published: a data input guide for SWIFT II (Reeves et al., 1986b), and verification-validation tests for the SWIFT II code (Ward et al., 1984).

The SWIFT II model is designed to simulate flow and transport processes in both single- and double-porosity media. In the fractured regions of the system where dual porosity is to be applied, two sets of equations are solved, one for the fracture processes and the other for the matrix processes. The flow and transport processes occurring within the rock matrix are conceptualized as being one-dimensional in a lateral direction relative to the direction of transport in the fractures. Thus, it is assumed that the fractures provide the only means for large-scale movement of water and solutes through the entire system while the matrix provides most of the storage of the system. Full details on the governing equations utilized in the SWIFT II model are presented and discussed by Reeves et al. (1986a).

For the purposes of the design calculations presented in Chapter 3, it is assumed that reactions between fluid and solid take place only in the matrix. The concentration on the solid phase can be assumed to be a function of the concentration in solution and expressed:

$$S = f(C_m) \quad (1-1)$$

One can define the partition coefficient (K) as a parameter relating these two concentrations:

$$K = \frac{S}{C_m} \quad (1-2)$$

In a general sense, K will vary spatially and temporally as a function of the solute species properties, the geochemical environment, and the mineralogy of the geologic system. Controls on the partition coefficient are discussed further in Chapter 5.

2.0 SELECTION OF SITE FOR THE SORBING TRACER TEST

2.1 Criteria

This section describes the criteria and approach for selecting the preferred location for conducting the first sorbing tracer test at the Waste Isolation Pilot Plant (WIPP) site (Figure 2.1). The general site selection criteria used to assist in identifying the optimal location for the sorbing tracer test include:

- (1) the site should be characterized with respect to its hydraulic characteristics;
- (2) the site should be characterized with respect to its physical solute-transport characteristics using conservative tracers;
- (3) the geochemistry of Culebra formation water at the site should be well characterized;
- (4) it is preferable that the site be located on a potential flow path (under natural ground-water flow conditions) in the Culebra in the event of a repository breach;
- (5) the sorbing tracer test should have an operational period of two to five years; and
- (6) the site should be located so as to permit geochemical extrapolation of the reactive solute-transport results to as large a region as practical at the WIPP site.

Because both multi-well hydraulic interference tests and conservative tracer tests have been conducted at the H-2, H-3, H-4 and H-6 hydropads, these hydropads were under consideration as primary sites. Secondary sites were those hydropads with multiple wells where hydraulic interference tests have been conducted (i.e., H-5, H-7, H-9 and H-11 hydropads). Tertiary sites are single-well locations (e.g., DOE-1, DOE-2, H-8, H-10, H-12, WIPP-12, WIPP-13, WIPP-18, WIPP-19, WIPP-21, and WIPP-22).

In addition to the larger data base available for the primary sites, they also offer the advantage of requiring less site-preparation time, because they each have three wells that have been completed, developed, and tested in the Culebra. It is possible that one or more of the primary or secondary sites could be suitable in meeting the objectives of the sorbing tracer test. Sites at locations where wells are not currently installed were not considered in the site-selection process. The selection of the recommended test location utilized the general site selection criteria listed above.

2.2 Hydraulic Characterizations

Single-well and multi-well interference tests have been conducted in most of the single-well and/or hydropad locations with wells completed in the Culebra. The majority of previously reported analyses from these tests utilized a porous-medium conceptualization for ground-water flow.

The analysis of hydraulic tests utilizing a double-porosity or fractured porous-medium conceptualization has been reported for DOE-2 (Beauheim, 1986). Recent analyses of the drawdown and recovery data at the pumping well for the H-3 multipad pumping test have been conducted using a double-porosity (fracture-flow) formulation (Beauheim, in preparation).

The hydropads that have had the most intensive hydraulic-testing program are H-2, H-3, H-4, H-5, H-6, H-9, and H-11. A series of slug and/or pumping tests have been conducted on wells at each of these hydropads. Hydraulic-test analyses have been conducted for the H-4, H-5, and H-6 hydropads (Hydro Geo Chem, in preparation, a,b,c). These analyses, utilizing a porous-medium conceptualization, provided a measure of the degree of anisotropy or heterogeneity at the hydropad scale for the H-4, H-5, and H-6 hydropads. Further hydraulic-test data analyses to investigate double-porosity effects are planned for the H-2, H-3, H-4, H-6, and H-11 hydropads. These analyses, in combination with laboratory core

investigations (i.e., permeability, porosity and mineralogy) and analysis of conservative tracer tests using a double-porosity conceptualization (where appropriate), will provide a more complete and accurate description of the hydraulic characteristics of the Culebra at specific hydropads. With respect to satisfying the hydraulic characterization criterion for site selection, the H-2, H-3, H-4, H-5, H-6, H-9, and H-11 hydropads have had adequate field testing for providing hydraulic characterizations. While additional interpretation is needed to complete the hydraulic characterization, the present interpretations are adequate for site selection.

2.3 Solute-Transport Characterizations

Tracer tests have been conducted at the H-2, H-3, H-4 and H-6 hydropads to evaluate the physical transport process (i.e., advection, dispersion and diffusion) in the Culebra at the hydropad scale. Two types of tracer tests were conducted: (1) convergent-flow, with pumping of one well and addition of tracers to one or more of the other wells at that hydropad; and (2) two-well injection-withdrawal, with pumping of one well and injection of the pumped water and tracers to a second well. The tracers utilized in these tests were organics and were assumed to be conservative. However, the various organic tracers did, in some cases, exhibit different transport behavior reflecting either different diffusive losses from the fractures to the matrix, chemical interactions between the tracer and the Culebra, or tracer losses as a result of microbial activity.

Even though all of the organic tracers may not have exhibited ideal transport behavior (i.e., exactly representative of the rate of movement of the ground water), the tracer tests provided a measure of the transport rates expected for specific pumping rates for the tracers at four of the hydropads. The relative transport rates, based on the times of first detection and peak concentration for the tracers from water

samples taken at the pumping well, of the organic tracers for the tracer tests conducted at the H-2, H-3, H-4, and H-6 hydropads are summarized in Table 2.1. The values of first detection of a particular tracer depend on the specific tracer and the analytical procedures.

Analyses using a porous-medium conceptualization have been reported for the two-well tracer test conducted at the H-2 hydropad (Hydro Geo Chem, 1986) and the convergent-flow tracer tests conducted at the H-6 hydropad (Hydro Geo Chem, in preparation, d). The convergent-flow tracer tests conducted at the H-3 and H-4 hydropads have been analyzed using the SWIFT II model which utilizes a double-porosity conceptualization for both flow and solute transport (Kelley and Pickens, 1986). These analyses have provided a more representative and complete description of the hydraulic and solute-transport characteristics of the Culebra at the H-3 and H-4 hydropads. Through conducting a sensitivity analysis on the values of the various physical solute-transport parameters, the relative importance of fracture flow, fracture spacing, and the diffusion of the tracers into the rock matrix was evaluated for the tracer test at the H-3 hydropad.

With respect to the site-selection criterion of solute-transport characterization, only those hydropads which have undergone tracer tests (i.e., H-2, H-3, H-4, and H-6) may be considered suitable. The present information obtained from these tracer tests is adequate for site selection. The results from interpretations of these tests, including double-porosity conceptualizations, where appropriate, are very valuable in terms of design and scoping calculations for the sorbing tracer test (Chapter 3).

2.4 Geochemical Characterization

Water samples have been collected from one or more wells at all hydropads. Analyses of samples taken between 1976 and 1980 are reported by Mercer (1983) and by Ramey (1985). Since 1984, as part of the

ecological monitoring program at WIPP (Westinghouse, 1985), many hydropad wells have been resampled. As of the date of preparation of this report (August 1986), analyses were obtained for samples from the H-2, H-3 (two samples), H-4, H-5, and H-11 hydropads.

An overview of the hydrochemistry of the Culebra is presented in Appendix E of Haug et al. (in preparation). Table E-1 of that report shows that the total dissolved solids content of the recently collected samples range from over 100 grams per liter (g/l) at H-5, H-11, H-12, and DOE-1, to 56 g/l at H-3, and 20 g/l at H-4. The geochemical modeling required to characterize the environment of the highly saline waters at H-5, H-11, H-12, and DOE-1 cannot be done reliably using presently-available computer codes. Reliable geochemical characterization of the H-3 and H-4 hydropads, however, is possible with available geochemical models (Haug et al., in preparation, Appendix E).

From the standpoint of geochemical characterization, the H-3 or H-4 hydropads are suitable sites for sorbing tracer tests with the preference given to H-3 because of the availability there of two recently-collected water samples of high quality. As codes suitable for modeling more highly saline solutions become available, geochemical characterization of the H-5, H-11, and H-12 sites will also be possible and they too may turn out to be suitable.

2.5 Potential Flow Paths from Repository

Previous hydrologic characterizations of ground-water flow in the Culebra (e.g., Mercer, 1983) including modeling investigations (e.g., INTERA Environmental Consultants, 1981; Barr et al., 1983; Haug et al., in preparation) have indicated that, at the present time, the general flow direction is from north to south through the center of the WIPP site. Using the criterion of locating the sorbing tracer test on a potential flow path from a repository breach under present natural

ground-water flow conditions (i.e., excluding the brine-reservoir breach scenario) indicates that the H-5 and H-6 hydropads, DOE-2, and the WIPP-series wells in the Culebra north of the WIPP site are unsuitable. On the basis of location, the primary and secondary sites located immediately south of the center of the WIPP site (i.e., H-2, H-3, H-4, and H-11) are considered the most suitable.

2.6 Tracer-Test Operational Period

The recommended operational design for the sorbing tracer test is a convergent-flow tracer test consisting of one pumping well and several peripheral wells used for the addition of conservative and sorbing tracers. A number of sorbing tracers will be selected in order to investigate a range of possible retardations.

By choosing hydropads with intermediate to high transmissivities and transport rates, a larger group of potential sorbing tracers can be utilized in the sorbing tracer test. Examination of the transport rates for tracers for the four hydropads at which conservative tracer tests have been conducted indicates a direct correlation between the transmissivity and relative transport rates; that is, high transport rate for the H-3 and H-6 hydropads, and low transport rates for the H-2 and H-4 hydropads (see Table 2.1).

From an operational viewpoint, the transport rate of the sorbing tracers selected for the sorbing tracer test will vary as a function of the type and extent of interaction between the sorbing tracers and the Culebra. Even for weakly-sorbing tracers, one should expect significant bulk retardation factors. For more strongly-sorbing tracers, retardation factors may be so large that the tracers would not arrive at the pumping well at detectable concentrations during the tracer-test operational period.

Examination of the tracer first-detection times for the conservative tracers under representative pumping conditions (see Table 2.1) indicates that the H-2 and H-4 hydropads are not suitable and that the H-3 and H-6 hydropads are suitable for meeting the tracer-test operational-period criterion of obtaining useful results in two to five years (i.e., a well-defined breakthrough curve).

2.7 Extrapolation of Tracer-Test Results to a Larger Scale

The sorbing tracer test will investigate the gross retardation of selected sorptive solutes (tracers) under field conditions in the Culebra dolomite at the scale of a single hydropad. The data from the sorbing tracer test will thus be site specific. Correlation of the transport rates and sorption mechanisms to a larger region can be accomplished, at least qualitatively, through the development of an understanding of the controls on solute mobility (e.g., through a detailed examination of the chemistry of the ground water, the chemistry of the selected tracers, and the physical solute-transport and mineralogical characteristics of the Culebra at both the experimental site and at other areas where it is desirable to extrapolate the results of the sorbing tracer test).

Physical laboratory measurements (i.e., matrix permeability and porosity) and mineralogical studies have been conducted on core samples and fracture surfaces from the Culebra at the H-2, H-3, H-4, and H-6 hydropads (Core Laboratories, 1986a,b). These measurements were conducted on from 2 to 7 samples from each of these hydropad locations. These studies provided mineralogical data for evaluating water-rock interactions in the matrix and on fracture surfaces, evidence of mineral dissolution or precipitation, and the relative amount and identity of mineral phases which have a high ion-exchange or surface sorption capacity.

Conducting the above preliminary investigations on core samples and fracture surfaces from these four hydropad locations has provided data for an initial evaluation of the variability of the physical and mineralogical characteristics of the Culebra on a regional scale. This data base, in combination with regional hydrologic characterization studies and the regional geochemical and isotopic investigations will provide at least a qualitative basis for extrapolation of the results of the sorbing tracer test.

2.8 Summary and Recommendations

The preceding discussion has outlined the selection criteria and the characteristics of potential sites for conducting the first sorbing tracer test. The multi-well hydropad sites have been emphasized in this review because they offer the advantages of a larger instrumentation configuration in place and a larger data base with respect to their physical transport parameters. The results of the review of the information base and the suitability of site selection criteria for the multi-well hydropad locations are summarized in Table 2.2.

In terms of meeting the general site-selection criteria, the H-3 hydropad is considered to be the optimum location for conducting the first tracer test. The H-3 hydropad exhibits intermediate physical transport characteristics and also offers the advantage of presently having the most complete and extensive description of the ground-water flow and solute-transport characteristics as a result of hydraulic-test and tracer-test interpretations that have been conducted. The breakthrough times observed for the conservative tracer test at the H-3 hydropad indicate that the operational-time requirement for the sorbing tracer test can likely be attained. Geochemical characterization of this site is also possible because of the availability of recent water samples and the fact that the salinity of Culebra water there is within a range which can be modeled with available techniques. Lastly, the H-3 hydropad is closest to the center of the WIPP site and on a likely flow path from the site under natural flow conditions.

3.0 SOLUTE TRANSPORT IN THE CULEBRA AT THE H-3 HYDROPAD

As discussed in Chapter 2, the H-3 hydropad offers a number of advantages as the site for conducting the sorbing tracer test. The physical and transport characteristics of the Culebra at the H-3 hydropad and the design calculations for a range of partition coefficients are presented in this section.

The interpretation of the conservative tracer test conducted at the H-3 hydropad is presented in detail by Kelley and Pickens (1986). Portions of this interpretative report on the H-3 conservative tracer test are repeated below to summarize the characteristics of the Culebra and instrumentation at the H-3 hydropad and to provide an information base for the reader to assess the uncertainty in the interpreted physical solute-transport parameters.

3.1 Physical Characterization at the H-3 Hydropad

3.1.1 Geology

At the H-3 hydropad, the Culebra is a 7-m thick, primarily finely vugular dolomite with voids ranging from 0.5 to 5 cm in diameter. Figures 3.1 and 3.2 summarize the results of examination of the available Culebra core from the H-3 hydropad. The rock matrix ranges from strongly indurated dolomite to easily friable siltstone. The mineralogy of the Culebra is discussed in Chapter 4. The Culebra dolomite at H-3 has both vugs and fractures which often are filled with gypsum and, in some cases, halite. Core recovery from H-3b2 and H-3b3 was poor, suggesting a high degree of fracturing, vugs, and/or poor induration due to a high silt content. In both wells, total core recovery from the Culebra was less than 50 percent. No pieces of core exceeded 0.3 m in length and much of the core was present only as rubble.

Below the Culebra, there is a pervasive claystone generally 2 m or less in thickness, reddish-brown at its base darkening upward to black close to the base of the dolomite. This claystone exhibits textures characteristic of both detrital sediments and of solution residues (Core Laboratories, 1986b). The clay contains detrital gypsum clasts, secondary gypsum, and commonly authigenic potassium feldspar and quartz.

3.1.2 Well Configurations

The H-3 hydropad is located approximately 1.2 km south of the center of the WIPP site. The H-3 hydropad consists of three wells, H-3b1, H-3b2, and H-3b3, arranged in an approximate equilateral triangle with 30.5 m sides. Their surface separations and relative positions at the Culebra depth are shown in Figure 3.3. A satellite elevation survey conducted at the WIPP site (Hydro Geo Chem, 1985) determined top-of-casing elevations (TOC) for well H-3b1 at 1033.19 m, well H-3b2 at 1032.95 m, and well H-3b3 at 1032.58 m. The well-construction details are illustrated in Figure 3.4.

Well H-3b1 (originally designated H-3) was drilled under the direction of the United States Geological Survey and was completed August 12, 1976 (Powers et al., 1978). This well was drilled to a total depth of 274.9 meters. The 6-5/8 inch outside diameter (O.D.) steel casing is perforated in the Magenta dolomite from 171.3 to 179.8 m below ground surface (BGS), in the Culebra dolomite from 205.7 to 211.5 m BGS, in the "dissolution residue" below the Culebra from 211.5 to 214.3 m BGS, and at the Rustler-Salado contact from 247.8 to 255.1 m BGS. A bridge plug was set to separate the Culebra and Rustler-Salado contact zone, and a production-injection packer was set to separate the ground waters of the Magenta and Culebra dolomites. The relationship between casing depths, perforated intervals, and stratigraphic units is illustrated in Figure 3.4.

Wells H-3b2 and H-3b3 were drilled in 1983 to form the triangular array of wells on the H-3 hydropad (Hydro Geo Chem, 1985). Well H-3b2 was originally drilled to a depth of approximately 205.1 m and then on November 11, 1983, 5-1/2 inch O.D. steel casing was cemented in to that depth. The well was then further deepened to 221.0 m BGS in order to access the Culebra interval. The lower 17.3 m of the well is a 12.1 cm diameter open hole.

Well H-3b3 was drilled to a total depth of approximately 222.5 m BGS in December 1983. Well H-3b3 was left open until January 30, 1984 when 5-1/2 inch O.D. steel casing was run in and cemented to a depth of 204.4 m (Hydro Geo Chem, 1985). The remainder of the hole (204.4 to 222.5 m BGS) is a 12.1 cm open hole.

3.1.3 Hydrogeology

The Culebra dolomite is locally fractured. The information base that supports the presence of fractures is discussed in Section 3.2.2. The transmissivity associated with the H-3 hydropad and reported in the literature is $2.0 \times 10^{-5} \text{ m}^2/\text{s}$ (Mercer, 1983). This transmissivity is based upon a slug test performed in well H-3b1. A flood-wave response model was applied by Stevens and Beyeler (1985) to pressure-response data measured at the H-3 hydropad as a result of the influence of exploratory shaft construction occurring at the WIPP site. In this study, the transient pressure history at the H-3 hydropad was matched using a hydraulic diffusivity of $4.6 \times 10^{-2} \text{ m}^2/\text{s}$. While reported values for the storage coefficient for the Culebra dolomite range from 1×10^{-9} to 8×10^{-4} (Seward, 1982; Mercer, 1983; Gonzalez, 1983a; Beauheim, in preparation), values near 2×10^{-5} are the most common. Assuming this value as representative, the diffusivity obtained by Stevens and Beyeler (1985) is equivalent to a transmissivity of about $1 \times 10^{-6} \text{ m}^2/\text{s}$. Beauheim (in preparation) has interpreted the pressure-response data for a long-term pump test (2 months pumping and 4 months

recovery) conducted at the H-3 hydropad. He concluded that the pressure response indicated the presence of fractures and obtained a transmissivity of $2 \times 10^{-6} \text{ m}^2/\text{s}$ using a double-porosity interpretive model.

A ^{131}I tracer-injection test to define the presence of inflow zones was conducted on the perforated Culebra interval of H-3b1 (Mercer and Orr, 1979). The interpretation of the results of downhole tracer logging indicated major liquid losses of 36% in the depth interval 208.5 to 210.9 m and of 64% in the interval 210.9 to 211.8 m. In the Culebra perforated interval at H-3b1 (205.7 to 214.3 m with three 1.3 cm shots per 0.3 m vertical), it is apparent that flow was predominantly in the lower 50% of the Culebra. Since the upper 1.5 m of the Culebra was not perforated and one cannot be sure that the shot perforations are hydraulically well connected with all of the significant fractures, it is uncertain whether the upper 50% of the Culebra at H-3b1 is or is not an important transport medium. In addition, data is not available to judge the areal homogeneity of the Culebra at the hydropad scale.

The hydraulic gradients under undisturbed conditions (before shaft construction) at the H-3 hydropad are estimated to be 4×10^{-3} to the south-southeast (Haug et al., in preparation).

3.2 Physical Transport Characteristics from the Conservative Tracer Test at the H-3 Hydropad

A convergent-flow tracer test, utilizing conservative organic tracers was conducted in the Culebra dolomite at the H-3 hydropad from May 9 to June 12, 1984 by Hydro Geo Chem, Inc. under contract to Sandia National Laboratories. Full details on the operation of the tracer test, the tracer breakthrough curves obtained from water samples from the pumping well, and the interpretation of the tracer test to determine the physical solute-transport parameters of the Culebra at the H-3 hydropad are presented in Kelley and Pickens (1986).

3.2.1 Tracer-Test History

The H-3 hydropad tracer test was a convergent-flow tracer test in which well H-3b3 was pumped at a nominally constant rate of 0.19 l/s while 1 kg each of tracers meta-trifluoromethylbenzoate (m-TFMB) and pentafluorobenzoate (PFB) were injected into wells H-3b1 and H-3b2, respectively.

The breakthrough curves obtained for the m-TFMB and PFB tracers from water samples from the pumping well H-3b3 are shown in Figure 3.5a and the arrival times, first-measured and peak concentrations, and percent tracer recovery at the pumping well are summarized in Table 3.1. The concentration data, expressed as micrograms per liter ($\mu\text{g/l}$), for the tracer breakthrough curves were reported by Hydro Geo Chem (1985).

First detection of m-TFMB (reported concentration of $56 \mu\text{g/l}$) at the pumping well was obtained from water samples taken 22.1 hours (0.92 days) after tracer injection at well H-3b1. The maximum observed concentration ($3379 \mu\text{g/l}$) was recorded 62.08 hours (2.59 days) after tracer injection. Figure 3.5b expresses m-TFMB concentrations in terms of mass per unit mass. By integration for the mass below the m-TFMB breakthrough curve over the duration of the test, it is estimated that approximately 53% of the injected tracer mass was recovered at the pumping well.

First detection of PFB (reported as trace concentration) at the pumping well was obtained from water samples taken 90.25 hours (3.76 days) after tracer injection at well H-3b2. The following sample taken at 95.25 hours (3.97 days) had a reported concentration of $20 \mu\text{g/l}$. The maximum observed concentration ($444 \mu\text{g/l}$) was recorded 553 hours (23.04) days) after injection (Figure 3.5a). Only two samples were collected after the peak concentration was reached. These samples had concentrations 12% lower than the peak concentration. Sufficient

samples to better determine the falling limb of the breakthrough curve were not obtained. Figure 3.5b expresses concentrations in terms of mass per unit mass for both tracers PFB and m-TFMB. By integrating for the mass below the PFB breakthrough curve over the duration of the test, recovery of approximately 15% of the injected tracer mass is estimated. The PFB breakthrough curve exhibits a peak concentration about a factor of eight lower than the m-TFMB breakthrough curve and a time to reach the peak concentration delayed by a factor of nine when compared to the m-TFMB breakthrough curve.

3.2.2 Interpretation Approach

The objectives of the interpretation of the H-3 tracer test were to develop a consistent conceptualization of the governing physical solute-transport processes operating in the Culebra at the H-3 hydro- pad and to develop quantitative estimates of the respective transport parameters. From a review of the information base for the H-3 hydro- pad, it was concluded that a double-porosity interpretation approach was the most appropriate. This information base included:

- identification of open fractures in core samples;
- observation of a very rapid transport rate between the tracer- addition wells and the pumping well, suggesting transport in fractures;
- the hydraulic conductivity representing the full Culebra thickness (including the effects of the presence of fractures) is about one order of magnitude larger than the hydraulic conductivity obtained from core-sample measurements;
- the identification of a double-porosity pressure response from the analysis of the pumping test at the H-3 hydro- pad (Beauheim, in preparation).

Because of the relatively high matrix porosity of the Culebra, solute transport between the fractures and the matrix by diffusion is expected to be a significant process. Therefore, a discrete fracture model with transport in the fractures only is not considered an appropriate conceptualization for analyzing the H-3 tracer test. The double-porosity approach following fracture-matrix interactions is described below.

Inherent to double-porosity theory is the conceptualization that transport occurs in two separate media possessing different intrinsic transport properties. The primary medium is considered to possess properties which are the result of primary sedimentary processes, and the secondary medium to possess properties resulting from secondary processes such as mechanical deformation and dissolution. Using the classification approach of Streltsova-Adams (1978) for dual-porosity systems, the Culebra dolomite may be classified as a fractured medium, at least on a site-specific basis. In a fractured medium, the primary medium has the greater porosity and effectively represents the bulk of the "storage" capacity of the unit, and the secondary medium has intrinsic "transport" properties which make it the transport medium. Also inherent in double-porosity theory is the concept that any representative finite volume of the collective media contains both primary and secondary media.

In the conceptualization of a double-porosity medium, various assumptions are necessary to allow the system to be represented mathematically. One very important assumption, as noted above, is that the system can be characterized as fractures and matrix units with a relatively simple interaction between them. The SWIFT II model (Reeves et al., 1986a), utilized in the analysis of the H-3 tracer test, allows the geologic system to contain either one fracture set or three orthogonal fracture sets. With this conceptualization, the matrix units are mathematically represented as slabs (for a single fracture set) and cubes or spheres (for three fracture sets). While these

mathematical idealizations cannot be expected to truly represent natural geologic systems, they do allow the solution for double-porosity transport at the field scale to be a tenable problem. Conceptually, one should consider these ideal representations as approximations of the natural system, where one is attempting to quantitatively attain consistency between the fracture fluid volume and the surface area available for diffusion.

Further assumptions were also made regarding the conceptual basis for this analysis. The flow field in the study area was assumed to be radial around the pumped well and at steady-state conditions during the tracer test. Since the hydraulic conductivity of the matrix is low and the flow regime is approximately at steady state, the advective transfer from the fractures to the matrix and advective transport in the matrix were assumed to be negligible. Therefore, the transport of the tracer from the fracture to the matrix and within the matrix was assumed to occur by diffusion only. The double-porosity medium was assumed to be homogeneous and isotropic.

Three alternative approaches were considered for solution of the transport equations: (1) a Cartesian coordinate system, (2) a curvilinear coordinate system, or (3) a radial geometry. The simulation of the transport of the initial tracer input using a Cartesian coordinate system would be impractical because of the very large number of grid blocks and time steps that would be required to prevent numerical problems. Since the coding has not been developed for the curvilinear approach, the radial-geometry option of SWIFT II was chosen. Additional reasons for choosing the radial approach for simulating the H-3 tracer test are: (1) it offers advantages in meeting the numerical criteria of the model, and (2) the field data base on heterogeneity is not sufficient to warrant utilizing the Cartesian approach, which is much more difficult to implement.

A schematic representation of the global discretization in both plan view and cross section is shown in Figure 3.6 for the pumping well and a typical tracer-addition well. The pumping well resides at the center of the radial system and is given a constant discharge rate consistent with that measured during the tracer test. Both upper and lower boundaries of the system are considered to be no-flow boundaries. At the outer edge of the radial system, a Dirichlet pressure boundary condition is prescribed. Using the radial simulation approach, the initial tracer distribution surrounding the tracer-additional well is approximated as being distributed in a concentric ring surrounding the pumping well. The actual initial tracer-input zone at the end of the short-duration tracer-injection phase and the approximated zone for modeling purposes are shown schematically in Figure 3.6. Further details on the calculation procedures for estimating the mass of tracer introduced into each of the global grid blocks at the input zone are outlined in Appendix F of Kelley and Pickens (1986).

The radial discretization implemented for the global system assumes that the geologic system is both homogeneous and isotropic. As a result, flow paths for tracers m-TFMB and PFB were analyzed separately. Results from anisotropy determinations from pumping tests performed at the H-4, H-5, and H-6 hydropads at the WIPP site (Gonzalez, 1983b) have yielded anisotropy ratios of 2.7:1, 2.4:1, and 2.1:1. This degree of anisotropy is weak in magnitude and cannot clearly be differentiated from the effects of aquifer heterogeneity. Although it is felt that hydropad-scale heterogeneities are present at the H-3 and H-4 hydropads, the quantification of the spatial variability of the medium properties is not possible from the existing information base.

3.2.3 Simulation Model

The SWIFT II model was selected for simulation of the tracer test at the H-3 hydropad and for design calculations for the sorbing tracer

test because it has the capability to simulate flow and transport processes in double-porosity media. A comprehensive description of the theory and implementation of the SWIFT II model is presented in Reeves et al. (1986a). The discretization of the global (fracture) and local (matrix) systems and the time-step specification for simulating the breakthrough curves from the conservative tracer test are discussed in Kelley and Pickens (1986).

3.2.4 Model Input Parameters

As discussed earlier, the Culebra dolomite at the H-3 hydropad is conceptualized as a double-porosity system for modeling purposes. Parameters characterizing the Culebra, tracers, tracer-test operating conditions, fractures, and matrix were utilized in fitting the m-TFMB and PFB breakthrough curves determined from water samples taken from the pumping well. These parameters include:

- tracer free-water diffusion coefficient;
- matrix tortuosity;
- longitudinal dispersivity;
- fracture porosity;
- matrix porosity;
- matrix-block size;
- pumping rate;
- Culebra thickness;
- distance between tracer-addition and pumping wells;
- tracer mass introduced;
- initial tracer input-zone dimensions.

The following is a discussion of the estimation of values for each of these parameters:

Tracer Free-Water Diffusion Coefficient

Free-water diffusion coefficients for m-TFMB and PFB have been reported by Walter (1982). He calculated the free-water diffusion coefficients using the Nernst expression and data from laboratory experiments conducted to determine the limiting ionic conductances of the tracer species. The calculated diffusion coefficients for m-TFMB and PFB were 7.4×10^{-6} and 7.2×10^{-6} cm²/s, respectively (Walter, 1982).

Tortuosity

The solute diffusion coefficient in the porous matrix is defined as follows for use in the SWIFT II code:

$$D^* = \phi_m \tau D_o \quad (3-1)$$

where D^* = the solute diffusion coefficient in the porous matrix;
 ϕ_m = the matrix porosity;
 τ = the tortuosity; and,
 D_o = the free-water diffusion coefficient.

In studying solute transport by diffusion, tortuosity is a parameter whose magnitude ($0 < \tau > 1$) is a measure of the tortuous nature of the pores through which the solute is diffusing. As the resistance to diffusional transport for a conservative species increases, the magnitude of tortuosity decreases. Bear (1972) has presented a review of tortuosity values in the range of 0.3 to 0.7. Bear states that tortuosity is correctly defined as:

$$\tau = (L/L_e)^2 \quad (3-2)$$

where L = straight-line distance;
 L_e = mean length of the diffusional path in a porous matrix.

Although not stated, his review appears to have been for studies utilizing unconsolidated media. Tortuosity values for consolidated materials like dolomite are rare. Tortuosity values of 0.02 to 0.17 were calculated from the diffusion coefficients of Cl^- in chalk samples by Barker and Foster (1981). From diffusion experiments on crystalline rock samples, Katsube et al. (1986) calculated tortuosity values of 0.02 to 0.19. It is expected that the tortuosity will vary spatially within the Culebra. For simulation purposes in interpreting the tracer test at the H-3 hydropad, tortuosity values of 0.15 and 0.45 were chosen as reasonable. In addition, utilizing two values for calibration of the breakthrough curves allows the evaluation of the effect of varying tortuosity on other parameters determined from the calibration (e.g., effective matrix-block size).

Longitudinal Dispersivity

In fitting tracer breakthrough curves for transport in a single-porosity medium, longitudinal dispersivity is often the key parameter utilized in the calibration (i.e., fitting breakthrough-curve shape and peak concentration). In a double-porosity system, the transport of solutes between the fractures and matrix by diffusion can have a very large effect on the breakthrough curve, thus causing the interpretation of the best-fit longitudinal dispersivity to be difficult.

A review of the literature on the magnitude of longitudinal dispersivity for various tracer-test scales and contamination-plume sizes (e.g., Lallemand-Barres and Peaudecerf, 1978; Pickens and Grisak, 1981) suggests that longitudinal dispersivity can be expressed as a function of the mean travel distance of the tracers or contaminants. In many situations, the longitudinal dispersivity is from 5% to 10% of the travel-path length. Since the well spacings at the H-3 hydropad were approximately 30 m, longitudinal dispersivities of 1.5 to 3.0 m were chosen for simulation of the breakthrough curves.

Fracture Porosity

From examination of the tracer-breakthrough curves, it was concluded that the rapid arrival of the m-TFMB tracer at the pumping well could have been dominated by transport in fractures along the H-3b1 to H-3b3 flow path. A first estimate for the fracture porosity was calculated from the relation:

$$\phi_f = Q\bar{t} / \pi r^2 h \quad (3-3)$$

where ϕ_f = the fracture porosity;
Q = the discharge rate at the pumping well;
 \bar{t} = the time to reach the peak concentration;
r = the distance between the tracer-addition and pumping wells; and,
h = the aquifer thickness.

This equation is based on the assumption that transport is occurring in the fractures only with no tracer losses to the matrix. Therefore, it will yield an overestimate for the fracture porosity.

Using equation 3-3, the calculated fracture porosity based on the m-TFMB breakthrough curve for the H-3b1 to H-3b3 flow path was approximately 2.0×10^{-3} . The PFB breakthrough curve for the H-3b2 to H-3b3 flow path exhibited a much later first detection of tracer and did not have a well-defined peak concentration. Therefore, only the fracture porosity determined from the m-TFMB breakthrough curve was utilized. Because of the large difference between the breakthrough curves for m-TFMB and PFB, it is recognized that the estimated fracture porosity is uncertain and its representativeness to both flow paths may be questionable. However, no other estimates are available for simulating the tracer breakthrough curves.

Matrix Porosity

Porosity determinations conducted on six core samples from boreholes H-3b2 and H-3b3 ranged from 0.11 to 0.24 (Core Laboratories, 1986a) with an average value of approximately 0.2. A matrix porosity of 0.2 was chosen for simulating the tracer breakthrough curves.

Matrix-Block Size

As discussed in Section 3.2.2, the conceptualization of the double-porosity system involves mathematically representing the natural system as a homogeneous, idealized configuration of fractures and matrix units. Even though the natural system is heterogeneous, one must attempt to develop a reasonable approximation of the correct fracture fluid volume and the surface area available for diffusion from the fractures to the matrix.

For modeling the tracer breakthrough curves at the H-3 hydropad, the matrix units were assumed to be defined by three orthogonal fracture sets. Fracture sets both horizontal and vertical (or near vertical) have been observed in core samples, shaft excavations and outcrop areas. A spherical representation of the matrix units was chosen for simulation purposes. Because the time scale of the tracer tests is not very long with the depth of penetration of the tracer into the matrix units not large, the spheres are mathematically equivalent to the cube representation through a consistent correlation of fracture fluid volume and surface area available for diffusion. This assumption in the simulation approach is discussed further by Kelley and Pickens (1986).

The characteristic matrix-unit size is expected to vary considerably over the WIPP-site area and also vertically at any location as a result of the high degree of heterogeneity observed in the Culebra.

Matrix-block sizes from 0.15 to 1.0 m are considered a reasonable range based on examination of core samples. These matrix-block sizes were utilized as initial estimates for simulating the tracer-breakthrough curves using the SWIFT II model. Additional discussion of fracturing in the Culebra is presented in Kelley and Pickens (1986).

Pumping Rate

The discharge rate at the pumping well was relatively constant throughout the tracer test. The pumping rate was approximately 0.19 l/s for the first 23 days of the test, at which time the rate increased by 0.02 l/s over the following 4 days and continued at the higher rate (0.21 l/s) for the last 6 days of the test. The portion of the breakthrough curves that were most sensitive during calibration involved the first 23 days of the test. Therefore, a constant pumping rate of 0.19 l/s was chosen as adequate for simulating the tracer breakthrough curves.

Culebra Thickness

The definition of the bottom and top of the Culebra has been reviewed using available geophysical logs (Beauheim, personal communication, 1986). Recommended values are:

Well	Depth Interval Below Land Surface (ft)	Thickness (m)
H-3b1	670 - 694	204.2 - 211.5
H-3b2	676 - 699	206.1 - 213.1
H-3b3	673 - 696	205.1 - 212.1

A Culebra thickness of 7.0 m, corresponding to the thickness estimate at the pumping well, was chosen for simulating the tracer-breakthrough curves.

Distance Between Tracer-Addition and Pumping Wells

Distances between the boreholes at the Culebra depth were calculated based on the surveys of the borehole locations at ground surface and borehole-deviation surveys (Saulnier et al., in preparation). The distances between H-3b1 and H-3b3 for the m-TFMB flow path and H-3b2 and H-3b3 for the PFB flow path are 30.66 and 26.80 m, respectively (see Figure 3.3).

Tracer Mass Introduced

Hydro Geo Chem (1985) reported injecting 1 kg of m-TFMB into well H-3b1 and 1 kg of PFB into well H-3b2.

Initial Tracer Input-Zone Dimensions

The tracer-test history was presented in Section 3.2.1. The tracer injection procedure consisted of mixing the tracer in an initial volume of water, injecting the tracer-labelled volume, and injecting a second volume of water to displace the tracer-labelled water into the formation. Since the injection was of short duration, it was assumed that the tracer moved out under plug-flow conditions through the fractures only and resulted in an initial tracer input zone that was cylindrical in shape and encompassing a region dependent on the volume injected and the fracture porosity. The two fluid volumes that are injected determine the initial tracer-zone dimensions in the aquifer. Natural gradients were assumed to have a negligible effect upon the initial tracer-mass distribution around the injection well. For a fracture porosity of 1.9×10^{-3} (value determined through calibration

of the breakthrough curves at the pumping well) and the respective fluid volumes injected, the initial tracer-input ring of the m-TFMB tracer surrounding well H-3b1 had radii of 1.0 and 1.7 m, and for the PFB tracer surrounding well H-3b2 had radii of 1.5 and 1.7 m. The procedure for distributing this mass in the global grid-block system of SWIFT II is shown schematically in Figure 3.6 and discussed in detail in Appendix F of Kelley and Pickens (1986).

The input parameters discussed above are represented by a constant value for each simulation during calibration of the breakthrough curves. However, input-parameter values for different simulations are adjusted systematically, within ranges judged as reasonable, in an attempt to match the observed tracer-breakthrough curves.

3.2.5 Analysis of Tracer-Breakthrough Curves

From initial inspection of the two breakthrough curves (Figure 3.5), one can identify major differences in tracer breakthrough. The m-TFMB curve peaks sharply early in the test, whereas the PFB curve is very broad, of much lower concentration, and requires a significant portion of the test period to reach maximum observed concentration. With the current double-porosity conceptualization, it was possible to achieve reasonable breakthrough-curve matches with system parameters consistent with the current physical and conceptual understanding of the Culebra. A sensitivity analysis using a range of values for the model input parameters for the m-TFMB breakthrough curve was conducted (Kelley and Pickens, 1986). The sensitivity analysis provided additional information for assessing the uncertainty in the parameters determined from the calibration of the tracer-breakthrough curves.

The basis for initial estimates for each of the model-input parameters is described above. Using these initial estimates, calibration of the observed breakthrough curves for m-TFMB and PFB was performed. The best-fit parameters are summarized in Table 3.2.

Figures 3.7a and 3.7b show the comparison of the observed and simulated breakthrough curves for the m-TFMB tracer on the H-3b1 to H-3b3 flow path for tortuosities of 0.15 and 0.45. A longitudinal dispersivity of 3.0 m and a fracture porosity of 1.9×10^{-3} provided the best-fit simulated breakthrough curve. Effective matrix-block sizes of 1.2 and 2.1 m were interpreted for assumed tortuosities of 0.15 and 0.45, respectively.

The observed and simulated breakthrough curves for PFB for the H-3b2 to H-3b3 flow path are shown in Figures 3.8a and 3.8b for tortuosities of 0.15 and 0.45. As discussed earlier, the breakthrough curve for PFB did not indicate fracture-controlled transport. Using the same fracture porosity as for fitting the m-TFMB breakthrough curve, a dispersivity of 1.5 m, and assumed tortuosities of 0.15 and 0.45 resulted in effective matrix-block sizes of 0.25 and 0.44 m, respectively.

Dispersivity is defined and applied consistent with a Fickian conceptualization in the SWIFT II model. The longitudinal dispersivities obtained for the two flow paths are within a factor of two. From a sensitivity analysis (Kelley and Pickens, 1986), it was found that increasing dispersivity alone caused an earlier tracer arrival and higher peak concentration. The difference in dispersivities for the two flow paths can be viewed as a measure of either differences in heterogeneity between the two flow paths traveled by the tracers or a result of difficulties in providing a unique fit of observed and simulated breakthrough curves for processes described by such a large number of parameters.

The tortuosity value chosen during calibration has a direct effect on the subsequent estimate of the matrix-block size. As the tortuosity increases, the diffusive loss increases and, therefore the matrix-block size must also increase in order to obtain the same tracer-

breakthrough response. From the literature review of tortuosities for consolidated materials, the lower tortuosity value is considered to be more representative.

The characteristic matrix-block sizes estimated from calibration of the breakthrough curves varied between flow paths. Between H-3b1 and H-3b3, 1.2 to 2.1 m block sizes (depending on specified tortuosity values) provided the best fit, whereas between wells H-3b2 and H-3b3, 0.25 to 0.44 m gave the best fit. Given the degree of heterogeneity expected within the Culebra even over relatively short distances, it is not surprising to have evidence of differences in matrix/fracture geometry at the hydropad scale. The difference in matrix-block sizes implies that directional fracture/matrix properties are present at the hydropad scale. It should be noted that the calculated matrix-block sizes are consistent with observations from core samples, shaft excavations, and outcrop areas. However, the uncertainty in the matrix-block sizes determined for the H-3b2 to H-3b3 flow path (PFB tracer path) is considered larger since the fracture porosity utilized in the calibration was chosen the same as for the H-3b1 to H-3b3 flow path (m-TFMB tracer path) where fracture-dominated transport was more clearly evident.

It is recognized that uncertainty exists in the assumed or calibrated values for tortuosity, fracture porosity, matrix porosity, and matrix-block size used to describe solute transport at the H-3 hydropad. Reduction in this uncertainty would require additional laboratory and field testing (e.g., additional drilling and coring, additional matrix-porosity determinations on core, diffusion experiments, and additional field tracer testing). The results obtained from the conservative tracer test are adequate, however, to indicate that fracture flow and matrix diffusion dominate solute transport in the Culebra at the H-3 hydropad. Further, the parameters derived to fit the m-TFMB and PFB breakthrough curves are consistent with current conceptualizations of the Culebra at the H-3 hydropad.

3.3 Design Calculations for Sorbing Tracer Test

Model calculations were performed using SWIFT II to evaluate the significance of the magnitude of the partition coefficient (defined in Chapter 1) to the transport of generic sorbing tracers in the Culebra Dolomite Member at the H-3 hydropad. These calculations should be considered as scoping in nature and are not intended to represent specific tracers. For each of these simulations, the partition coefficient was assumed to be constant spatially and temporally.

Simulations were conducted using a range of partition coefficients and the best-fit parameters determined from analysis of the convergent-flow conservative tracer test conducted at the H-3 hydropad. The parameters are summarized in Table 3.3. The free-water diffusion coefficients utilized for interpretation of the conservative tracer test with the organic tracers are similar in magnitude to those for a range of cations. Therefore, diffusion coefficients were not treated as a variable in the simulations. A single tortuosity of 0.15 was chosen for the design calculations. Thus, effective block sizes of 1.2 and 0.25 m were utilized to represent the H-3b1 to H-3b3 and the H-3b2 to H-3b3 flow paths, respectively. A pumping rate of 0.19 l/s, identical to the pumping rate used in the previously-conducted conservative tracer test, was chosen. Future evaluations and design calculations could investigate both the suitability and effect of using larger pumping rates and the effects of different diffusion coefficients.

The mass of a specific tracer that would be added to a tracer-addition well was set at 1 kg and the injection volumes and times were chosen identical to those utilized for the previously-conducted conservative tracer test at the H-3 hydropad. These tracer masses and injection volumes were chosen for calculation purposes only and are assumed independent of any possible tracer-solubility constraints. The design calculations using SWIFT II provide estimates of the concentrations that

would be present in water samples from the pumping well. These concentrations are expressed in Table 3.4 both as micrograms per liter sample per 1 kg input ($\mu\text{g}/\text{l}/\text{kg}$) and as dimensionless dilution factors (mass per kg of sample pumped/mass injected). The density of H-3 Culebra water is about 1.04 kg per liter (kg/l) so the conversion between the two concentrations units becomes

$$\text{Dilution factor} = (\mu\text{g}/\text{l}/\text{kg}) \times 0.96 \times 10^{-9} \quad (3-4)$$

A range of partition-coefficient values was chosen, with higher values utilized for the H-3b1 to H-3b3 flow path because this path exhibited a more rapid transport rate for conservative tracers. Partition coefficients of 0.1, 1.0, 10.0, and 50.0 ml/g and 0.1, 1.0, 2.0, and 10.0 ml/g were utilized for the H-3b1 to H-3b3 and the H-3b2 to H-3b3 flow paths, respectively. For these two flow paths, the simulated breakthrough curves for the pumping well are shown in Figures 3.9a and 3.9b, and the peak concentrations, times to reach the peak concentration, and times to reach 1% of the peak concentration are summarized in Table 3.4. In evaluating the results of these simulations, one should consider the uncertainties associated with the estimates of the physical solute-transport parameters for the Culebra at the H-3 hydropad (Section 3.2), the limitations in the use of partition coefficients to represent overall transport behavior of reactive species (Sections 1.2 and 4.0), and the simplifying assumptions used in the design calculations.

4.0 GEOCHEMICAL CONTROLS ON TRANSPORT IN THE CULEBRA AT THE H-3 HYDROPAD

The common mathematical description of the transport of substances by flowing ground water includes a term to account for retardation by chemical reactions between solutes and solid phases. This term, which we refer to as the partition coefficient (K), is defined in Section 1.2 as the ratio of the mass of substance fixed on the solid phase in a given volume of aquifer to the mass dissolved in the fluid in that volume.

If it is assumed that the mass fixed on the solid is linearly proportional to its concentration in solution, the partition coefficient can be identified with the distribution coefficient (K_d) used to describe simple linear sorption. There are practical advantages to making this assumption. First, it yields transport equations which are amenable to closed-form solutions. Second, numerical values for partition coefficients for sorption processes can, in principle, be determined from batch laboratory tests.

In reality, sorption is not the only process which can change the relative concentration of solute in the fluid and in the solid. Processes such as mineral solution and precipitation, and ion exchange can also influence the value of the partition coefficients. Prediction of how a substance will be transported and interpretation of observations of its transport behavior both require an understanding of how a substance will behave in solution. They also require the identification of the geochemical processes by which the solute is partitioned between the stationary solids of the aquifer and the moving fluid.

Once identified, the geochemical processes must be defined in sufficient detail to permit a mathematical description which at least bounds the expected behavior. This requires a conceptual model for the thermodynamic behavior of solutes and for their interactions with solid phases. The conceptual model must be appropriate for the type of system being examined

(for example, a brine as opposed to a dilute solution) and there must be sufficient thermodynamic data to support the model.

Site-specific data are also required and are generally drawn from both field and laboratory activities. Field activities include the collection of representative samples of fluids and solids, and field measurements of such quantities as formation temperature and geochemical parameters which may change rapidly during sample storage or as a result of the sampling activity itself. Such parameters may include pH and platinum-electrode potential. In this report, the term "platinum-electrode potential" refers to values found using this common field-measurement technique. The term "Eh" refers only to theoretical values derived from or related to redox reaction potentials.

Laboratory activities include descriptions of the mineralogy, petrology and chemistry of solid phases, particularly those which have the potential either to control the bulk chemistry of the formation fluid or to react with specific substances of interest in the transport problem. Laboratory activities also include the chemical analyses of preserved samples of formation fluid. Finally, special laboratory investigations may be required, such as direct studies of water-rock interactions using batch, column, or wafer methods.

This chapter describes the geochemical processes which influence transport in the Culebra in the vicinity of the H-3 hydropad. It begins by summarizing the data which are presently available on the chemistry of water and the composition of solid phases from boreholes at the H-3 hydropad. It continues with an interpretation of these data and leads to a description of specific processes which control bulk water chemistry and may otherwise influence transport at this location. The chapter concludes with a summary of the geochemical constraints on the design of a sorbing tracer test at the H-3 hydropad.

4.1 Formation Water Chemistry

Chemical analyses are available for three samples of Culebra water taken from wells at the H-3 Hydropad. The results of the analyses of a sample collected March 17, 1977 from a well designated as H-3 (now H-3b1) were reported by Mercer (1983) and by Ramey (1985). Two samples were taken more recently from the H-3b3 borehole as part of the Ecological Monitoring Program. Some data on these samples are given by Westinghouse Electric Corporation (1985), and complete analytical data will be published by Robinson (in preparation).

Analyses of all three samples are shown in Table 4.1. All the data for the March 17, 1977 sample are as given in Mercer (1983). The concentrations of dissolved solids for the samples taken in 1984 and 1985 are from analyses reported by Bendix which will appear in Robinson (in preparation). The pH used for the 1985 sample is that shown in Figure 10.6 of Westinghouse Electric Corporation (1985). The sample taken in 1984 was assumed to have the same pH.

No density values were reported for either the 1984 or the 1985 samples. A series of specific-gravity measurements made during hydraulic testing of the Culebra at the H-3 hydropad indicate values ranging from 1.037 to 1.040 (INTERA Technologies, 1986, Table A5-1). As discussed in Appendix E of Haug et al. (in preparation), the densities of water from the Culebra at standard temperature and pressure (STP) conditions are a function of their chemistry. Based on the chemistry of these samples, their densities should be about 1.04 kilograms per liter (kg/l) at STP conditions. A value of 1.04 kg/l is used for the density of all three of the samples. Values of solution density are required to convert concentrations measured in milligrams per liter solution (mg/l) to molal concentrations (moles per kilogram water).

Temperatures of water produced during a sixty-two day pumping test of the Culebra at the H-3 hydropad are given in Table A5-1 of INTERA Technologies (1986). After about 3 days of pumping, the temperature reached 24°C (measured on water samples discharged at ground surface) and it remained at essentially this value for the remainder of the test. For calculation purposes, the temperature of the formation was taken as 24°C. Downhole temperature measurements would be required to obtain an improved estimate of the representative formation-water temperature.

The results of tests on the internal consistency of these samples are also shown in Table 4.1. These include a charge balance test and a mass balance test. The sum of the charges of the anions and cations balance within 3% in all three analyses. The sum of the analyzed dissolved solids for the 1977 sample is within 9% of the measured residue on evaporation. The residue on evaporation was measured at 105°C (Mercer, 1983) and may therefore have included some water of hydration of the residual salts. The fact that it is higher than the sum of analyzed constituents is therefore neither surprising nor of concern. The values for residue on evaporation were not available for the samples taken in 1984 and 1985 and, therefore, this test of internal consistency could not be applied to them.

Overall, the compositions of these three samples are consistent with one another and with the regional pattern of water chemistry in the Culebra. The regional Culebra water chemistry is discussed briefly in Appendix E of Haug et al. (in preparation).

The overall chemical consistency among the three samples from the H-3 hydropad is evident from inspection of Table 4.1. The results of the analyses of the 1984 and 1985 samples agree particularly well. However, some values reported for the 1977 sample are clearly discordant from the later samples. These include values for the concentrations of

potassium, magnesium, sulfate, alkalinity, and silica. Except for the alkalinity, the differences could reflect analytical errors or the remnants of fluid used to construct and develop the well which were not adequately pumped before the sample was taken. The alkalinity discrepancy is discussed further in Section 4.3.2.

4.2 Identity and Distribution of Solid Phases

The mineralogy of aquifers exerts strong controls on the chemistry of water within them. Mineralogical information on the Culebra at the H-3 site was gathered on selected samples of cores from boreholes H-3b2 and H-3b3. The samples were examined by thin-section petrographic techniques, X-ray diffractometry, and scanning electron microscopy by Core Laboratories Inc. The following discussion is based on a report of this work (Core Laboratories, 1986b) which is summarized in Table 4.2. The core samples were chosen both from zones from which intact core was available and from zones from which only rubble and rock fragments were collected. Thus, the analyzed core samples should have provided representative mineralogical and physical properties for characterization of the Culebra. The validity of this assumption cannot be evaluated from the existing data base.

The majority of the Culebra at the H-3 hydropad, including the part through which most ground-water flow is thought to occur, can be described as a vuggy, fractured dolostone. Samples of this material range from 81 to 99 weight percent dolomite with the balance composed of gypsum, halite, mica, bassanite, quartz, and clay minerals. The clay fraction is dominated by mixed-layer chlorite-smectite which has 40% to 50% expandable interlayers and shows some degree of ordering. Discrete chlorite, illite, and kaolinite are also present.

Immediately above and below the dolostone are silty claystones. These units are composed of detrital quartz, mica, dolomite, and gypsum in a

clay matrix. Feldspar, halite, pyrite, metal oxides, and calcite also occur in minor amounts. It is probable that most water flow in the system occurs through the dolostones, so that minerals present in the adjacent claystones are likely to have little influence on the chemistry of water in the Culebra, particularly on the time scale of the test.

Materials which may enter an aquifer during the drilling and completion of boreholes can also bring about changes in the aquifer water chemistry and influence the transport of substances in the vicinity of the borehole. The construction of the wells at the H-3 hydropad is discussed in Section 3.1.2. Although drilling fluids are not discussed in the well construction section, the discussion of water chemistry presented suggests drilling fluids are not a problem in the H-3 hydropad water sampling, except possibly for the first (1977) sample.

4.3 Characterization of Geochemical Environment

Water chemical analyses and information on formation mineralogy can be used to explore possible mineral controls on water chemistry. To do this requires a model of the geochemistry of the system. Before describing the results of the examination of the data, it is necessary to discuss the model used.

4.3.1 Geochemical Modeling

A model for the thermodynamic behavior of solutions is necessary to translate the results of water analyses to parameters used in the mathematical treatment of chemical equilibria involving solutions and mineral phases. The conceptual model used in this work is the ion-pair model (Garrels and Christ, 1965).

As shown in Table 4.1, the ionic strength of Culebra water at the H-3 hydropad is slightly above one molal, with the dissolved constituents

dominated by sodium and chloride. Thus, these waters can be studied with an ion-pair model, particularly when it is used with a modified formulation for the calculation of individual ion activity coefficients. Activity coefficients were therefore calculated using the WATEQ or Truesdell-Jones form of the extended Debye-Huckel equation (Truesdell and Jones, 1974; Nordstrom and Munoz, 1985). A discussion of this equation is included in the Appendix to this report.

The ion-pair model of solution behavior is embodied in a number of the computer codes commonly available for making geochemical calculations (Nordstrom et al., 1979). The code used for this work, PHREEQE (Parkhurst et al., 1980), was chosen because it embodies the ion-pair model and includes an option to calculate individual ion activity coefficients using the WATEQ Debye-Huckel expression. In addition, it is efficiently coded to minimize computer run time, and is written so that all the reactions it models are entered as part of the thermodynamic data base rather than hard-programmed into the code. The particular version of the code employed was prepared for use in the Salt Repository Project of the U.S. Department of Energy and is documented to meet nuclear waste quality assurance requirements (INTERA Environmental Consultants, 1983).

The reliability of geochemical modeling is determined by the quality of the thermodynamic data base supporting the model. Data required for the calculations made for this report include values for the equilibrium constants for ion association reactions and for the formation of minerals which might influence the water chemistry. In addition, ion-specific parameters for the equation used to calculate individual ion activity coefficients must be specified. Finally, the temperature dependence of all equilibrium constants is needed along with the temperature-dependent values of certain of the properties of the solvent, water.

The thermodynamic data used are included in the Appendix. This Appendix also includes references to the sources of the data chosen and a description of the procedure used to select the data.

4.3.2 Formation-Water Interactions

From the mineralogical data described in Section 4.2, the Culebra at the H-3 hydropad can be broadly characterized as a gypsiferous dolostone. As described in Appendix E of Haug et al. (in preparation), a number of studies have been performed on waters from aquifers of this type including studies of:

- the Floridan aquifer;
- the Edwards aquifer of central Texas; and
- the Muschelkalk and other dolomitic aquifers of northern Switzerland.

Waters in these aquifers are characterized by:

- Saturation with respect to calcite, even if the residence time of the water being sampled is as short as a few years.
- Saturation with respect to dolomite, if the residence time of the water sampled is several hundred years or more.
- Saturation with respect to gypsum. In formations in which there has been limited fresh-water circulation so that plentiful gypsum remains, gypsum saturation can occur in waters with residence times of only a few tens of years.
- Saturation with respect to celestite. This is particularly common in waters saturated with gypsum. Strontium is not as frequently analyzed in water samples as is calcium but where data are available, they show that solutions saturated with gypsum are generally also saturated with celestite.
- Undersaturation with respect to halite, even though halite is present in some of these formations as it is in the Culebra. This

probably occurs because halite is so very soluble and dissolves so rapidly that even a limited amount of ground-water circulation can remove accessible halite from a formation. Thus, higher chloride concentrations in waters from such formations tend to be present in waters taken at points distant from outcrops and recharge areas or in areas which for other reasons have limited ground-water circulation.

4.3.2.1 Saturation Index Calculations

Mineral saturation calculations were made for the three Culebra water samples to examine the possible mineral controls on water chemistry. The calculations were made using the PHREEQE code and the thermodynamic data given in the Appendix. The results in Table 4.3 are expressed as saturation indices (SI), which are defined as:

$$SI = \log IAP - \log KT \quad (4-1)$$

where $\log KT$ is the logarithm of the equilibrium constant for the dissolution of the mineral at the temperature of the solution, and $\log IAP$ is the logarithm of the ion activity product. The $\log IAP$ for gypsum ($\text{CaSO}_4 \cdot 2\text{H}_2\text{O}$), for example, is:

$$\log IAP_{\text{gypsum}} = \log a(\text{Ca}^{+2}) + \log a(\text{SO}_4^{-2}) + 2 * \log a(\text{H}_2\text{O}) \quad (4-2)$$

where a = thermodynamic activity

while that for calcite (CaCO_3) is:

$$\log IAP_{\text{calcite}} = \log a(\text{Ca}^{+2}) + \log a(\text{CO}_3^{-2}). \quad (4-3)$$

At equilibrium, the $\log IAP$ and $\log KT$ will be equal and the saturation index will be zero. A negative saturation index indi-

undersaturation, while a positive saturation index indicates oversaturation of the solution with respect to the mineral.

Saturation indices for several minerals calculated from the analyses given in Table 4.1 are shown in Table 4.3. The gypsum saturation indices are between 0.04 and 0.11. As shown in Figure E.3 of Haug et al. (in preparation), the gypsum saturation index for all but one of the Culebra samples taken in 1984 and 1985 is between 0.0 and 0.1. This tight grouping of saturation indices is strong evidence that the chemistry of these waters is controlled by saturation with respect to gypsum. A similar tight grouping would be found for saturation indices of anhydrite (CaSO_4), but with a mean value of -0.34 SI units, the amount by which anhydrite is more soluble than gypsum at 24°C (see Appendix).

Celestite (SrSO_4) saturation indices can be calculated only for the 1984 and 1985 samples because strontium was not analyzed for the sample taken in 1977. The saturation indices of the latter samples, however, are close to 0.0 and suggest control of the solution composition by saturation with respect to celestite.

Saturation indices of minerals containing carbonate are sensitive to the pH of the solution. Carbonate (CO_3^{-2}) concentrations in solutions of pH values of less than 8.5 or 9 cannot be measured directly. Instead they are calculated from the measured solution alkalinity which, in solutions of pH values less than 8 to 8.5, essentially equals the bicarbonate (HCO_3^-) content of the solution. The carbonate activity is calculated from the bicarbonate and the pH using the expression:

$$\log a(\text{CO}_3^{-2}) = \log K_T(\text{HCO}_3^-) + \text{pH} + \log a(\text{HCO}_3^-) \quad (4-4)$$

where $\log K_T(\text{HCO}_3^-)$ is for the dissociation reaction for bicarbonate.

Combining this expression with the definition of the saturation index (Eq 4-1) shows that the saturation index for calcite varies directly with variations in the pH.

The log IAP for dolomite ($\text{CaMg}(\text{CO}_3)_2$) is:

$$\log \text{IAP}_{\text{dolomite}} = \log a(\text{Ca}^{++}) + \log a(\text{Mg}^{++}) + 2 \log a(\text{CO}_3^{-2}) \quad (4-5)$$

The dolomite saturation index varies as twice the pH because the activity of carbonate appears twice in the expression for the dolomite saturation index.

Because pH values of ground waters can change during sample collection and storage, it is good geochemical practice to measure pH in the field. Even when this is done, it is often difficult to assure that the value measured at the surface represents that of the ground water as it was in the formation. Although the analytical error in pH measurements is far less than 0.01 pH unit, uncertainties associated with pH values of ground waters, even when carefully determined in the field, are from 0.05 to 0.1 pH units.

To compare the saturation states of a solution with respect to several carbonate minerals it is convenient to use expressions from which the possibly uncertain carbonate ion activity has been eliminated. To compare calcite and dolomite, the expression:

$$2 \text{SI}_{\text{calcite}} - \text{SI}_{\text{dolomite}} \quad (4-6)$$

is useful because its value is independent of the activity of carbonate.

The calcite and dolomite saturation indices calculated for the 1985 sample and shown in Table 4.3 are -0.11 and -0.18, respectively.

While these negative saturation indices could be taken as an indication that this water is undersaturated with respect to these minerals, undersaturation with calcite, at least, is uncommon in ground waters with residence time in excess of several decades. Thus, it is more likely that the measured pH is slightly below that in the formation, and that the water actually is saturated with respect to both calcite and dolomite.

The calcite and dolomite saturation indices for the 1984 sample are -0.06 and -0.08, respectively. These values are well within the ranges to be expected for a water saturated with calcite and dolomite, given the possible uncertainties in measured pH values. The pH value used for these calculations though was that measured for the 1985 sample because the 1984 value was not reported. This detracts somewhat from the confidence with which saturation indices for this sample can be used.

Uncertainties in the saturation indices for calcite, dolomite, and gypsum due to uncertainties in the thermodynamic data and the conceptual model used in their calculation are estimated to be less than 0.05 SI units.

Two sets of saturation indices are given in Table 4.3 for the sample collected in 1977. The calcite and dolomite saturation indices calculated using the reported alkalinity (see Table 4.1) are 0.38 and 0.72 respectively. These strongly positive values indicate that a water of this composition would be oversaturated with respect to both these minerals at the measured pH.

Waters with such strongly positive saturation indices for these minerals are generally not found in nature. Although positive calcite and dolomite saturation indices have been reported from some ground waters, these can usually be explained as a result of mixing

of waters or of CO₂ gas loss during or just prior to the time of sample collection (Pearson et al., 1978).

Table 4.1 shows that the alkalinity reported for the 1977 sample is considerably higher than the values reported for the 1984 and 1985 samples. If it is assumed that the alkalinity reported for the 1977 sample is in error and that its true value is the mean of the 1984 and 1985 values, saturation indices of 0.01 and -0.01 result for calcite and dolomite, respectively (Table 4.3).

Comparison of the calcite and dolomite saturation indices of these samples using the expression $2SI_{\text{calcite}} - SI_{\text{dolomite}}$ to eliminate uncertainties in the carbonate values are also shown in Table 4.3. For the 1977 sample the value is 0.04 while for both the 1984 and 1985 samples the value is -0.04. If the Culebra formation water is in equilibrium with calcite and dolomite, and if the thermodynamic data used in the calculations of the saturation indices are correct, the likely cause for these values not equaling 0.00 would be errors in the analyses for dissolved magnesium.

4.3.2.2 Redox Controls

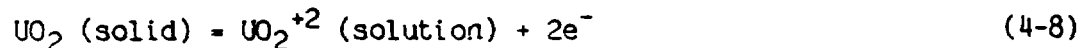
The solubility and the identity of the dominant aqueous species of a number of elements depend on the oxidation state of the element in solution. It has been common practice to treat aqueous solutions as if all redox couples within them were responding to the same oxidation potential - that is, following Garrels and Christ (1965), to write of the oxidation potential (Eh) of a solution, or following Stumm and Morgan (1981), to consider pE as a master solution variable. As more data on the concentrations of redox-sensitive species in ground waters become available, it is increasingly evident that it is not possible to describe solutions using a single oxidation potential to characterize all possible redox reactions (Lindberg and Runnells, 1984; Pearson, 1985).

The characteristics of the dominant species of an element in a given ground water will determine the extent to which the transport of that element may be retarded by geochemical processes. Many elements present in nuclear waste or of interest as potential tracers can exist in several oxidation states in ground waters. Their transport behavior might be quite different if they are in one state than if they are in another. Thus it is important to examine the oxidation states of certain elements in Culebra ground water to aid both in tracer selection and in the design of the tracer matrix solution.

The solubilities of both iron and uranium in ground waters are sensitive to oxidation state. Ferric, Fe (III), oxides and hydroxides are common iron-bearing phases in many aquifers. Only ferrous, Fe (II), species occur in measurable quantities in waters like those in the Culebra. Thus the concentration of iron in Culebra formation water could be controlled by such a reaction as:



The most common uranium-bearing phase is the U(IV) oxide UO_2 . Measurable uranium in solution, however, is dominated by the uranyl ion (UO_2^{+2}) in which uranium is present as U(VI). The uranium concentration in many ground waters appears to be controlled by the reaction:

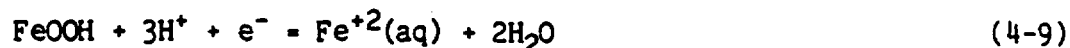


Oxidation potentials have been calculated for the H-3 Culebra samples of Table 4.1 under three assumptions:

- 1: That the analyzed dissolved uranium is in equilibrium with uraninite (UO_2);

- 2: That the analyzed dissolved iron is in equilibrium with goethite, (Fe OOH) and;
- 3: That the analyzed dissolved iron is in equilibrium with amorphous Fe(OH)₃.

The dissolution of goethite, for example, can be written:



with

$$\log K_{T(\text{goethite})} = \log a(\text{Fe}^{+2}(\text{aq})) + 2 \log a(\text{H}_2\text{O}) + 3 \text{pH} + \text{pE} \quad (4-10)$$

where $\text{pH} = -\log a(\text{H}^+)$ and $\text{pE} = -\log a(\text{e}^-)$. pE can readily be converted to Eh, in volts, as described in Section A.3.4 of the Appendix.

The results of these calculations are shown in Table 4.4. No uranium-bearing minerals were identified in the core analyses, although were any such minerals present they would be in such low concentrations that great care would be necessary to find them. The mineral goethite was identified in the claystone immediately overlying the Culebra dolomite. As shown in the Appendix, a wide range of thermodynamic properties are reported in the literature for minerals called goethite. Using the value chosen and the iron concentrations of the samples lead to calculated Eh values between -0.106 and -0.151 volts as shown in Table 4.4. These values, while more negative than the values calculated using uranium data for the same samples, are at least of the same order as the uranium values. This suggests that metals in solution in the Culebra can be treated as if they are responding to oxidation potentials in the range of +0.05 to -0.15 volts.

If the analyzed iron values do not represent those of the formation water, there will be additional uncertainty in the estimated Eh values. Lambert and Robinson (1984) report that the iron concentrations of samples from many WIPP wells decrease with pumping and suggest that the early higher iron values may have resulted from corrosion of iron well casings. Pearson (1985) has also found iron from this source in water samples taken from wells in northern Switzerland.

The dissolved iron contents of the three H-3 samples range from 0.05 to 0.57 mg/l (Table 4.1). This range is reflected in the 0.045 volt difference between the highest and lowest Eh value calculated for each iron mineral (Table 4.4). If the iron content of the formation water is an order of magnitude lower than the lowest sample measured, the calculated Eh values would be about 0.04 volts more positive, or roughly -0.06 and +0.05 volts for goethite and $\text{Fe}(\text{OH})_{3\text{am}}$, respectively. These values are still in the range of 0.05 to -0.15 volts estimated for the Culebra.

In making Eh calculations as done here, it has been assumed that solid-solution equilibrium has been reached. The size of the error, if any, introduced into the results by this assumption cannot be estimated.

4.4 Summary

From analyses of ground water and core samples collected from the Culebra from wells at the H-3 hydropad, the following conclusions can be drawn:

- The generally good agreement between the chemistry of water samples taken in 1977, 1984, and 1985 suggests that all represent the chemistry of Culebra formation water.

- The water-bearing zone of the Culebra is a gypsiferous dolomite, bounded by claystones dominated by mixed layer chlorite-smectite minerals and with goethite present as an additional iron-bearing phase.
- Calculations of the saturation indices of the water samples suggest that the formation water is in equilibrium with the minerals calcite, dolomite, gypsum, and celestite and has a pH of 7.3 to 7.4. The water chemistry therefore appears to be controlled by its host rock, a gypsiferous dolomite.
- The observed concentrations of iron and uranium in the water samples are consistent with the assumption of near-equilibrium with the minerals goethite or amorphous $\text{Fe}(\text{OH})_3$, and uraninite, respectively, at Eh values of between 0.05 and -0.15 volts.

5.0 PRELIMINARY DESIGN OF TRACER-TEST SOLUTION

The design of the tracer-test solution has had two objectives:

- that the tracer solution will not bring about geochemical changes in the aquifer system which would modify the natural transport properties of the system; and
- that the tracers used will breakthrough within the period of the test and be a source of information about the transport properties of the aquifer.

It is assumed that for the purposes of assessing expected behavior of the WIPP facility, that the results of mixing of Salado and Culebra brines can be investigated either in the laboratory or by calculations, and that during transport within the Culebra, the fluid chemistry will be, in general, dominated by the Culebra itself.

The first section of this chapter develops a design for a matrix fluid in which the tracers could be introduced and presents a recipe for its preparation. The second section discusses a number of reactive and conservative tracers which would be useful for characterizing the transport properties of Culebra within a test period of from two to five years.

5.1 Injection-Fluid Matrix Composition

The tracer fluid should have a composition which will not react with the formation, nor should mixtures of the tracer fluid with formation water react with the aquifer. Such reactions as mineral dissolution or precipitation could change the hydraulic properties of the formation during the course of the tracer test. More important, precipitating solids could remove tracer from the solution, leading to erroneously

high estimates of the extent of sorption in the system. Properties influencing the flow of the tracer fluid, such as its density and viscosity, should also mimic those of the native ground water. The design of an artificial solution which will be compatible with Culebra water at the H-3 hydropad is described in this section.

The procedure by which the tracer fluid is introduced into the formation is also important and is discussed below. The procedure adopted must minimize changes which might occur in the tracer solution due to exposure to the atmosphere or to foreign solids during handling prior to injection or during injection itself.

This section concludes with a description of how a solution simulating Culebra formation water could be produced. Artificial Culebra water should be used as a matrix for the introduction of tracers into the Culebra aquifer as well as in the laboratory for performing small-scale transport tests in Culebra material.

5.1.1 Design Constraints

The introduction of a foreign water into a formation may have several effects. If the water is under-saturated with respect to minerals in the formation or with respect to solids associated with the borehole, it may dissolve or otherwise react with them. Dissolution of solids will not have an important effect on tracer transport unless a sufficient mass is dissolved to modify the hydraulic properties of the system or unless reaction with or dissolution of one solid brings about precipitation of another.

Foreign water could also be over-saturated with respect to solids. If tracers co-precipitate with solids precipitating from such water, the tracers will be retarded. Even if the foreign water itself is not reactive with aquifer and borehole substances, it is necessary to

guard against the occurrence of mixtures between the foreign and formation waters which could dissolve or precipitate solid phases.

As shown in the previous chapter, Culebra formation water is in equilibrium with the carbonate minerals calcite and dolomite, and with the sulfate minerals gypsum and celestite. Reactions between ground water and carbonate and sulfate solids are rapid enough that they could influence water chemistry during a period of a few years, within the expected duration of the tracer test. Thus, a constraint on the tracer injection fluid is that it be non-reactive with respect to calcite, dolomite, gypsum, and celestite.

The tendency of a tracer solution to undergo oxidation or reduction reactions in the formation may have as much effect on tracer transport as dissolution or precipitation of major mineral phases. While it is relatively easy to design an injection solution which will minimize the possibility of precipitation or dissolution of major solids, it is not practically possible to control potential redox reactions except within rather broad limits. Thus, no attempt will be made to tightly constrain the redox state of the tracer solution.

Even if practical difficulties did not exist there are other reasons why there is no need to try to control the redox state of the tracer solution except within broad limits. First, as discussed in the preceding chapter, the field and laboratory data on the composition of formation water from the Culebra do not permit an unequivocal definition of the state of redox reactions in the system. Second, the necessity for close control of redox state can be avoided by choosing tracer substances which are insensitive to changes in redox state over relatively broad limits.

5.1.2 Constraints on Tracer-Injection Procedures

The tracer solution will be designed to be non-reactive with carbonate and sulfate minerals, and to have an oxidation state which is within a certain broad range. While such conditions can be achieved in the laboratory where the solution will be prepared, it is also necessary to design the procedures by which the solution is introduced into the formation so that conditions do not change during that introduction.

The saturation state of the solution with respect to carbonate minerals is a function of the partial pressure of CO_2 of solution. As Table 4.1 shows, the partial pressure of CO_2 in water from the Culebra is about $10^{-2.9}$ bars. This is higher than the partial pressure of CO_2 in the atmosphere, $10^{-3.5}$ bars, and so Culebra formation water, or water closely resembling it, will slowly lose CO_2 when exposed to the atmosphere. With this loss, the solution pH will rise and the solution will become over-saturated with respect to carbonate minerals. Thus, it is important to minimize the CO_2 loss from the fluid between the time it is first made up in a laboratory and the time it is introduced into the formation.

Tracers will be chosen which will be stable over a relatively broad range of redox states. However, it will be necessary to protect the injection solution from conditions which would drive redox conditions beyond the range in which the tracers are stable.

If the tracer solution receives more than momentary exposure to the atmosphere, it will dissolve atmospheric oxygen. This would have two effects. First, it would bring about strongly oxidizing conditions in the solution which could change the chemical behavior of certain tracers and affect their stability in the tracer solution itself or their transport properties in the aquifer. Second, if oxygenated tracer solution entered the aquifer and mixed with less oxidizing

formation water, redox-sensitive species dissolved in the formation water would be affected. If such oxygenation caused the precipitation of iron or manganese oxides or hydroxides, the transport behavior of all cationic tracers could be affected because these iron and manganese solids are strong sorbents. Thus, it will be important to minimize the exposure of the tracer solution to air to prevent both loss of CO₂ and dissolution of oxygen.

It will be necessary also to minimize the exposure of the tracer solution to any strongly reducing substances during its injection into the aquifer. The substance of this type to which the solution is most likely to be exposed is metallic iron, which may be present in materials used to construct the borehole or in the apparatus used to transmit the tracer solution from the surface through the borehole to the formation at depth. The corrosion of iron by ground water leads to the production of hydrogen gas and to high dissolved iron concentrations. High dissolved iron levels formed by corrosion caused by the injection solution could bring about precipitation of iron hydroxides in the formation as the tracer solution mixes with formation water. These highly sorbent iron hydroxides would tend to retard any cationic tracers being used and possibly restrict the hydraulics of the well and inhibit injection efficiency.

Hydrogen is a strong reducing agent, and if any were formed by corrosion of metal by the tracer solution, it could also influence the behavior of tracers in the injection fluid or after introduction to the aquifer itself. It will be important to design the tracer-injection procedure in a way that minimizes any contact between the tracer solution and metals with which that solution could react.

Since one (H-3b1) of the existing three wells at the H-3 hydrograd consists of perforated steel casing at the Culebra interval, it is assumed that one additional new hole will be drilled. The location of

the new hole should be chosen such that it intercepts the rapid-transport pathway between H-3b1 and H-3b3.

5.1.3 Preparation and Handling of Injection Matrix Fluid

Considerations for the preparation of tracer matrix solution summarized from the discussion above, are as follows:

- The solution should be closely similar in chemical composition and physical properties to the formation fluid.
- The solution should neither dissolve nor precipitate calcite, dolomite, gypsum, or celestite.
- The oxidation state of the solution should neither be as oxidizing as would be caused by the presence of dissolved oxygen nor as reducing as would be caused by the presence of metallic iron.

This section provides instruction on the formulation of a solution to meet these constraints.

The chemistry of water samples taken from the Culebra at the H-3 hydropad is discussed in the previous chapter and the analyses themselves are shown in Table 4.1. Based on the chemistry of the samples taken in 1984 and 1985, an estimate of Culebra formation water chemistry can be developed. This Culebra water chemistry is shown in Table 5.1. The following considerations went into its development.

- There are no systematic differences between the 1984 and 1985 analyses which would suggest that one is inherently more reliable than the other. Thus, the concentrations of most dissolved constituents were taken as the mean of the values reported for the two samples.

- A solution must maintain strict electrical neutrality, or charge balance. Charge balance was achieved by choosing the lower of the two reported chloride values and adjusting the sodium concentrations. The resulting sodium concentration is virtually the same as was measured in the 1985 sample.

Table 5.2 shows the saturation indices of several minerals and the total dissolved carbonate and $\log P_{CO_2}$ values for the Culebra formation fluid at two pH values: 7.3, the value reported for the 1985 sample (see Table 4.1); and 7.394, at which the water has a calcite saturation index of 0.00. The true pH of the Culebra formation water lies between 7.3 to 7.4. The total dissolved carbonate content is from 0.78 to 0.81 millimolal and the logarithm of P_{CO_2} (bars) is between -2.9 and -3.0.

The dissolved solids composition of the Culebra formation water of Table 5.1 has been restated as masses of anhydrous salts in Table 5.3. This provides a recipe by which artificial Culebra water can be produced for use as tracer injection matrix fluid or for laboratory experiments.

The procedure to make artificial Culebra water is as follows:

- Begin with high quality distilled or deionized water.
- Exclude dissolved atmospheric gases from this water by boiling or purging with an inert gas (nitrogen or argon) just prior to use, and store under inert gas.
- Dissolve the masses of reagent grade salts shown in Table 5.3 in the distilled water and bring the solution up to volume.
- Adjust the pH to between 7.3 and 7.4 with reagent grade, concentrated HCl or NaOH solution.
- Store the solution under a minimum volume of inert gas to avoid loss of CO_2 from the solution.

Table 5.4 compares the composition of the solution produced using this recipe with the composition of formation water in the Culebra at the H-3 hydropad as estimated above. The concentrations are expressed as molarity (moles per liter solution) rather than as molality (moles per kilogram water) and thus the numbers in the second column of Table 5.4 are not identical with the numbers in the third column of Table 5.1, though both refer to the same water. The only differences between the artificial water and the Culebra water will result from an inability to precisely add very small quantities of certain salts. As Table 5.3 shows, for example, only 0.2 mg of NaI are required per liter of solution. To match the iodide concentration of the artificial solution more closely to that of Culebra water would require that the amount of salt added be specified more precisely than to the nearest 0.1 mg.

5.2 Tracers and Tracer Concentrations

There are several practical considerations which should be considered during the process of selecting tracers and designing the tracer solutions. These will be described briefly here before beginning the more detailed discussion leading to recommendations for specific tracers.

Conservative as well as sorbing tracers will be required. Tests using conservative tracers have already been performed at the H-3 hydropad with results described in Kelley and Pickens (1986), and summarized in Chapter 3 above. Inclusion of conservative tracers in the tracer solution along with tracers likely to be retarded will establish the time when the breakthrough of non-retarded transport occurs, against which the retardation of the other tracers will be measured. In addition, interpretation of the conservative-tracer breakthroughs by the same techniques used for the test already completed will provide a second estimate of physical transport parameters in the system which can be compared to those deduced from the interpretation of the first test. For the sorbing tracer test, it is assumed that tracers will be

introduced into two or more wells. To distinguish breakthrough from each of them, different conservative tracers should be used in each well.

Prime considerations in the choice of sorbing tracers are that they will travel from the injection to the observation well during the time allotted for the test and that their concentrations at breakthrough will be measurable. Calculated tracer-breakthrough times and concentrations using SWIFT II for various values of partition coefficients are given in Table 3.4 (Section 3.3). The physical transport parameters used in these sensitivity calculations are based on the interpretation of the conservative tracer test already carried out at the H-3 hydropad and summarized in Chapter 3.

The sorbing tracer test is planned to last from two to five years. In order that some definition of the tail of the breakthrough curve is possible and to allow for uncertainties in the estimates of the transport parameters needed to design these tests, the test is designed for peak arrival times in the range of 1.5 to 2 years. Figures 5.1 and 5.2 are graphs of data given in Table 3.2, and show the peak arrival times calculated for various assumed partition coefficient values using the physical parameters calculated from the conservative tracer test already performed at the H-3 hydropad. Figure 5.1 is for transport along the flow path from well H-3b1 to H-3b3. As this figure shows, a partition coefficient of 50 leads to a peak arrival time of about two years. Figure 5.2 is for transport along the path from well H-3b2 to H-3b3. For peak arrival in two years or less along this flow path, tracers with partition coefficients of 2.5 or less are necessary.

Figures 5.3 and 5.4, which are also based on the data in Table 3.4, show the logarithms of the breakthrough peak concentrations in micrograms per liter plotted against the logarithm of the peak arrival time in years. The curves on Figure 5.3 are for the H-3b1 to H-3b3 flow path and on

Figure 5.4 are for the H-3b2 to H-3b3 flow path. It can be seen from both these figures that for a tracer input of 1 kg, the concentration of a peak arriving at two years will be about 10 micrograms per liter ($\mu\text{g/l}$).

The actual masses of tracer which it will be practical to introduce into the formation at the start of a test will be of the order of milligrams to grams rather than kilograms. Thus, the peak concentrations to be expected will be in the range of 10 nanograms per liter (ng/l) to 10 picograms per liter (pg/l). Radionuclides are a class of substances which can be analyzed at very low concentrations, and so they are the only tracers considered in this preliminary design report.

There are a number of regulatory constraints on the use of radioisotopes to protect the health of individuals carrying out the injection, sampling, and analytical operations, and the safety of the environment into which nuclides would be emplaced. Possible regulatory or procedural constraints on the selection or recommendation of tracers given below or on other aspects of test conduct, such as the disposal of the fluid withdrawn from the aquifer during the test, have not been considered in preparing this preliminary design report.

Several additional constraints on choosing tracers need to be considered. Only small proportions of the tracers injected will be recovered from the aquifer during the test. The rest will remain in the system and migrate with regional ground-water flow. If the tracers were radionuclides in the waste to be emplaced at WIPP, and if one of them appeared at a regional discharge point sometime in the future, it could be taken erroneously as evidence of the escape of waste from the repository. Thus isotopes which will be important in the waste itself would not be suitable tracers. On the other hand, if the tracers are chemically similar to the waste nuclides, the results of the tracer tests could provide support to site performance-assessment activities.

Therefore, substances which are chemically analogous with but not identical to important nuclides in the waste are desirable.

Finally, it is also important that the tracer solution not introduce into the formation any substances which could enhance the transport of waste nuclides, should any escape the repository. Chelating agents such as EDTA are often employed to stabilize tracers and prevent their retardation during transport. Such agents could also prevent retardation of waste nuclides and, therefore, should not be introduced into the aquifer.

5.2.1 Constraints on Tracer Concentrations

Tracer concentrations are constrained by the conditions both during their introduction into the aquifer and during their recovery at the pumping well. Conditions during injection tend to limit the maximum concentrations which are acceptable, while at recovery certain minimum concentrations are required. Specification of these conditions is important so they can be balanced during tracer selection to assure that the tracers chosen meet both sets of conditions.

Conditions limiting the maximum concentration of possible tracers in the injection fluid are that:

- the concentration should be low enough that the injection fluid is not significantly different physically or chemically from native ground water; and
- the concentration should be low enough to avoid oversaturation and the resulting precipitation of any tracer-bearing solid phases.

The concentration of tracer in the fluid recovered during the test must be high enough that the breakthrough curve can be defined to the required degree of precision given:

- the analytical sensitivity for the tracer;
- the dilution factor to be expected during transport; and
- radioactive decay during transport.

Both sorbing and conservative tracers should be present in the solutions injected. Breakthrough of the conservative tracer will serve as a reference against which retardation of the sorbing tracers will be measured. Furthermore, an interpretation of the conservative breakthrough curve similar to that made of the results of the test already carried out at the H-3 hydropad will allow evaluation of the reliability of the values of the physical transport parameters deduced from the interpretation of the earlier test (Kelley and Pickens, 1986). If new holes are drilled on the H-3 hydropad, physical solute-transport properties along the new flow paths during the test will be interpreted on the basis of the behavior of the conservative tracers. For convenience, and to permit standardization of sampling and analytical procedures, conservative and sorbing tracers should be of the same type - that is, they should all be radioisotopes, substances to be analyzed by neutron activation, etc. The discussion of the selection of conservative tracers will follow the discussion of sorbing tracers.

5.2.2 Sorbing Tracer Selection

5.2.2.1 Projected Waste Elements

To make the tracer test results most useful in support of site performance-assessment activities, the selection of sorbing tracers was begun by considering elements likely to be important in the waste. The transport behavior of all isotopes of a given element will be the same. Considering radioisotopes as tracers leads to the possibility of choosing almost perfect surrogates for waste elements by using radioisotopes not present in the waste to represent other isotopes of the same elements which are present in the waste.

The compositions of wastes intended for the WIPP facility are summarized in Tables A-7 (Contact Handled (CH) TRU waste) and A-8 (Remote Handled (RH) TRU waste) of U.S. Department of Energy (1985). The isotopes listed in Tables 5.5 and 5.6 of this report were developed from these tables. Table 5.6 includes all transuranic isotopes occurring in either the (CH) or the (RH) waste and Table 5.5 includes fission products which have half-lives of greater than 10 years. The group of fission products in an average canister greater than 50 years old which will be present in quantities greater than 10 millicuries (mCi) is the same as the group listed in Table 5.5

Fission-product nuclides are shown in Table 5.5. They include three lanthanides: ^{151}Sm , ^{152}Eu , and ^{154}Eu . As discussed below, lanthanide partition coefficients are likely to be very high - of the order of 10,000 or greater. Thus, lanthanides could not move the full distance from the injection to the pumping well during the course of the test and so would not be tracers for which breakthrough curves could be measured.

The other three fission-product nuclides, ^{63}Ni , ^{90}Sr and ^{137}Cs , are expected to have partition coefficients of less than 50. Thus, other nuclides of these three elements might be suitable as tracers if they can be injected in sufficient masses to have detectable concentrations at breakthrough.

Nuclides of actinide elements of possible importance in the projected WIPP waste inventory are shown in Table 5.6. Of the six actinides listed only uranium, neptunium, and possibly plutonium have partition coefficients low enough that other isotopes of these elements could be considered as tracers.

5.2.2.2 Partition Coefficients

Estimates of partition coefficients are crucial to the selection of tracers to be used. The partition coefficient is a lumped parameter which includes all processes which can change the ratios of the concentration of tracer in solution to its mass stationary in the aquifer. The processes include precipitation or co-precipitation in solids, congruent or incongruent dissolution of solids, ion exchange and sorption. A first step in refining estimates of partition coefficients is to design the test so that some of the processes will be unimportant. The tracer solution suggested here should not precipitate solids and the tracers chosen will not be substances which could dissolve from the aquifer or from borehole construction material. Thus, the processes setting the partition coefficient will be restricted to ion exchange and sorption.

A number of measurements have been reported on the ability of material from cores of the Culebra to exchange with and (or) sorb various nuclides from solution (Serne et al., 1977; Dosch and Lynch, 1978; Lynch and Dosch, 1980; Dosch, 1981). Several solutions have been used for these measurements because the extent of both exchange and sorption are strongly influenced by the composition of the carrier solution used when they are measured (Wahlberg and Fishman, 1962; Wahlberg et al., 1965; Wahlberg and Dewar, 1965). The composition of these solutions must be considered in deciding which of the measured sorption coefficient values might be appropriate for the Culebra in the presence of water of the type found at the H-3 hydropad.

Table 5.7 shows the composition of six waters. Those labeled Brine "A", Brine "B", Culebra water, and Solution "C" have been used for the measurement of distribution coefficient (K_d) values on material taken from cores taken from the Culebra. As noted in Section 4.0,

the distribution coefficient is the same as the partition coefficient if it is assumed that the mass fixed on the solid is directly proportional to its concentration in solutions. The values for the distribution coefficients are often reported in ml/g. The composition of Culebra formation water at the H-3 hydropad and of the "WIPP" water used by Cleveland et al. (1985) in studying actinide speciation are also given in Table 5.7. The total dissolved solid contents of the solutions used in determining Kd's range from over 300,000 mg/l to less than 3,000 mg/l, while that of the H-3 Culebra water has about 55,000 mg/l total dissolved solids. Kd values, whether from ion exchange, sorption, or both, tend to vary inversely with total solution concentration (Wahlberg and Fishman, 1966; Wahlberg et al., 1965). The Kd values appropriate for the Culebra at the H-3 hydropad should thus be higher than those measured for Brines "A" and "B", but lower than those measured for Solution "C" and Culebra water.

Saturation indices, total dissolved carbonate concentrations, and values of CO₂ partial pressures are also given for four of the six waters in Table 5.7. No calculations were made for either of the brines, because their concentrations are beyond the range of validity of the aqueous model used. The Culebra water (with pH = 7.5 as given by Dosch, 1981, rather than pH = 8.4 as given by Lynch and Dosch, 1980) has calcite and gypsum saturation indices which are virtually zero but a negative dolomite saturation index. The calculated log P_{CO₂} of this water is -2.8 and its total carbonate is 1.0 millimolal. It is similar to the H-3 Culebra water except for its lower salinity.

Solution "C" and "WIPP" waters have gypsum and celestite saturation indices which are virtually zero, but positive calcite and dolomite saturation indices. The "WIPP" water has a higher pH and lower P_{CO₂} than the other three low salinity waters in the table. A loss of

CO₂ corresponding to a partial pressure change from 10^{-2.8} to 10^{-3.2} bars would raise the pH of the sample from 7.5 to 7.9, its calcite saturation index from 0 to 0.4, and its dolomite saturation index from 0.2 to 1.0.

The alkalinity of Solution "C" is considerably higher than that of the other three low-salinity waters in this table. If the alkalinity is high by a factor of 2, it would cause the calcite saturation index to be high by a factor 0.3, and the dolomite saturation index to be high by a factor of 0.6.

Distribution coefficients reported for a number of nuclides on Culebra core material are given in Table 5.8. The estimated partition coefficients given in Tables 5.5 and 5.6 are based on these values. The tracer solution is designed so that no precipitation of solids will occur. Thus, the tracer behavior of these substances should be influenced only by ion exchange and/or sorption, and should be well characterized by these distribution coefficients.

The distribution coefficients for cesium measured by Serne et al. (1977) and by Dosch and Lynch (1978) are similar, and range from values of less than 1 to 2 ml/g in the brines to values from 7 to 16 ml/g in the dilute Solution "C". Wahlberg and Fishman (1962) measured the adsorption of cesium on several clay minerals from solutions of various NaCl concentrations. The K_d values in their system are proportional to the reciprocal of the sodium concentration. If the same proportionality holds for cesium in the Culebra, the K_d for cesium in H-3 water should range from 2 to 5 ml/g based on the sodium contents of the waters in which Serne et al., and Dosch and Lynch measured their K_d values.

Lynch and Dosch (1980) report Kd measurements for cesium between 9 and 68 ml/g in their Culebra water. Their water contained no matrix cesium while that used by Serne et al., and by Dosch and Lynch contained 1 ml/g of cesium in addition to the tracer used. The H-3 Culebra water contains less than 0.007 mg cesium/l (Table 4.1) and therefore its Kd for cesium may be closer to that measured by Lynch and Dosch than to values measured by the other investigators. For conservatism in the tracer test design, a distribution coefficient of less than 50 ml/g is estimated for cesium in Table 5.5.

Several sets of reported values for distribution coefficients for strontium are also shown in Table 5.8. Those measured by Dosch and Lynch (1978) vary from less than 1 to 2 ml/g in the brines to 4 to 5 ml/g in the dilute Solution "C". Serne et al. (1977) report similar but slightly lower values, while Lynch and Dosch (1980) report values of 0.3 to 0.6 ml/g in their Culebra water. These relatively low Kd values can be attributed to the fact that there is a relatively high common strontium content to these waters and that 13% of the dissolved strontium is present as the uncharged ion pair SrSO_4^0 (Table 5.9). For conservative tracer test design a distribution coefficient for strontium of less than 2 ml/g has been estimated in Table 5.5.

The distribution coefficient for europium found by all investigators is of the order of 10,000 ml/g or greater. This element is probably present in solution as the +3 ion and thus could be strongly sorbed or exchanged, as this very high distribution coefficient would suggest. It is also possible that the solubility limit for this element was exceeded in the experiments performed, and that the high distribution coefficient is simply a result of precipitation of some solid europium phase. In any case, europium, or any similar lanthanide such as samarium, is likely to be retarded too strongly to be of interest as a tracer in this test.

One set of distribution coefficients for iodide have been reported, and all coefficients are less than 1 ml/g in all solutions. Iodide is an anion and present in the native ground water in greater than trace concentrations. Thus it should sorb only weakly, if at all, and should be suitable for consideration as a conservative tracer.

Uranium distribution coefficients range from 0 to 27 ml/g in the brines and from 0 to 69 ml/g in the dilute solutions. In the H-3 formation water, uranium is present dominantly in the VI oxidation state as one of several negatively charged uranyl carbonate solution complexes. Under these conditions it is likely to be only weakly sorbed and thus its estimated partition coefficient in Table 5.6 is shown as less than 10 ml/g.

The neptunium distribution coefficients ranged from 6 to 12 ml/g in both the brine and the dilute solution in which they were measured. The aqueous speciation of neptunium is not as well known as that of uranium but it is likely that neptunium is present in the V oxidation state, and may also be present as an anionic solution complex. Its partition coefficient is estimated in Table 5.6 for H-3 Culebra water as less than 20 ml/g.

Distribution coefficients for plutonium range from less than 500 to over 7,000 ml/g in both brines and fresh waters. If plutonium is present in solution in the III oxidation state, a high distribution coefficient like that observed for europium is not surprising. However, Cleveland et al. (1985) suggest that plutonium may be present in Culebra water in the oxidized V and VI states. In these oxidation states, plutonium may have a distribution coefficient of the order of those measured for uranium VI or estimated for neptunium V. Because of this possibility and of the importance of all new data on plutonium transport, it would be of great interest to include plutonium in the suite of tracers used, with the under-

standing that it might not break through. Thus, in Table 5.6, a partition coefficient is estimated as low as 50 ml/g for plutonium in the V and VI states. Plutonium in the III state, on the other hand, would have a much higher estimated partition coefficient.

The distribution coefficients for americium and curium range from several hundred to several thousand ml/g. These elements, like europium, will be present in the III oxidation state and so relatively high distribution coefficients for them are not surprising. Values of greater than 1,000 ml/g for americium and curium are estimated in Table 5.6. Values for both elements are high enough that neither need be considered further as possible tracers for this test.

Distribution-coefficient values have not been reported for nickel, but from the chemical properties and solution behavior of this element it is possible to estimate a Kd value appropriate for nickel in this system. Under the redox conditions prevailing in the H-3 Culebra water, dissolved nickel will be present in the II valence state. The ion size of Ni(II) is 0.72 Angstrom Units (AU), while that of Fe(II) is 0.76 AU. Because of their similar charge densities, both ions should exhibit similar solution behavior.

Table 5.9 shows the dominant solution species of several divalent cations in H-3 Culebra water. Iron, which most closely resembles nickel, is present 90% as Fe^{+2} ion and 10% as the $FeSO_4^0$ ion pair. The other divalent ions shown have similar distributions of species, although their ion sizes differ from that of iron much more than does the size of the nickel ion.

As mentioned above, the distribution coefficient for strontium appears to be 2 ml/g or less in H-3 Culebra water. Although the charge and solution species behavior of nickel are similar to those

of strontium, its ion size is smaller so that its Kd value is likely to be larger than that for strontium. For purposes of test design, a value of 50 ml/g has been estimated for nickel and is given in Table 5.5. No assertion is made that this is a particularly accurate estimate, only that the Kd of nickel is likely to be small enough that it could be a useful tracer in this test.

5.2.2.3 Tracer Nuclides

The elements nickel, strontium, cesium, uranium, neptunium, and plutonium have been identified as being possibly suitable sorbing tracers for an H-3 Culebra test because:

- they have partition coefficient values low enough that they are likely to breakthrough within a two to five year test, and;
- they are elements of relatively long-lived nuclides in the projected WIPP waste.

It now remains to examine possible tracer radionuclides of these elements to determine whether any exist which could be injected into the solution in a reasonable total volume and remain detectable after a transport time of several years.

A nominal peak arrival time of two years has been selected. As Figures 5.3 and 5.4 show, for 1 kilogram of tracer injected, a concentration of 10 µg/l is to be expected after two years for flow along either the H-3b1 to H-3b3 or H-3b2 to H-3b3 flow paths. The dilution factor to be considered is therefore:

$$10 \text{ } \mu\text{g/l/kg} = 1 \times 10^{-8} \text{ mass per liter out per mass in .} \quad (5-1)$$

The analytical detection limit for many radionuclides quoted by a number of laboratories is about one picocurie per liter (pCi/l). As

mentioned above, it will be desirable to be able to detect the tracers at concentrations as low as 1% of their anticipated peak concentrations. Thus, a peak concentration of 100 pCi/l is taken as the nominal design value. To achieve this concentration given the above dilution factor will require a tracer input of 10 mCi of a tracer which will not decay significantly during the two-year period of the test.

The half-lives of many possible tracers are likely to be short enough that decay during the two year transport period will significantly affect their concentration in the ground water. This decay must be included in the calculations made to determine the amount of tracer to be added initially. The amount lost by radioactive decay will equal

$$\text{Decay} = e^{-\lambda t} \quad (5-2)$$

where $\lambda = \ln 2 / t_{1/2}$
 t = decay time
 $t_{1/2}$ = half-life

For this test, with decay time equal to the nominal peak arrival time of 2 years,

$$\text{Decay} = e^{-1.386/t_{1/2}} \text{ (years)}. \quad (5-3)$$

Combining this expression with the dilution factor above gives the following equation for calculating the tracer input required to yield a 100 pCi/l peak concentration at 2 years.

$$\text{Input (Ci)} = 0.01 / e^{-1.386/t_{1/2}} \text{ (yr)}. \quad (5-4)$$

Table 5.10 lists the elements identified as possible sorbing tracers and their solubilities. A list of isotopes of each element is given which includes the isotope present in the projected waste, from Tables 5.5 and 5.6, along with other nuclides possibly suitable as tracers. The last three columns express in several units the amount of the various nuclides which would have to be injected to reach a peak concentration of 100 pCi/l at two years at the pumping well.

This calculation does not consider what the actual peak arrival time for each tracer is likely to be, but treats them all as if they were to be retarded by the same amount. Tracers with peak arrival times shorter than two years will have peak concentrations greater than 100 pCi/l, while those with longer peak arrival times will have lower peak concentrations. The uncertainties in the estimates of partition-coefficient values are so great that only false precision would be achieved by making this calculation using different peak arrival times for the various nuclides.

The total input masses required, expressed as curies, are calculated from the nuclide half-life as described above. The total masses required in moles are calculated using:

$$\begin{aligned} \text{moles} = \text{curies} \times 3.7 \times 10^{10} \frac{\text{disintegration}}{\text{second-curie}} \times \frac{t_{1/2} \text{ (years)} \text{ atom-year}}{\ln 2 \text{ disintegration}} \\ \times 3.156 \times 10^7 \frac{\text{seconds}}{\text{years}} \times \frac{1}{6.023 \times 10^{23}} \frac{\text{mole}}{\text{atoms}} \end{aligned} \quad (5-5)$$

$$\text{moles} = \text{curies} \times t_{1/2} \text{ (years)} \times 2.80 \times 10^{-6} \quad (5-6)$$

The volume of tracer which must be injected equals the total number of moles of tracer required divided by the solubility of the tracer element. This quantity is given for each nuclide in the last column of Table 5.10.

Some general comments on the selection of suitable tracer nuclides for a given element are appropriate before beginning an element by element discussion of Table 5.10. Several attributes of nuclides are useful to rank their suitability as tracers for a given element. These include the half-life of the element, its analytical sensitivity, and its availability and cost.

Analytical sensitivity is not considered in the following discussion, except for the assumption made above that 1 pCi/l is a reasonable average detection limit. Nuclide availability is considered below only to the extent that the catalog of Isotope Products and Services of Oak Ridge National Laboratory (1985) was examined and the presence or absence of a nuclide in that catalog is noted. In selecting tracers as part of a final design for a sorbing tracer test, analytical sensitivity, availability, and cost need to be examined closely.

The half-life of a nuclide determines the initial number of curies which must be injected. From the standpoint of the safety of the injection and tracer nuclide cost, the fact that fewer curies of long-lived nuclides are required than of short-lived ones makes the former preferable. On the other hand, the longer the half-life of a nuclide, the larger its initial mass must be to achieve the number of curies required in the injection solution. The tracer concentration cannot exceed the solubility of the element in the matrix solution without there being danger of precipitation of the nuclide leading to a false high apparent retardation of the element in the system. Thus, if a large number of moles of a nuclide are required because of its long half-life, the volume of tracer solution which must be injected may become too large to be reasonable.

The elements in Table 5.10 fall into two groups, those which represent fission products in the waste and those which are actinides.

In general, the fission-product elements are more soluble than the actinides and nuclides available as tracers for them have half-lives ranging from days to years. Thus, the initial number of curies of these nuclides required could be of the order of tens or hundreds, but the volume of tracer solution required to inject them is quite small.

The actinides, on the other hand, are considerably less soluble than the fission-product elements, and tend to have only long-lived nuclides available as potential tracers. Thus, while the total curies of actinide tracers required is relatively small, the number of moles is larger than required for fission products, and the number of liters of tracer solution required for injection may be of the order of hundreds or more. These generalities are supported by the following discussion of the individual elements.

Two strontium isotopes exist which would make suitable tracers: ^{85}Sr with a 64-day half-life and ^{89}Sr with a 52-day half-life. Both isotopes appear in the Oak Ridge (1985) catalog and are among the isotopes routinely analyzed by several commercial laboratories. Because of their relatively short half-lives, tens to hundreds of curies of either would be required in the injection solution, which would be expensive. However, the tracer-solution concentrations could be high enough that injection volumes of less than 1 liter would be required. The distribution coefficient of strontium is low enough that the element would be a suitable tracer along either the H-3b1 to H-3b3 or H-3b2 to H-3b3 flow paths. ^{90}Sr would be an attractive tracer because its relatively long half-life minimizes the initial number of curies required in the injection solution and the isotope is readily available commercially. If its presence in the projected waste to be stored at the WIPP site would not be an objection to its use as a tracer, it should be strongly considered.

Only one isotope of cesium, ^{134}Cs , exists with a half-life suitable for use as a tracer. This isotope is attractive in that only a few millicuries would be required in the injection solution. However, it does not appear in the Oak Ridge (1985) catalog and may not be readily available. ^{137}Cs also would be a good tracer if its presence in the projected WIPP waste did not make its use as a tracer objectionable. Cesium is likely to have a relatively high distribution coefficient and therefore would be suitable as a tracer only along the H-3b1 to H-3b3 flow path.

The only nickel isotope of suitable half-life is ^{63}Ni . Only a few millicuries of this isotope would be required in the injection solution so it would be suitable as a tracer if its presence in the projected WIPP waste did not make its use as a tracer objectionable. If it were necessary to use nuclides which were not present in the projected waste, isotopes of cobalt would be suitable. The chemical properties of cobalt are so closely similar to those of nickel that it should have similar transport behavior. Two suitable cobalt isotopes are available, ^{58}Co with a half-life of 71.3 days and ^{60}Co with a 5.26-year half-life. ^{60}Co appears in the Oak Ridge (1985) catalog and only a few millicuries would be required in the injection solution. Because of the relatively high distribution coefficients estimated for nickel, either nickel or cobalt would be suitable only for a tracer along the H-3b1 to H-3b3 flow path.

Two uranium nuclides, ^{230}U and ^{232}U , are listed in Table 5.10 along with ^{233}U which is a component of projected WIPP waste. The half-life of ^{230}U , 20.8 days, is so short that it would require an unreasonably large number of curies in the input solution. The half-life of ^{232}U , 73.6 years, is long enough that decay does not seriously affect the number of input curies required (10.2 mCi are required as opposed to 10.0 mCi of a stable or very long half-life tracer). However, the solubility of uranium is so low that nearly

700 liters of tracer solution would be required. No uranium isotope exists with half-life between those of ^{230}U and ^{232}U so the uranium isotope of choice would be ^{232}U in spite of the large tracer volume required.

The estimated partition coefficient for uranium is less than 10 ml/g. Errors associated with these estimates of partition coefficients are large enough that it is not certain that uranium would not break through if used as a tracer along the slower H-3b2 to H-3b3 flow path. To assure tracer breakthrough, however, it would be best if uranium were used only as a tracer on the faster H-3b1 to H-3b3 flow path.

The only isotope of neptunium with a half-life which makes it remotely suitable for use as a sorbing tracer in a test of this type is ^{235}Np with a half-life of 410 days. Only 34 mCi of this isotope would be required in the input solution, but because of the very low solubility of this element, nearly 400 liters of tracer solution would be required. The partition coefficient of neptunium is estimated to be 20 ml/g or less, so it should be used as a tracer only along the H-3b1 to H-3b3 flow path. ^{235}Np does not appear in the Oak Ridge catalog.

Of the plutonium isotopes only ^{236}Pu and ^{241}Pu with half-lives of 2.85 and 13.2 years, respectively, can be considered as possible tracer nuclides. Because of the low solubility of plutonium, about 320 liters of tracer solution would be required if ^{236}Pu were chosen, and about 1000 liters if ^{241}Pu were selected. Both of these isotopes appear in the Oak Ridge catalog. However, both also are present in the projected WIPP waste inventory.

For plutonium to break through at all during this test, the assumption that it will be present in the Culebra water in the oxidized V

and VI state must be correct. Even under these conditions it may well have a partition coefficient of the order of 50 ml/g or more, and so could break through only along the H-3b1 to H-3b3 flow path.

The possible sorbing-tracer isotopes input masses and injection volumes required are summarized in Table 5.10. The selection of recommended tracers from this list should be conducted for the final design report after analytical sensitivities, analytical problems, isotope availability, isotope cost, health and safety requirements, and final tracer-test operational design have been evaluated.

5.2.3 Conservative Tracer Selection

Several radionuclides are commonly used as conservative ground-water tracers. These include ^3H , or tritium, which is introduced as part of the water molecule itself, and the dissolved halogen ions bromide and iodide (Moser and Rauert, 1980; Table 1). Laboratory measurements of the distribution coefficients of iodide with Culebra core material given in Table 5.8 support its use as a conservative tracer. Both bromide and iodide are present in the native Culebra water (Table 5.1) and in the suggested tracer matrix solution (Table 5.4).

The peak breakthrough of conservative tracers should occur at approximately 3.5 days along the H-3b1 to H-3b3 flow path and 26.3 days along the H-3b2 to H-3b3 flow path (Table 3.4). Thus, the quantities of conservative tracer required will be much less than those required for sorbing tracers, because there will be less dilution and decay of the conservative tracers than of the sorbing tracers.

The dilution factors for the conservative tracers can be derived from data in Table 3.4, following the procedure used to calculate dilution factors for the sorbing tracers in Section 5.2.2.3 above. For the H-3b1 to H-3b3 pathway dilution will be 3×10^{-6} and for the H-3b2 to

H-3b3 pathway it will be 3.5×10^{-7} . For a peak concentration of 100 pCi/l, inputs of 0.033 mCi and 0.29 mCi of stable tracer, respectively, would be required for the two paths.

The decay factor for the H-3b1 to H-3b3 path for a 3.5-day peak arrival time is:

$$e^{-2.426/t} \lambda_2 \text{ (days)} \quad (5-7)$$

and for H-3b2 to H-3b3 pathway with a 26.3-day peak arrival time:

$$e^{-18.23/t} \lambda_2 \text{ (days)} \quad (5-8)$$

The overall expressions for the input required for a conservative tracer along the H-3b1 to H-3b3 flow path are:

$$\text{Input (mCi)} = 0.033/e^{-2.426/t} \lambda_2 \text{ (days)} \quad (5-9)$$

and for the Hb2-b3 flow path:

$$\text{Input (mCi)} = 0.29/e^{-18.23/t} \lambda_2 \text{ (days)} \quad (5-10)$$

^3H has a half-life of 12.26 years. The nuclides of bromide and iodide commonly used as conservative tracers are ^{82}Br with a 1.48-day half-life and ^{131}I with an 8.07-day half-life.

Table 5.11 shows the concentrations of ^3H , ^{82}Br and ^{131}I , which would be required if they were to be used as conservative tracers on each of the two flow paths. The concentrations are given in millicuries and millimoles rather than in curies and moles as they were in Table 5.10. The last column in Table 5.11 shows the molality of the elements in the Culebra water at the H-3 hydropad. Hydrogen is part of the water molecule itself and so has a very high concentration (110 molal). The

bromide and iodide concentrations are those given in Table 5.1. As the table shows, the concentrations of tracer isotopes required for their use in this test are far below the ambient concentrations of the elements in H-3 Culebra water.

6.0 FURTHER REQUIREMENTS BEFORE FIELDING TEST

Prior to fielding of the sorbing tracer test, it is recommended that a detailed design/scoping report on the sorbing tracer test be completed. This report would contain:

- Re-evaluation of the objectives of the sorbing tracer test and a discussion of how these can best be addressed from both scientific, technical, and cost perspectives.
- Development and evaluation of a matrix of transport processes relevant to performance assessment at the WIPP site. The evaluation of all processes affecting transport at the WIPP site would enhance the integration of the site-characterization and performance-assessment activities. The evaluations pertaining to sorption mechanisms will include consideration of: effect of the presence of native or introduced organics; effect of molality of Culebra waters; importance of different fracture and matrix minerals; and properties of chosen radionuclide species. Specific recommendations will be developed on a design for the sorbing tracer tests that will result in a data base directly related to performance-assessment needs.
- Final selection of recommended conservative and sorbing tracers.
- Selection of operating conditions for the test (e.g., well configurations, pumping rates, etc.).
- Drilling, development, and hydraulic testing of one or more additional wells in the Culebra at the H-3 hydropad.
- Evaluations and integration of the data base obtained from the laboratory experimental program.

- Conducting detailed design calculations (similar to the approach of Chapter 3) using the best estimates of the tracer properties, the characteristics of the Culebra, and the tracer-test design operating conditions.
- Assessment of needs for additional mineralogical studies and laboratory tests on tracer/rock interactions.
- Development of a detailed work plan encompassing all site-preparation work, instrumentation required, test procedures, test schedule, staffing requirements for conducting the test, analytical techniques for tracer detection, and analytical/modeling requirements for data interpretation.
- Design, acquisition, installation and testing of all instrumentation required for the test. The details on the field instrumentation required will include items such as the on-site plumbing and packer systems, pumps, pumping-monitoring systems, and tracer-injection and tracer-monitoring systems.
- Development of the test schedule including such features as: site-preparation time; pre-test checking of plumbing, packers, and tracer-injection and tracer-monitoring systems; equipment-maintenance requirements; data-acquisition, handling, storage- and retrieval-system requirements; sampling and analysis frequency; transportation and disposal requirements for the pumped water; demobilization; data-interpretation requirements; and reporting requirements (progress and final reports).
- Development of quality-assurance procedures for addressing all aspects of conducting and interpreting the test.

- Evaluation of health and safety requirements for use of the selected tracers.
- Determination of, and compliance, with all regulatory requirements for conducting the test (e.g., necessary permits for use of selected tracers and for transportation and disposal of the pumped water).

7.0 SUMMARY AND CONCLUSIONS

Conducting field tests using sorbing tracers is one means of improving knowledge of the nuclide transport properties at one location in the Culebra dolomite at the WIPP site. To assist in the preparation for such a tracer test, data evaluation and preliminary design calculations were conducted for estimation of the range of values for the principal parameters governing solute transport and for identification and initial evaluation of potential tracers. This report presents the initial steps in preparing for a sorbing tracer test at the WIPP site and includes: (a) the selection of the best location for the first test at the WIPP site; (b) an evaluation of a conservative tracer test at the recommended site to provide estimates of the physical solute-transport parameters; (c) a hydrogeochemical and mineralogic characterization of the Culebra dolomite; (d) the rationale and recipe for the tracer-injection solution; (e) the compilation of a list of potential sorbing and conservative tracers; and (f) the identification of other needs before fielding the sorbing tracer test. The thermodynamic data base used to support the geochemical model (PHREEQE) used in this study is presented in an Appendix.

The general site selection criteria utilized in identifying the preferred location for conducting a sorbing tracer test are: (a) the site should be characterized with respect to its hydraulic characteristics; (b) the site should be characterized with respect to its physical solute-transport characteristics using conservative tracers; (c) the geochemistry of Culebra formation water at the site should be well characterized; (d) the site should be located on a potential flow path (under natural groundwater flow conditions) in the Culebra in the event of a repository breach; (e) the sorbing tracer test should have an operational period of two to five years; and (f) the site should be located to permit geochemical extrapolation of the reactive solute-transport results to as large a region as practical at the WIPP site.

In terms of meeting the general site-selection criteria, the H-3 hydropad is considered to be the optimum location for conducting the first tracer test. The H-3 hydropad exhibits suitable physical transport characteristics and also offers the advantage of presently having the most complete and extensive description of the ground-water flow and solute-transport characteristics as a result of hydraulic-test and tracer-test interpretations that have been conducted. The breakthrough times observed for the conservative tracer test at the H-3 hydropad indicate that the operational-time requirement for the sorbing tracer test can likely be attained. Geochemical characterization of this site is also possible because of the availability of recent water samples and the fact that the salinity of Culebra water there is within a range which can be modeled with available techniques. Lastly, the H-3 hydropad is closest to the center of the WIPP site and on a likely flow path from the site under natural flow conditions.

The H-3 hydropad complex consists of three wells arranged in an equilateral triangle with approximate 30 m sides. Each well is completed either open-hole or through perforated casing to the Culebra, which is about seven meters in thickness. Interpretation of a convergent-flow tracer test, performed at the H-3 hydropad in 1984 using two conservative organic tracers, meta-trifluoromethylbenzoate (m-TFMB) and pentafluorobenzoate (PFB), has yielded the following physical solute-transport characteristics: longitudinal dispersivity of 1.5 to 3 m, a fracture porosity of 1.9×10^{-3} , and effective matrix-block sizes ranging from 0.25 to 2.0 m. During this test, H-3b3 was the pumping well and tracers were introduced into wells H-3b1 and H-3b2. Using the above estimates, coupled with a laboratory-measured matrix porosity of 0.2, estimated tortuosities of 0.15 to 0.45, and free-water diffusion coefficients of 7.4×10^{-6} cm²/s (m-TFMB) and 7.2×10^{-6} cm²/s (PFB), the breakthrough curves for the two tracers were simulated using the flow and solute-transport code SWIFT II.

Design simulations for the sorbing tracer test were conducted assuming an injection of one kilogram of generic tracer and applying a range of

partition coefficients of 0.1 to 50.0 ml/g for the flow path with the higher transport rate (H-3b1 to H-3b3) and 0.1 to 10.0 ml/g for the flow path with the lower transport rate (H-3b2 to H-3b3) at the H-3 hydropad. The results of these simulations were utilized to assist in the compilation of a list of potential sorbing tracers that would break through within the two- to five-year period planned for the test.

From analyses of ground water and core samples collected from the Culebra from wells at the H-3 hydropad, the following conclusions can be drawn: (a) the generally good agreement between the chemistry of water samples taken in 1977, 1984, and 1985 suggests that all represent the chemistry of Culebra formation water; (b) the Culebra is a gypsiferous dolomite, bounded by claystones dominated by mixed-layer chlorite-smectite minerals and with goethite present as an additional iron-bearing phase; (c) calculations of the saturation indices of the water samples suggest that the formation water is in equilibrium with the minerals calcite, dolomite, gypsum, and celestite and has a pH of 7.3 to 7.4. The water chemistry, therefore, appears to be controlled by its host rock, a gypsiferous dolomite; and (d) the observed concentrations of iron and uranium in the water samples are consistent with the assumption of near-equilibrium with the minerals goethite or amorphous $\text{Fe}(\text{OH})_3$, and uraninite, respectively, at Eh values of between 0.05 and -0.15 volts.

Geochemical analysis of the Culebra formation water led to the development of a recipe for the solution into which the tracer will be mixed prior to injection. The composition of the tracer solution is such that it should mimic the properties of the natural formation water and neither alter the chemistry of the matrix or formation water of the Culebra, nor cause the tracer to precipitate or to become unstable under the existing redox conditions in the Culebra.

In considering sorbing and conservative tracers for the planned test at H-3, it was necessary to consider geochemical constraints on the injected tracers. The tracers must be able to be injected at concentrations low

enough to not significantly alter the injection fluid or to provoke any reaction which could cause precipitation of the tracer before or during injection. The concentration should be high enough to define the breakthrough curve while being relatively easy to analyze. The sorbing and conservative tracers should be compatible. Radionuclide tracers are considered to be the most appropriate tracers because they require low mass input, while still being extremely sensitive to detection, and they should mimic the transport characteristics of the projected waste inventory.

Radionuclide tracers most suitable for use as a sorbing tracer are either fission-products or actinides. Nuclides of nickel, cobalt, strontium, uranium, neptunium, and plutonium were reviewed for suitability as possible sorbing tracers because they have partition coefficients low enough to achieve breakthrough in a two- to five-year test, and they are elements with long-lived nuclides in the projected WIPP waste inventory. Based on their half-lives, the nuclides ^{63}Ni , ^{58}Co , ^{60}Co , ^{85}Sr , ^{89}Sr , ^{90}Sr , ^{232}U , ^{235}Np , ^{236}Pu , and ^{241}Pu are recommended for further consideration. One important consideration will be the presence of certain fission-products, such as ^{90}Sr , in the probable waste inventory, and whether objections might be raised over the use of such nuclides for testing. In order to provide data for interpretation of the physical solute-transport parameters along the flow paths between the wells (also, to provide a comparison to parameters from the previously-conducted conservative tracer test), conservative tracers should accompany the selected sorbing tracers. The most likely candidates are ^3H (tritium), ^{82}Br , and ^{131}I .

Prior to fielding a sorbing tracer test, a final detailed design report will be completed. This report will describe final tracer selection, detailed design calculations, site preparation, instrumentation requirements, staffing requirements, review of safety, health, and regulatory requirements and procedures, and determination of the optimum operational conditions for the test.

8.0 REFERENCES

- Baes, C.F. and R.F., Mesmer, 1976. The Hydrolysis of Cations. John Wiley and Sons, New York, 489 p.
- Barker, J.A. and S.S.D. Foster, 1981. A Diffusion Exchange Model for Solute Movement in Fissured Porous Rock. Quarterly Journal Eng. Geol., Vol. 14, p. 17-26.
- Barr, G.E., W.B. Miller, and D.D. Gonzalez, 1983. Interim Report on the Modeling of the Regional Hydraulics of the Rustler Formation. Sandia National Laboratories, SAND 83-0391, 58 p.
- Bear, J., 1972. Dynamics of Fluids in Porous Media. Elsevier, New York, 764 p.
- Beauheim, R.L., 1986. Hydraulic Test Interpretations for Well DOE-2 at the WIPP Site. Sandia National Laboratories, SAND 86-1364, 89 p.
- Beauheim, R.L., in preparation. Analysis of Pumping Tests of the Culebra Dolomite Conducted at the H-3 hydropad at the Waste Isolation Pilot Plant (WIPP) Site. Sandia National Laboratories, SAND86-2311.
- Cleveland, J.M., T.F. Rees, and K.L. Nash, 1985. Plutonium, Americium, and Neptunium Speciation in Selected Ground-Waters. Nuclear Technology, v. 69, p. 380-387.
- Core Laboratories, 1986a. Special Core Analysis Study for INTERA Technologies, WIPP Site. File Number: SCAL 203-850073, Core Laboratories Inc., Aurora, Colorado.
- Core Laboratories, 1986b. A Complete Petrographic Study of Various Samples for the Rustler Formation. Core Laboratories Inc., Aurora, Colorado.

- Dosch, R.G., 1981. Solubility and Sorption Characteristics of Uranium (VI) Associated with Rock Samples and Brines/Groundwaters from WIPP and NTS. Sandia National Laboratories, Albuquerque, NM, SAND 80-1595, 39 p.
- Dosch, R.G., and A.W. Lynch, 1978. Interaction of Radionuclides with Geomedia Associated with the Waste Isolation Pilot Plant (WIPP) Site in New Mexico. Sandia National Laboratories, Albuquerque, NM, SAND 78-0297, 49 p.
- Garrels, R.M. and C.L. Christ, 1965. Solutions, Minerals, and Equilibria. Harper and Row, New York, 450 p.
- Gonzalez, D.D., 1983a. Hydrogeochemical Parameters of Fluid-Bearing Zones in the Rustler and Bell Canyon Formations, Waste Isolation Pilot Plant (WIPP), Southeast New Mexico (SENM). Sandia National Laboratories, SAND 83-0210, 37 p.
- Gonzalez, D.D., 1983b. Groundwater Flow in the Rustler Formation, Waste Isolation Pilot Plant (WIPP), Southeast New Mexico (SENM): Interim Report. Sandia National Laboratories, SAND 82-1012, 39 p.
- Haug, A., V.A. Kelley, M. LaVenue, and J.F. Pickens, in preparation. Modeling of Ground-Water Flow in the Culebra Dolomite at the Waste Isolation Pilot Plant (WIPP) Site: Interim Report. Sandia National Laboratories, Contractor Report, SAND 86-7167.
- Hydro Geo Chem, 1985. WIPP Hydrology Program, Waste Isolation Pilot Plant, Hydrologic Data Report #1. Sandia National Laboratories, Contractor Report SAND 85-7206, 710 p.

Hydro Geo Chem, 1986. Two-Well Recirculation Tracer Tests at the H-2 Hydropad, Waste Isolation Pilot Plant (WIPP), Southeastern New Mexico (SENM). Sandia National Laboratories, Contractor Report SAND 83-7014, 45 p.

Hydro Geo Chem, in preparation, a. Aquifer Tests at the H-4 Hydropad, Waste Isolation Pilot Plant (WIPP), Southeastern New Mexico (SENM): Basic Data and Interpretations. Unpublished contractor report prepared for Sandia National Laboratories, 227 p.

Hydro Geo Chem, in preparation, b. Aquifer Tests at the H-5 Hydropad, 1981, Waste Isolation Pilot Plant (WIPP) Southeastern New Mexico (SENM): Basic Data and Interpretations. Unpublished contractor report prepared for Sandia National Laboratories, 174 p.

Hydro Geo Chem, in preparation, c. Aquifer Tests at the H-6 Hydropad, 1981, Basic Data and Interpretations. Unpublished contractor report prepared for Sandia National Laboratories, 190 p.

Hydro Geo Chem, in preparation, d. Convergent Flow Tracer Tests at the H-6 Hydropad, Waste Isolation Pilot Plant (WIPP), Southeastern New Mexico (SENM). Unpublished contractor report prepared for Sandia National Laboratories, 88 p.

INTERA Environmental Consultants, Inc. 1981. Hydrogeological Analysis (1980) in Support of the Waste Isolation Pilot Plant (WIPP) Program. Report prepared for Sandia National Laboratories under contract No. 771-006-01.

INTERA Environmental Consultants, Inc., 1983. PHREEQE: A Geochemical Speciation and Mass Transfer Code Suitable for Nuclear Waste Performance Assessment. prepared for Battelle Memorial Institute, Office of Nuclear Waste Isolation, Columbus, OH, ONWI-435, 304 p.

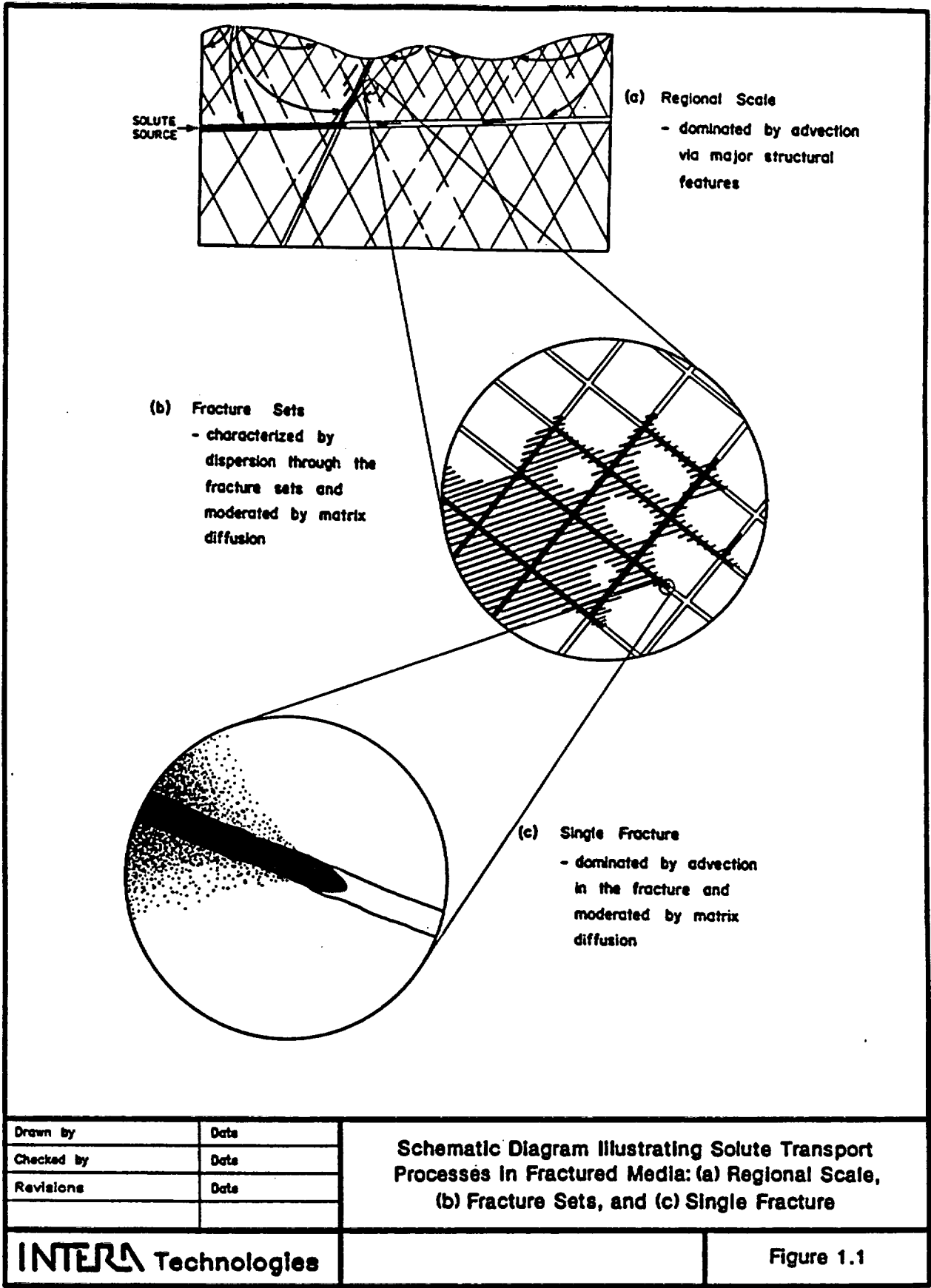
- INTERA Technologies, 1986. WIPP Hydrology Program, Waste Isolation Pilot Plant, Hydrologic Data Report #3. Sandia National Laboratories, Contractor Report SAND 86-7109.
- Katsube, T.J., T.W. Melnyk, and J.P. Hume, 1986. Pore Structure From Diffusion in Granitic Rocks. Atomic Energy of Canada Ltd., Technical Report TR-381.
- Kelley, V.A. and J.F. Pickens, 1986. Interpretation of the Convergent-Flow Tracer Tests Conducted in the Culebra Dolomite at the H-3 and H-4 Hydropads at the Waste Isolation Pilot Plant (WIPP) Site. Sandia National Laboratories, Contractor Report SAND 86-7161.
- Lallemand-Barres, A. and P. Peaudecerf, 1978. Recherche des Relations Entre la Valeur de la Dispersivite Macroscopique d'un Milieu Aquifere, Ses Autres Caracteristiques et les Conditions de Mesure. Bull. Bur. Geol. Minieres (Fr.) Sect. 3, 4:277.
- Lambert, S.J. and K.L. Robinson, 1984. Field Geochemical Studies of Groundwaters in Nash Draw, Southeastern New Mexico. Sandia National Laboratories, Albuquerque, NM, SAND83-1122, 38 p.
- Lindberg, R.D. and D.D. Runnels, 1984. Ground Water Redox Reactions: An Analysis of Equilibrium State Applied to Eh Measurements and Geochemical Modeling. Science, Vol. 225, p. 925-927.
- Lynch, A.W. and R.G. Dosch, 1980. Sorption Coefficients for Radionuclides on Samples from the Water-Bearing Magenta and Culebra Members of the Rustler Formation. Sandia National Laboratories, Albuquerque, NM, SAND80-1064, 21 p.

- Mercer, J.W., 1983. Geohydrology of the Proposed Waste Isolation Pilot Plant Site, Los Medanos Area, Southeastern New Mexico. U.S. Geological Survey, Water-Resources Investigation Report 83-4016, 113 p.
- Mercer, J.W. and B.R. Orr, 1979. Interim Data Report on the Geohydrology of the Proposed Waste Isolation Pilot Plant Site Southeast New Mexico. U.S. Geological Survey, Water-Resources Investigations Report 79-98.
- Moser, H. and W. Rauert, 1980. Isotopermethoden in der Hydrologie. Gebruder Borntraeger, Berlin, West Germany, 400 p.
- Nordstrom, D.K., L.N. Plummer, T.M.L. Wigley, T.J. Wolery, J.W. Ball, E.A. Jenne, R.L. Bassett, D.A. Crerar, T.M. Florence, B. Fritz, M. Hoffman, G.R. Holdren, Jr., G.A. Lafon, S.V. Mattigod, R.E. McDuff, F. Morel, M.M. Reddy, G. Sposito, and J. Thrailkill, 1979. A Comparison of Computerized Chemical Models for Equilibrium Calculations in Aqueous Systems: in Jenne, E.A., ed., Chemical Modeling in Aqueous Systems. American Chemical Society, Washington, DC, ACS Symposium Series 93, p. 857-892.
- Nordstrom, D.K. and J.L. Munoz, 1985. Geochemical Thermodynamics. The Benjamin/Cummings Publishing Co., Inc., Menlo Park, CA, 477 p.
- Oak Ridge National Laboratory, 1985. Catalog of Isotopes Products and Services. Distributed by Isotope Distribution Office, Oak Ridge, TN, 10/1/85 Revision of 1983 Catalog.
- Parkhurst, D.A., D.C. Thorstenson, and L.N. Plummer, 1980. PHREEQE - A Computer Program for Geochemical Calculations. U.S. Geological Survey Water-Resources Investigations 80-96, 210 p.

- Pearson, F.J., Jr., 1985. Sondierbohrung Bottstein - Results of Hydrochemical Investigations. Analysis and Interpretation: NAGRA, Baden, Switzerland, Technischer Bericht NTB85-05, 116 p.
- Pearson, F.J., Jr., D.W. Fisher, and L.N. Plummer, 1978. Correction of Ground-Water Chemistry and Carbon Isotopic Composition for Effects of CO₂ Outgassing. *Geochimica et Cosmochimica Acta*, Vol. 42, p. 1799-1807.
- Pickens, J.F. and G.E. Grisak, 1981. Scale-Dependent Dispersion in a Stratified Granular Aquifer. *Water Resources Research*, Vol. 17, No. 4, p. 1191-1211.
- Pourbaix, M., 1974. Atlas of Electrochemical Equilibria in Aqueous Solutions. National Association of Corrosion Engineers, Houston, TX, 644 p.
- Powers, D.W., S.J. Lambert, S.E. Shaffer, L.R. Hill, and W.D. Weart, 1978. Geological Characterization Report, Waste Isolation Pilot Plant (WIPP) Site, Southeastern New Mexico. Volumes I and II. Sandia National Laboratories, SAND 78-1596.
- Ramey, D.S., 1985. Chemistry of Rustler Fluids. Environmental Evaluation Group, Health and Environment Department, Santa Fe, NM, EEG-31, 61 p.
- Reeves, M., D.S. Ward, N.D. Johns, and R.M. Cranwell, 1986a. Theory and Implementation for SWIFT II, The Sandia Waste-Isolation Flow and Transport Model, Release 4.84. Sandia National Laboratories. NUREG/CR-3328 and SAND 83-1159, 189 p.
- Reeves, M., D.S. Ward, N.D. Johns, and R.M. Cranwell, 1986b. Data Input Guide for SWIFT II, the Sandia Waste-Isolation Flow and Transport Model, Release 4.84. Sandia National Laboratories, NUREG/CR-3162 and SAND 83-0242, 144 p.

- Robinson, K.L., (in preparation). Analysis of Solutes in Ground-Waters from the Rustler Formation at and Near the WIPP Site. Sandia National Laboratories. SAND 86-0917.
- Saulnier, G.J., Jr., G. Freeze, and W.A. Stensrud, in preparation. WIPP Hydrology Program, Waste Isolation Pilot Plant, Hydrologic Data Report #4. Sandia National Laboratories, Contractor Report SAND 86-7166.
- Seward, P.D., 1982. Abridged Borehole Histories for the Waste Isolation Pilot Plant (WIPP) Studies. Sandia National Laboratories, SAND 82-0080, 80 p.
- Serne, R.J., D. Rai, M.J. Mason, and M.A. Molecke, 1977. Batch Kd Measurements of Nuclides to Estimate Migration Potential at the Proposed Waste Isolation Pilot Plant in New Mexico. Battelle Pacific Northwest Laboratories, Richland, WA, PNL-2448, 47 p.
- Stevens, K. and W. Beyeler, 1985. Determination of Diffusivities in the Rustler Formation From Exploratory-Shaft Construction at the Waste Isolation Pilot Plant in Southeastern New Mexico. U.S. Geological Survey, Water-Resources Investigations Report 85-4020, 32 p.
- Streltsova-Adams, T.D., 1978. Well Hydraulics in Heterogeneous Aquifer Formations. Advances in Hydroscience, Vol. 11, p. 357-423.
- Stumm, W., and Morgan, J.J., 1981. Aquatic Chemistry, 2nd. ed. John Wiley & Sons, New York, 780 p.
- Truesdell, A.H. and B.F. Jones, 1974. WATEQ, a Computer Program for Calculating Chemical Equilibria of Natural Waters. U.S. Geological Survey Journal of Research, Vol. 2, p. 233-248.

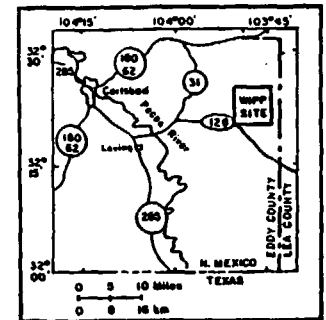
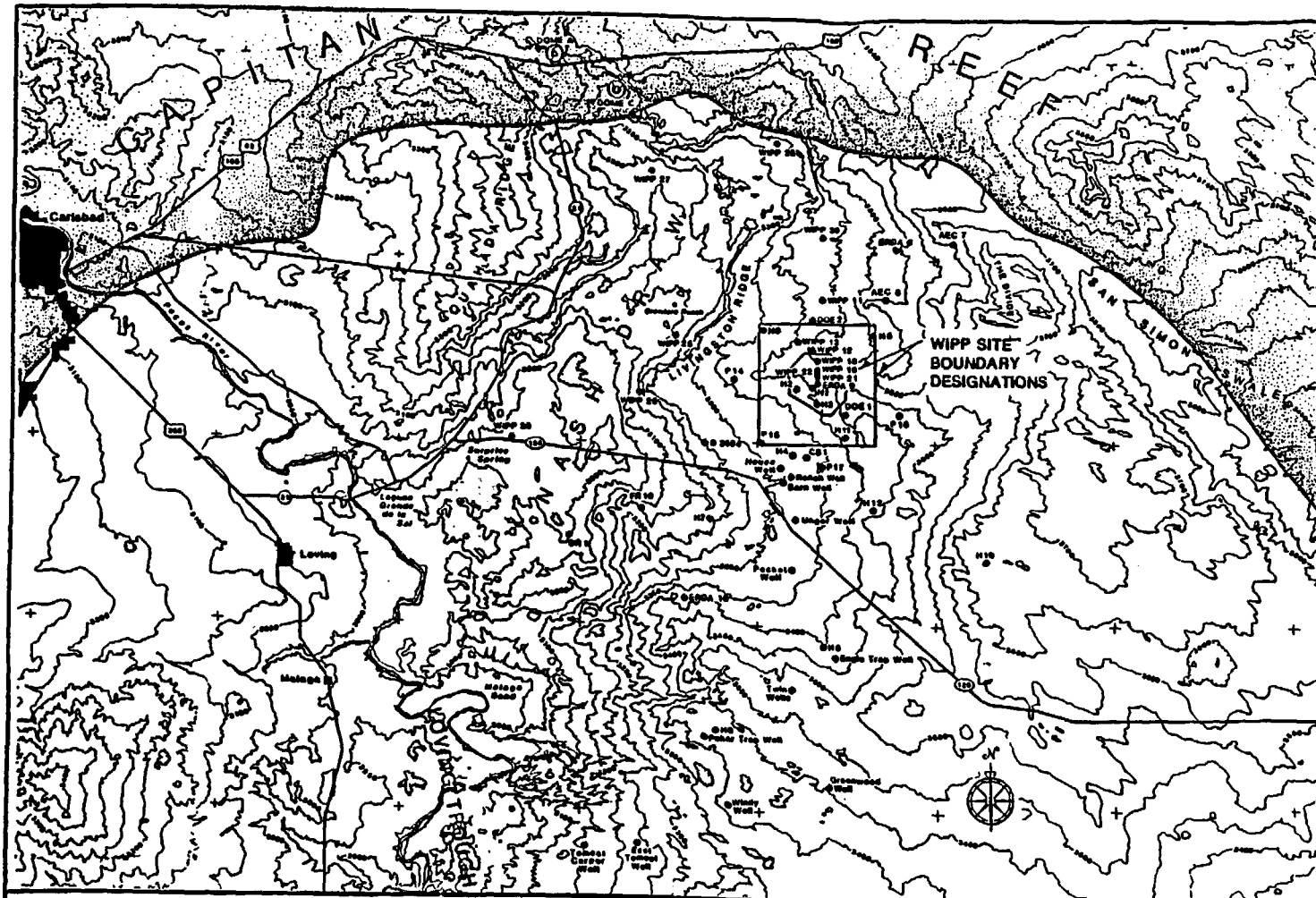
- U.S. Department of Energy, 1985. Assessment of Transuranic Activity Limits for WIPP TRU Waste. Waste Isolation Pilot Plant, Carlsbad, NM, WTSD-TME-062, 41 p.
- Wahlberg, J.S. and M.J. Fishman, 1962. Adsorption of Cesium on Clay Minerals. U.S. Geological Survey Bulletin 1140-A, p. A1-A30.
- Wahlberg, J.S. and R.S. Dewar, 1965. Comparison of Distribution Coefficients for Strontium Exchange From Solutions Containing One and Two Competing Cations. U.S. Geological Survey Bulletin 1140-D, p. D1-D10.
- Wahlberg, J.S., J.H. Baker, R.W. Vernon, and R.S. Dewar, 1965. Exchange Adsorption of Strontium on Clay Minerals. U.S. Geological Survey Bulletin 1140-C. p. C1-C26.
- Walter, G.R., 1982. Theoretical and Experimental Determination of Matrix Diffusion and Related Solute Transport Properties of Fractured Tuffs from the Nevada Test Site. Los Alamos National Laboratory, LA-9471-MS.
- Ward, D.S., M. Reeves, and L.E. Duda, 1984. Verification and Field Comparison of the Sandia Waste-Isolation Flow and Transport Model (SWIFT). Sandia National Laboratories, NUREG/CR-3316 and SAND 83-1154, 155 p.
- Westinghouse Electric Corporation, 1985. Ecological Monitoring Program at the Waste Isolation Pilot Plant; Second Semi-Annual Report Covering Data Collected January to June 1985. DOE/WIPP-85-002, prepared for U.S. Department of Energy, WIPP Project Office, Carlsbad, NM.



Drawn by	Date
Checked by	Date
Revisions	Date

Schematic Diagram Illustrating Solute Transport Processes in Fractured Media: (a) Regional Scale, (b) Fracture Sets, and (c) Single Fracture

Figure 1.1



0 1 2 3 4 Miles
0 1 2 3 4 5 6 km

NOTE: THIS MAP ILLUSTRATES THE PRINCIPAL FEATURES OF THE WIPP SITE AND VICINITY. CONTOURS SHOW APPROXIMATE RELIEF.

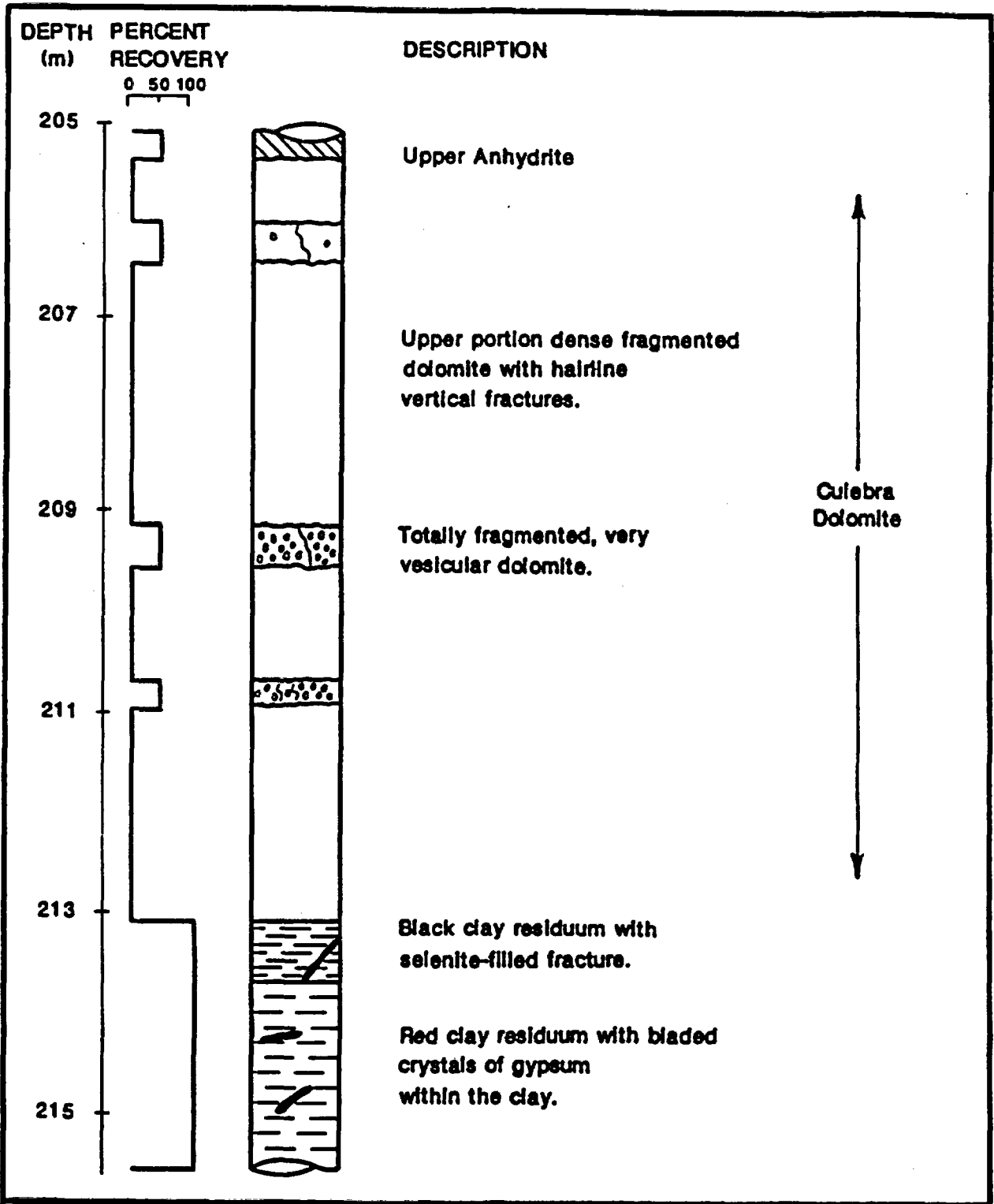
CONTOUR INTERVAL IS 50 FEET

Drawn by	Date
Checked by	Date
Revisions	Date

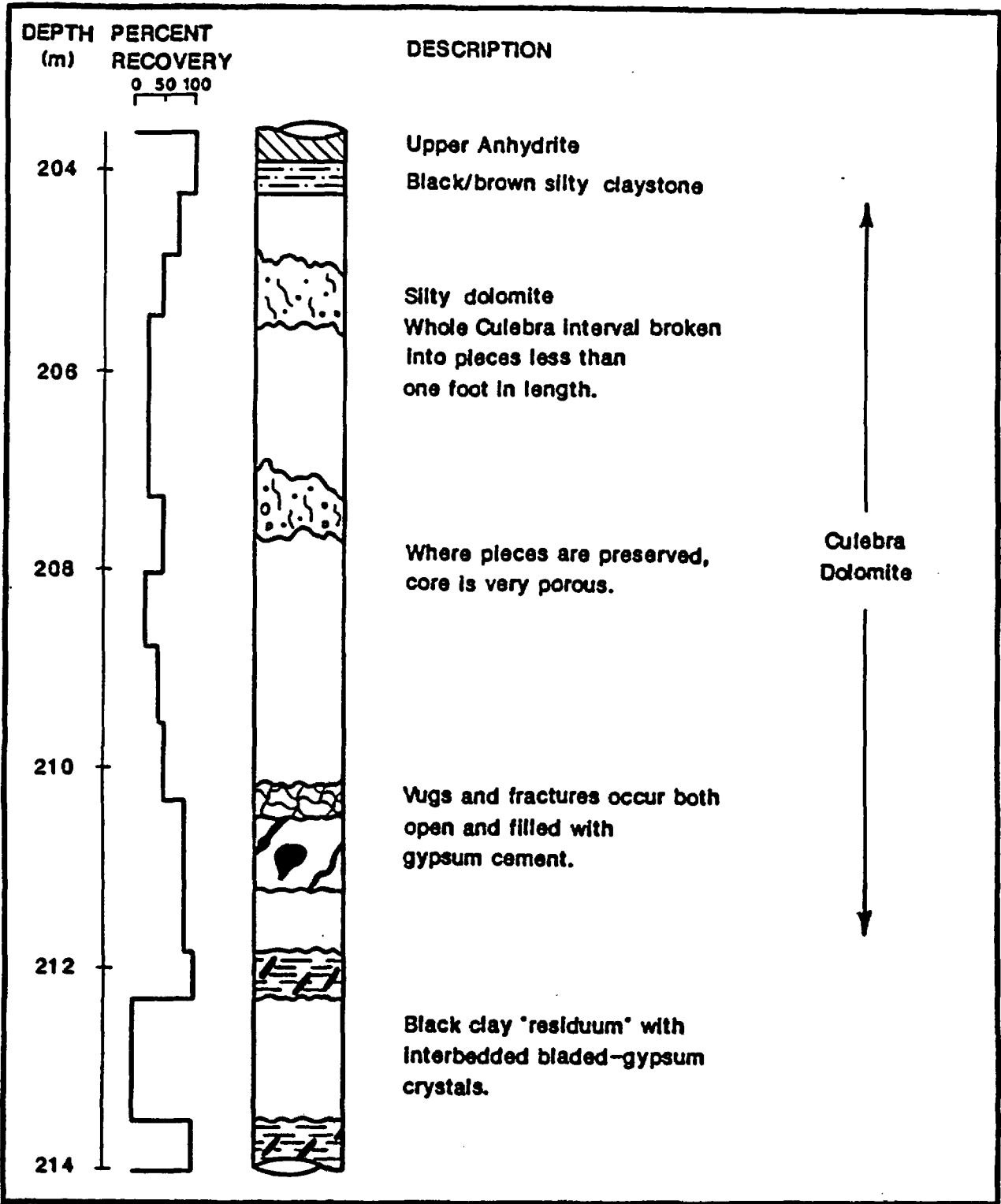
Site Locations for the Waste Isolation Pilot Plant Showing the Observation-Well Network for Regional Hydrogeologic Characterization Studies

INTERA Technologies

Figure 2.1



Drawn by	Date	Results of Core Examination of Culebra Dolomite from Borehole H-3b2
Checked by	Date	
Revisions	Date	

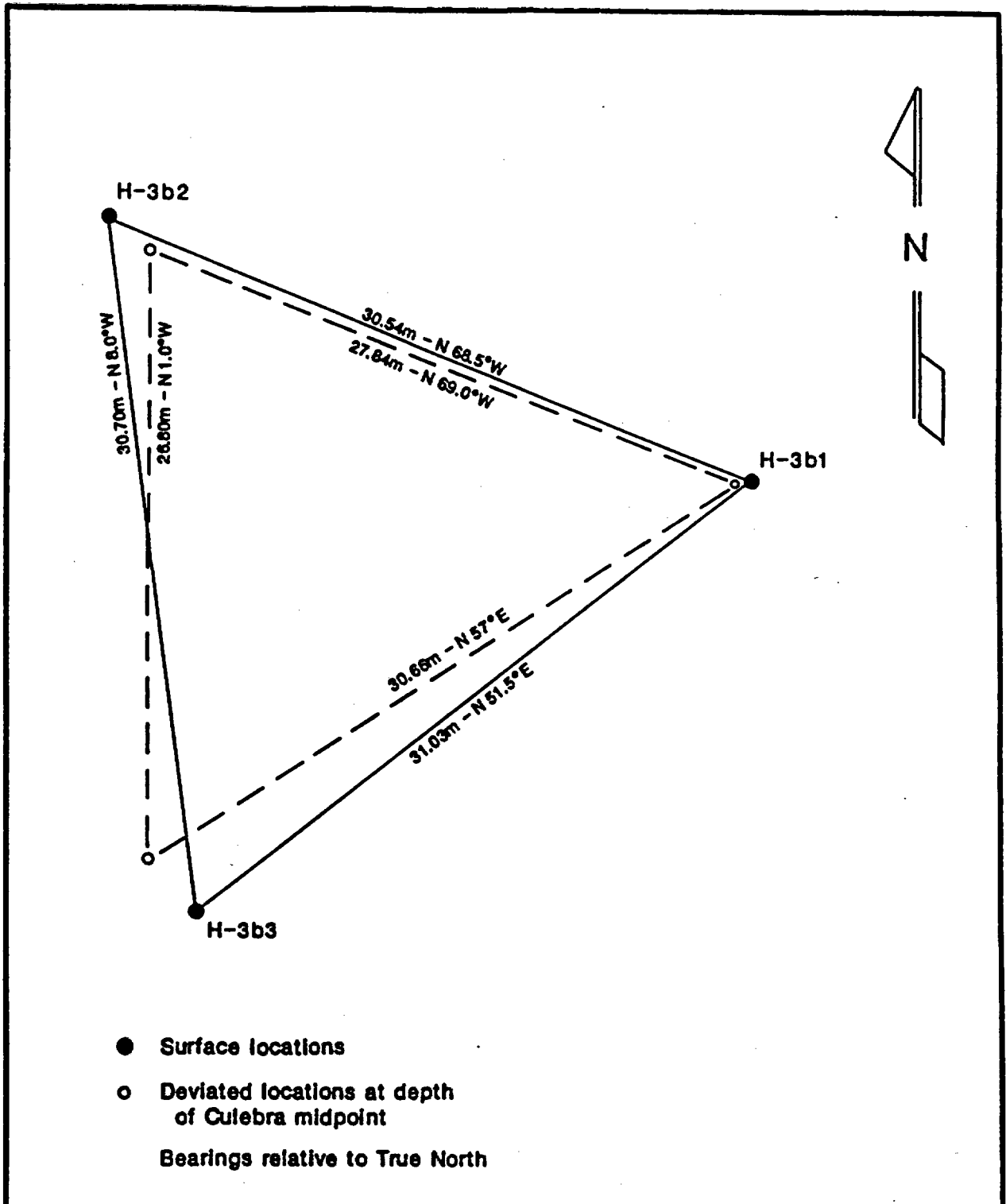


Drawn by	Date
Checked by	Date
Revisions	Date

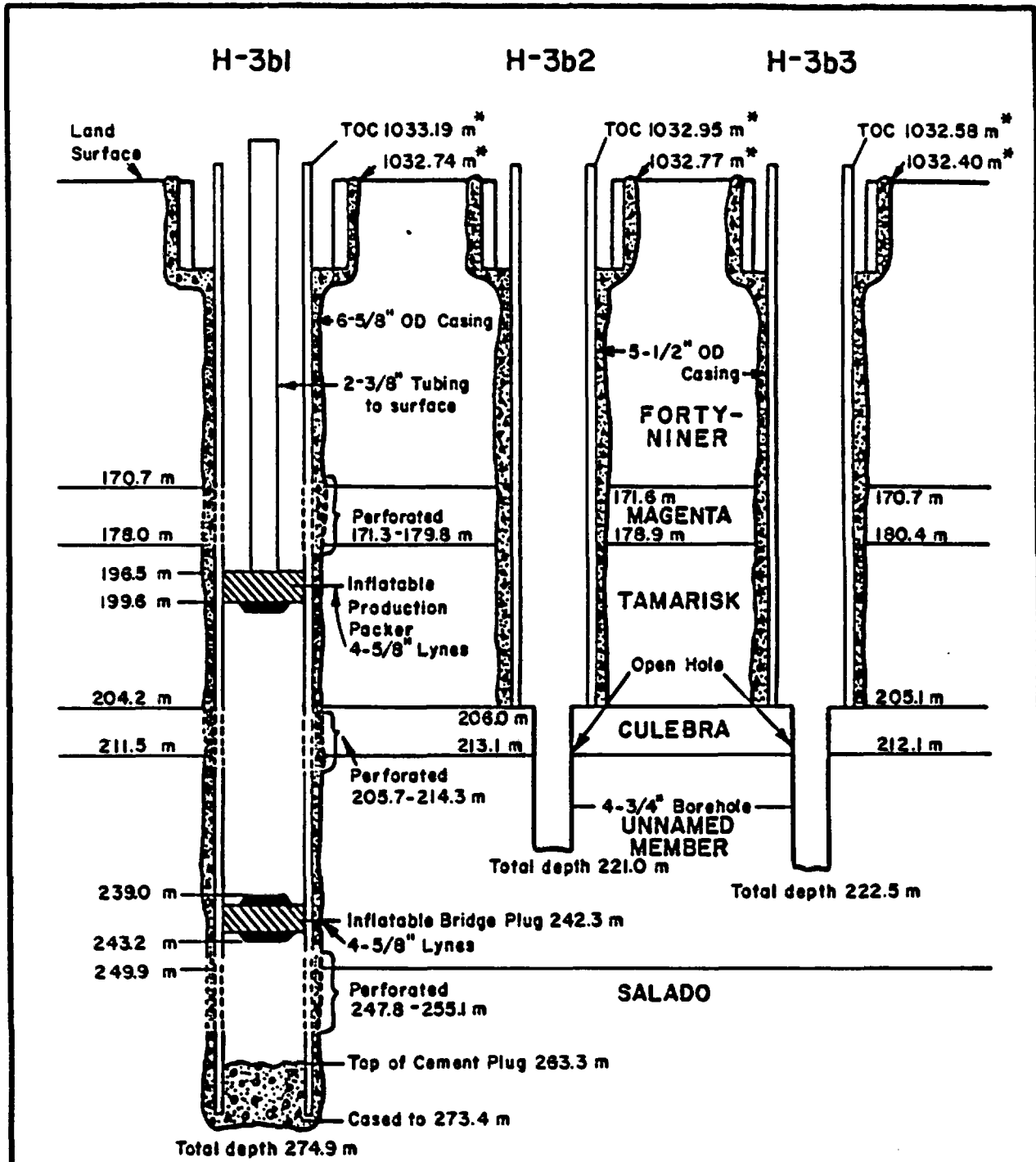
**Results of Core Examination of Culebra Dolomite
from Borehole H-3b3**

INTERA Technologies

Figure 3.2



Drawn by	Date	Plan View of Wells at the H-3 Hydropad Showing Distances Between Wells at Ground Surface and Culebra Depth
Checked by	Date	
Revisions	Date	



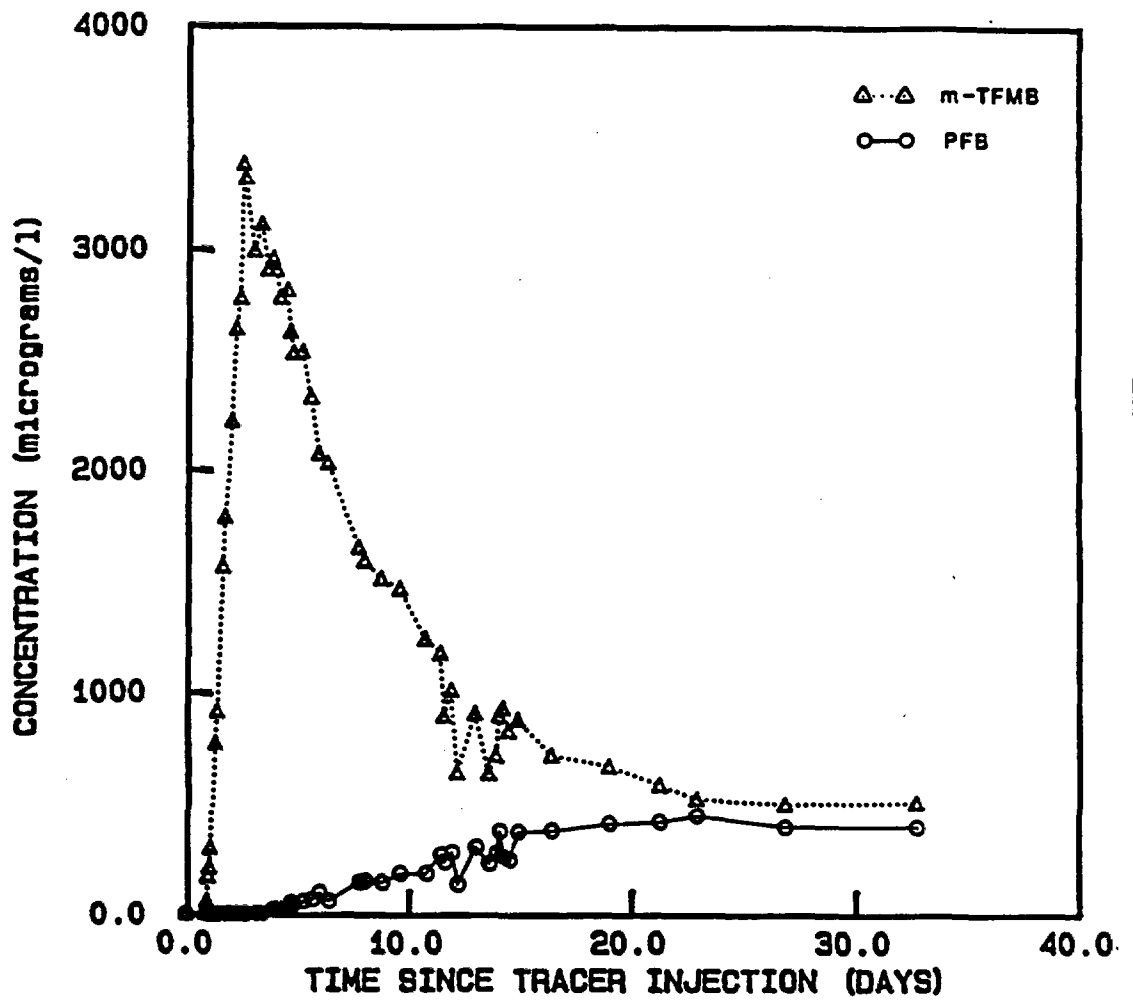
* Above sea level (Satellite Survey, Hydro Geo Chem, 1985 f)
 Depths in meters below ground surface

Drawn by	Date
Checked by	Date
Revisions	Date

Well Construction Details for the H-3 Hydropad

INTERA Technologies

Figure 3.4

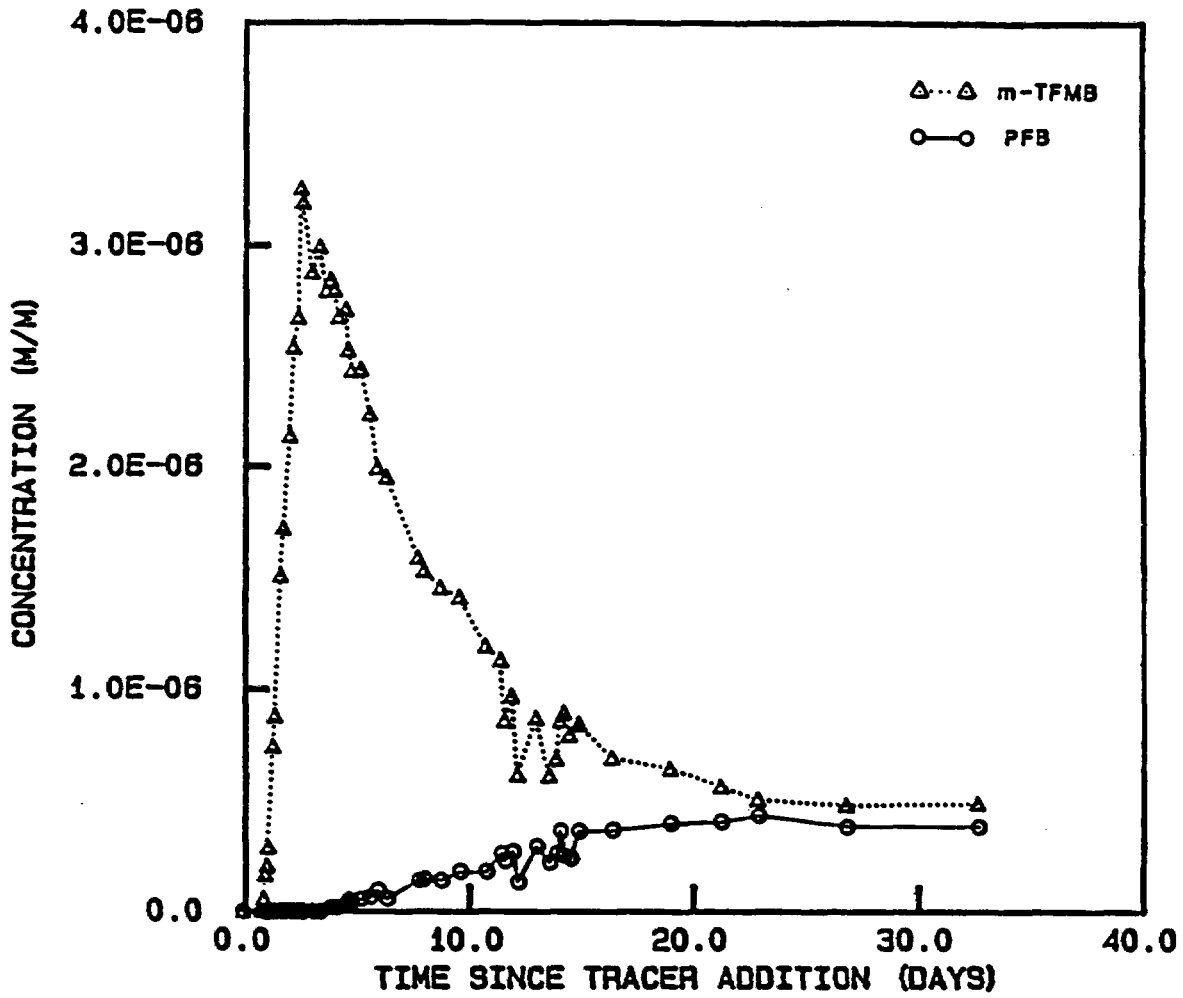


Drawn by	Date
Checked by	Date
Revisions	Date

Observed Tracer Concentration for PFB and m-TFMB
Expressed as (a) Micrograms per Liter

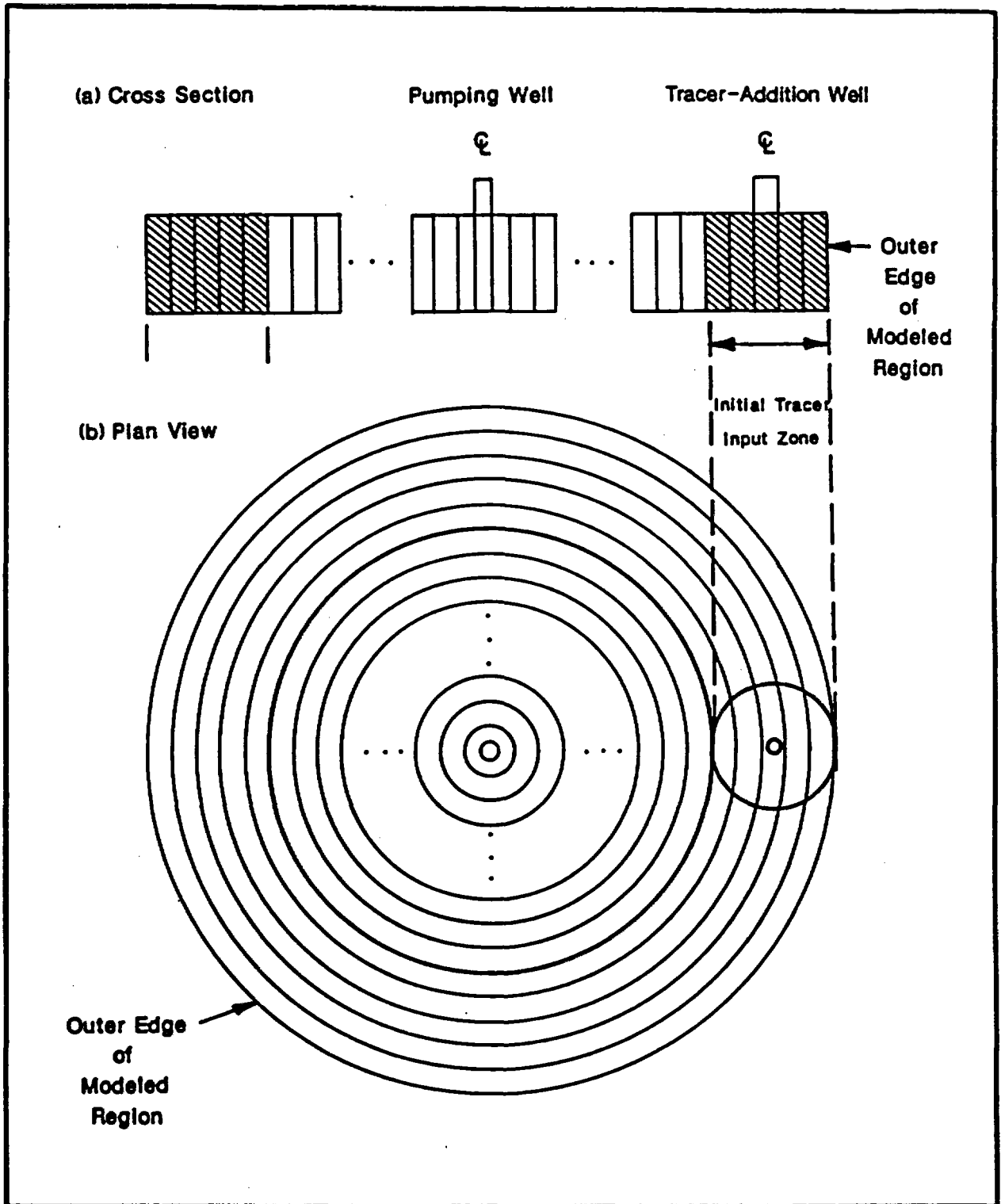
INTERA Technologies

Figure 3.5a



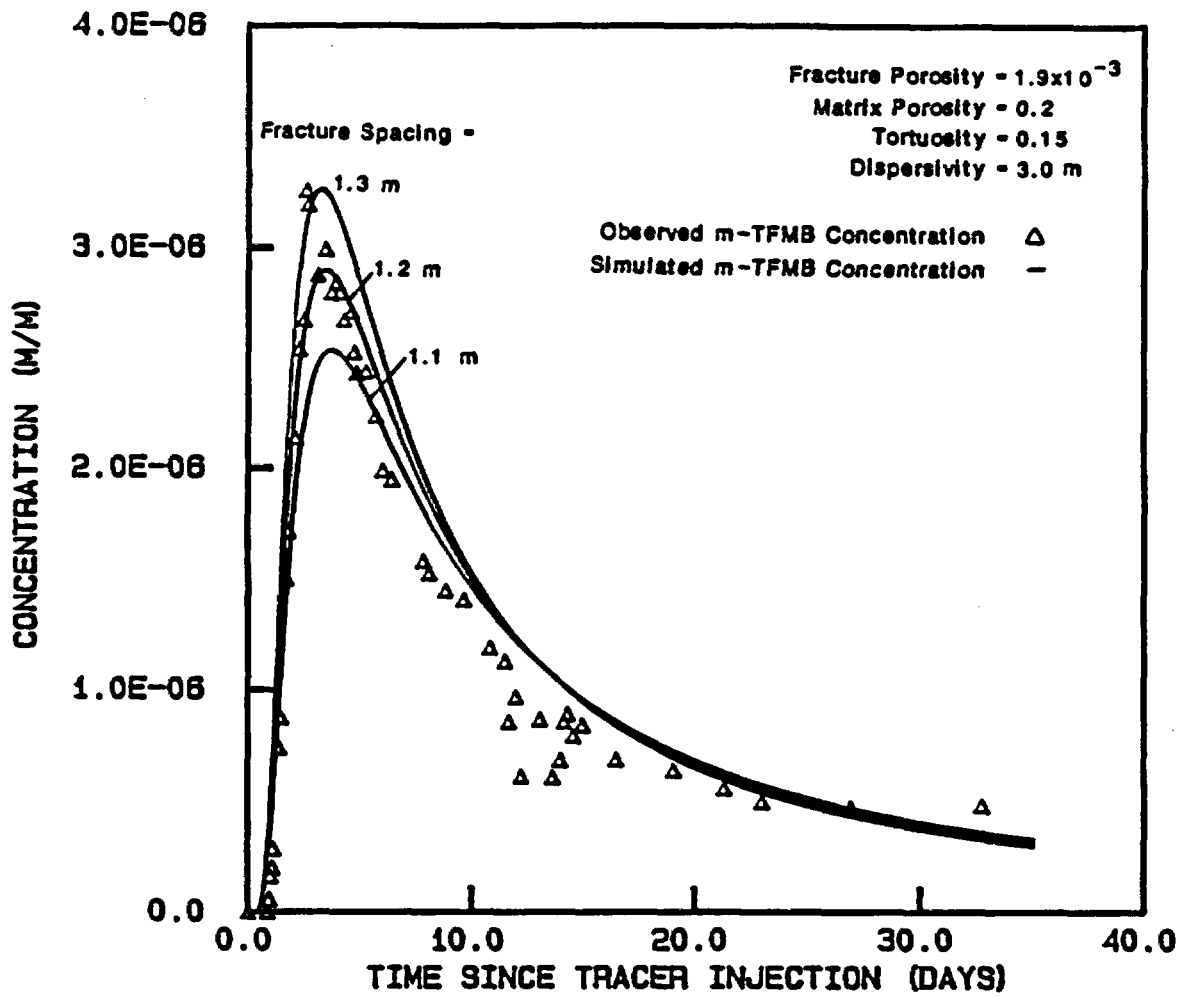
Drawn by	Date
Checked by	Date
Revisions	Date

Observed Tracer Concentrations for PFB and m-TFMB Expressed as (b) Mass per Unit Mass



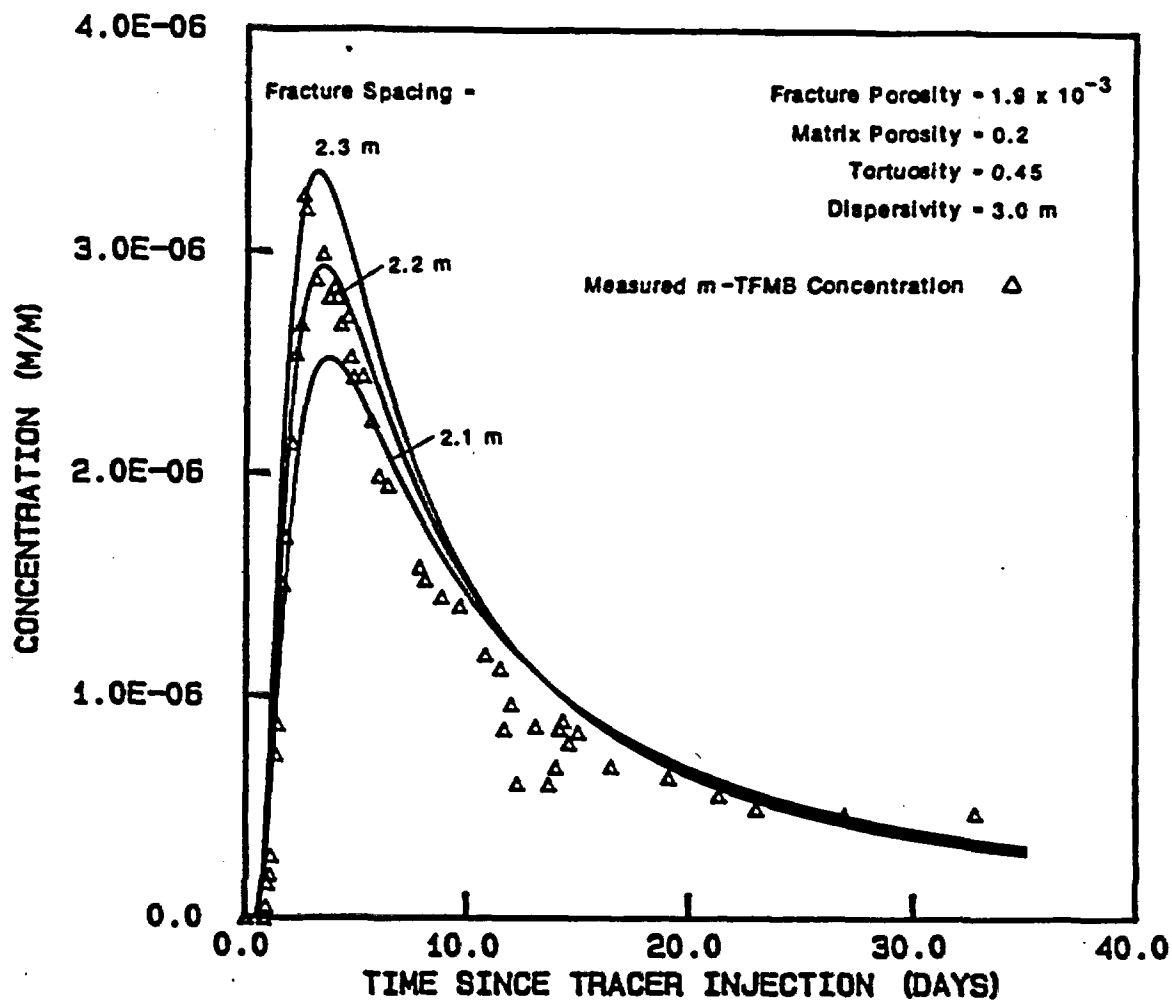
Drawn by	Date
Checked by	Date
Revisions	Date

Schematic Representation of the Modeled Region,
 (a) Cross Section, (b) Plan View



Drawn by	Date
Checked by	Date
Revisions	Date

Observed and Simulated Breakthrough Curves for Tracer m-TFMB for (a) Assumed Tortuosity of 0.15

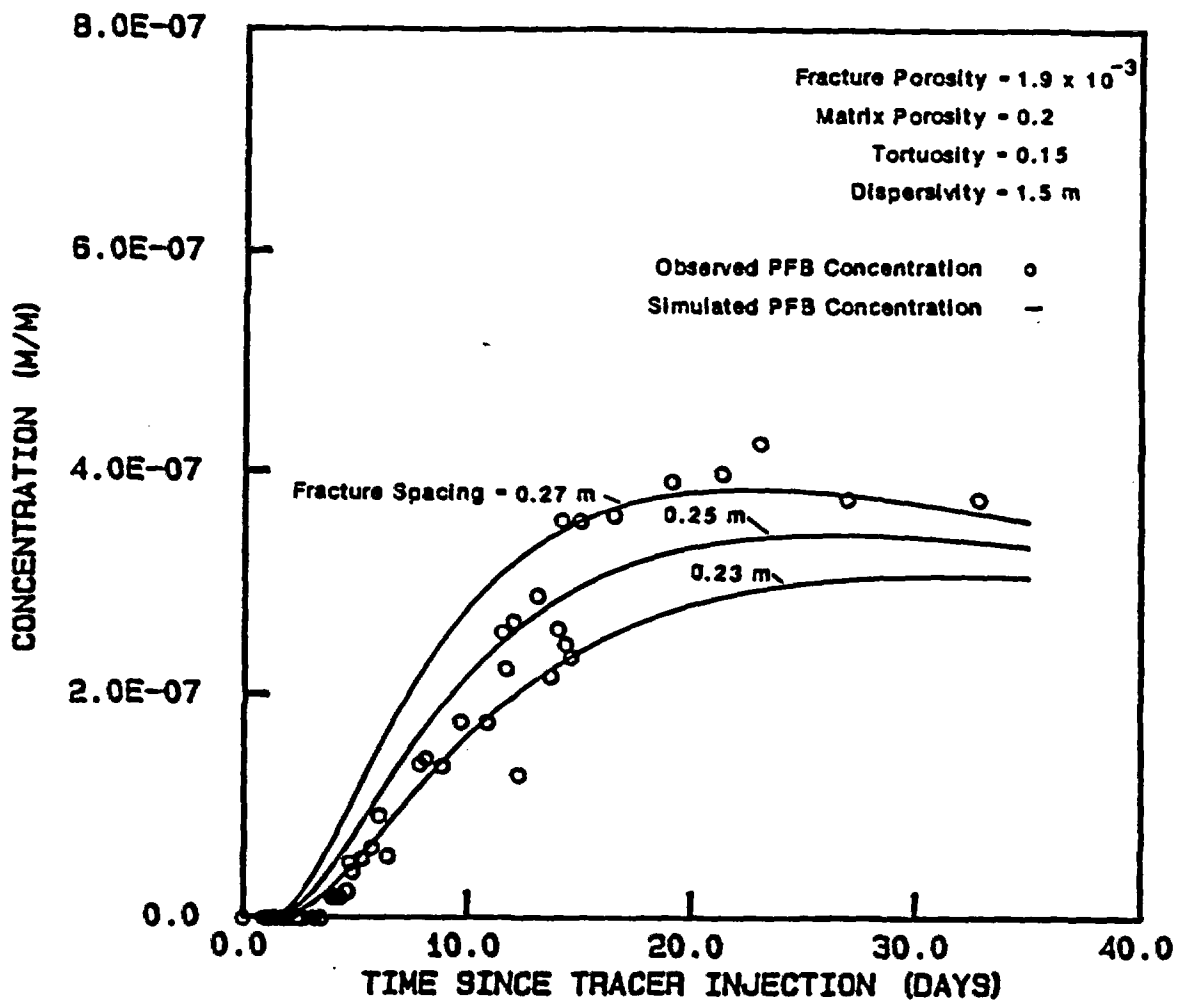


Drawn by	Date
Checked by	Date
Revisions	Date

Observed and Simulated Breakthrough Curves for Tracer m-TFMB for (b) Assumed Tortuosity of 0.45

INTERA Technologies

Figure 3.7b

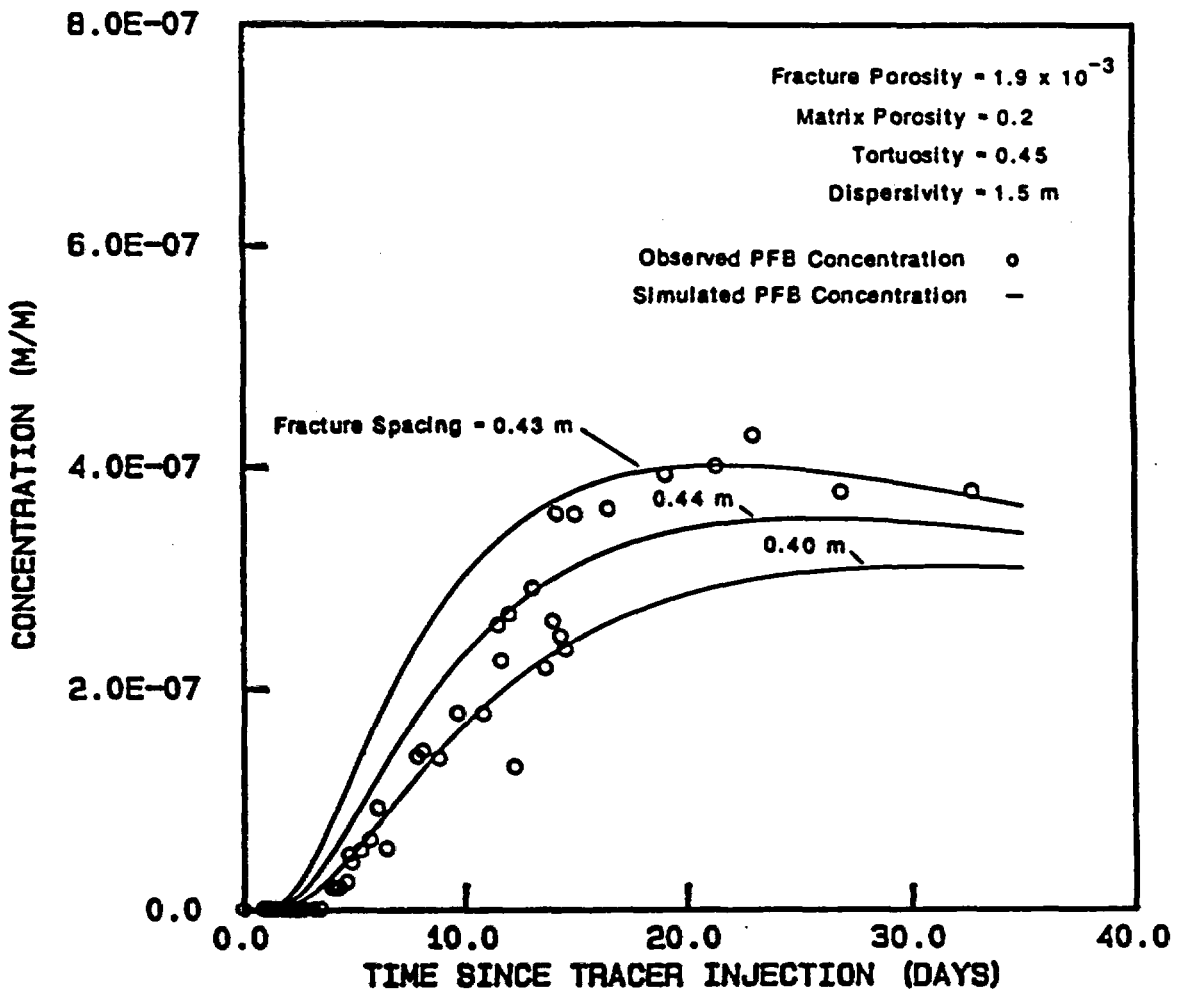


Drawn by	Date
Checked by	Date
Revisions	Date

Observed and Simulated Breakthrough Curves for Tracer PFB for (a) Assumed Tortuosity of 0.15

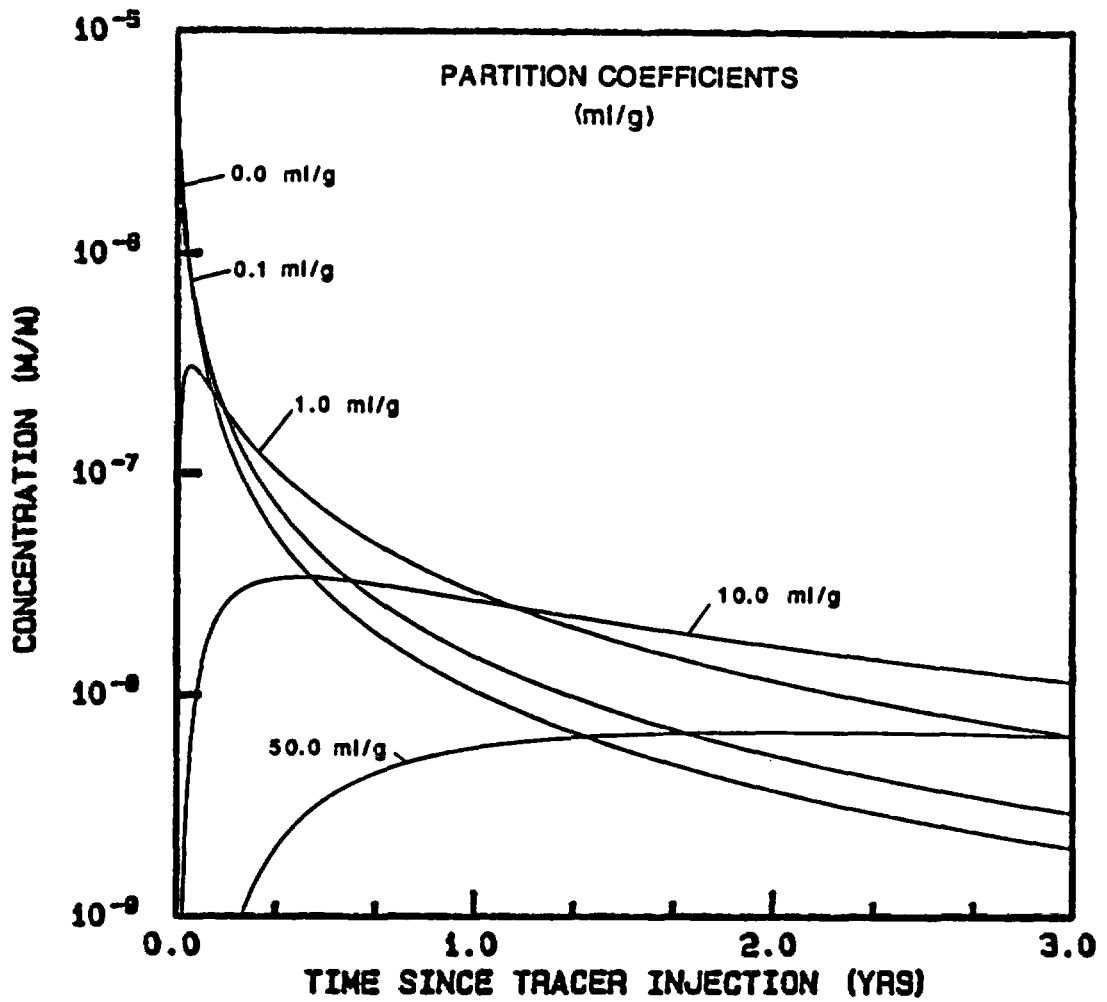
INTERA Technologies

Figure 3.8a



Drawn by	Date
Checked by	Date
Revisions	Date

Observed and Simulated Breakthrough Curves for Tracer PFB for (b) Assumed Tortuosity of 0.45



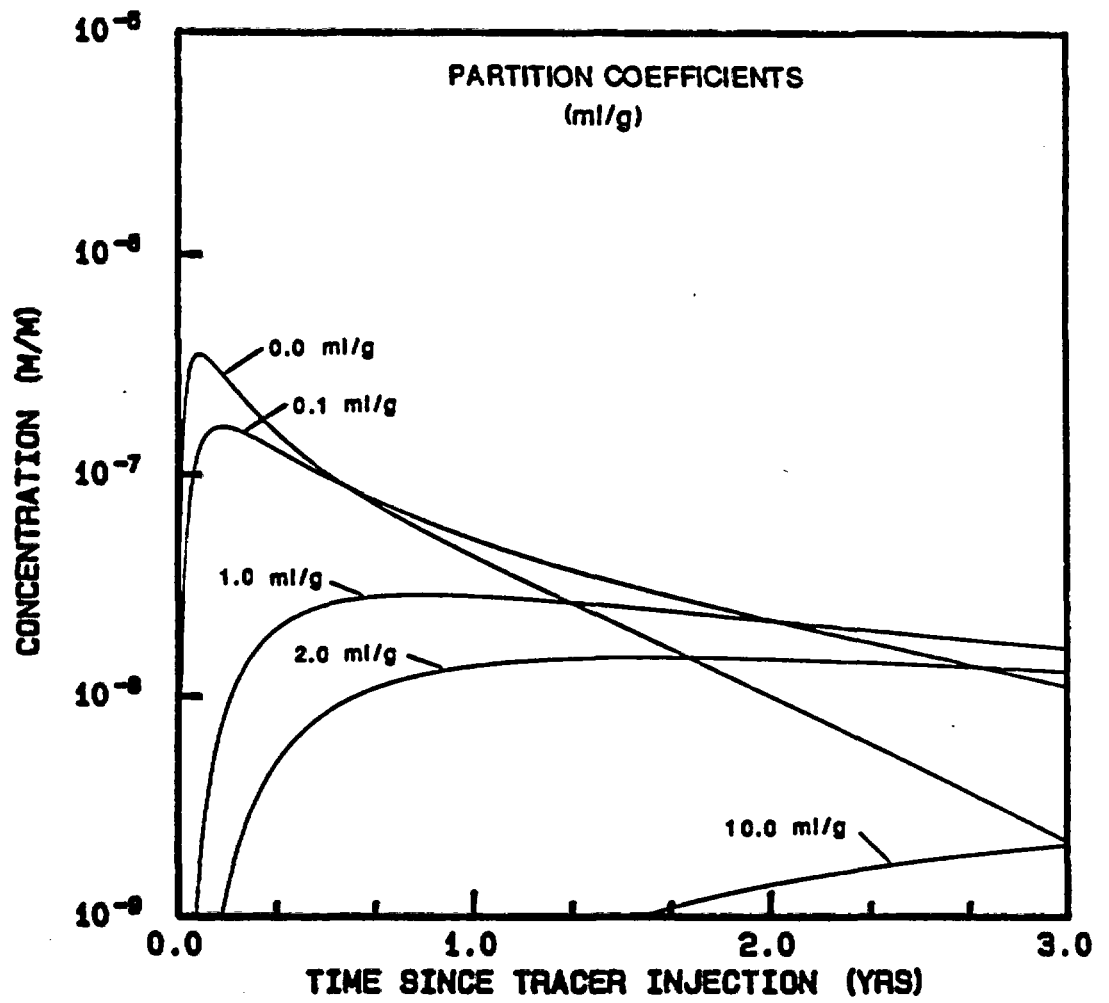
Note: 1 kg of tracer injected in tracer-addition well

Drawn by	Date
Checked by	Date
Revisions	Date

**Simulated Breakthrough Curves at Pumping Well
for a Range of Partition Coefficients for the
(a) H-3b1 to H-3b3 Flow Path**

INTERA Technologies

Figure 3.9a



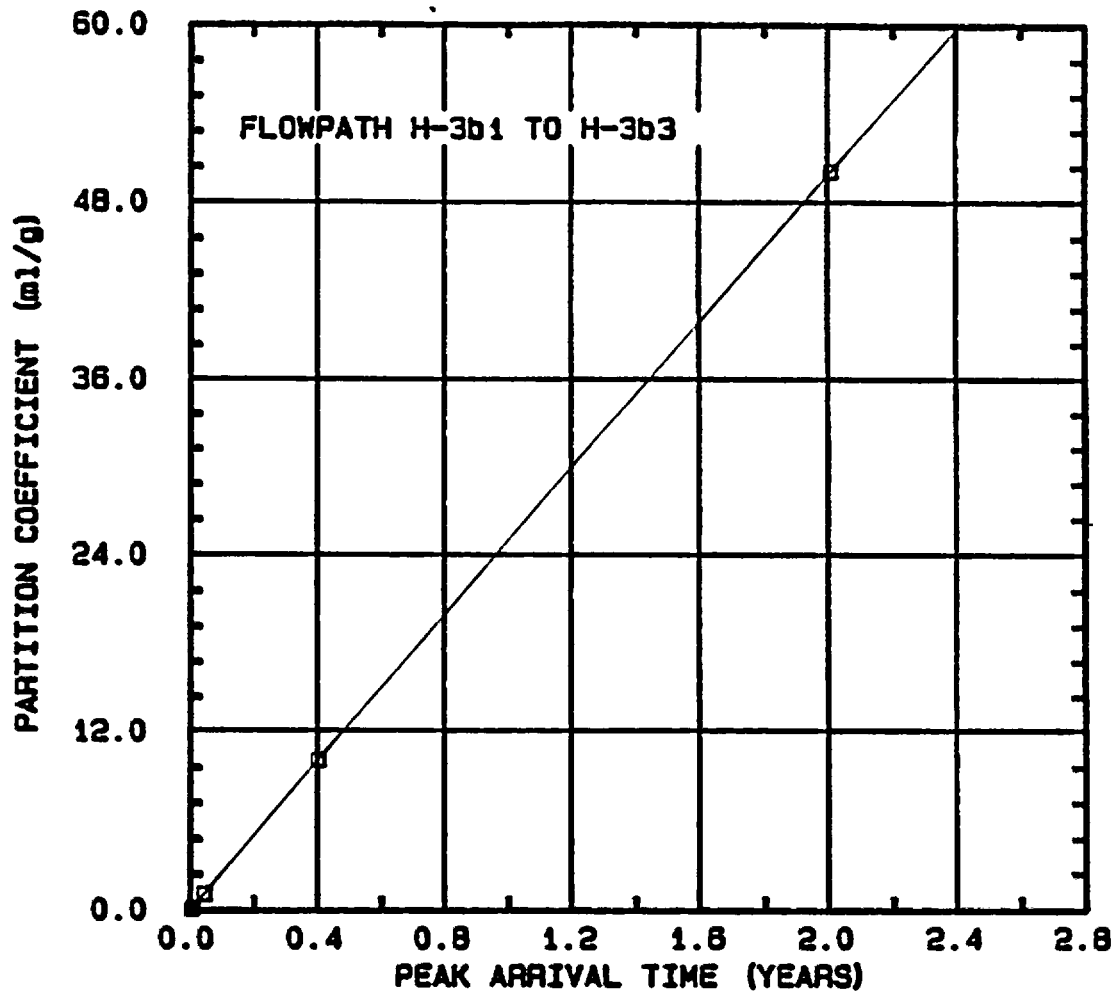
Note: 1 kg of tracer injected in tracer-addition well

Drawn by	Date
Checked by	Date
Revisions	Date

Simulated Breakthrough Curves at Pumping Well
for a Range of Partition Coefficients for the
(b) H-3b2 to H-3b3 Flow Path

INTERA Technologies

Figure 3.9b



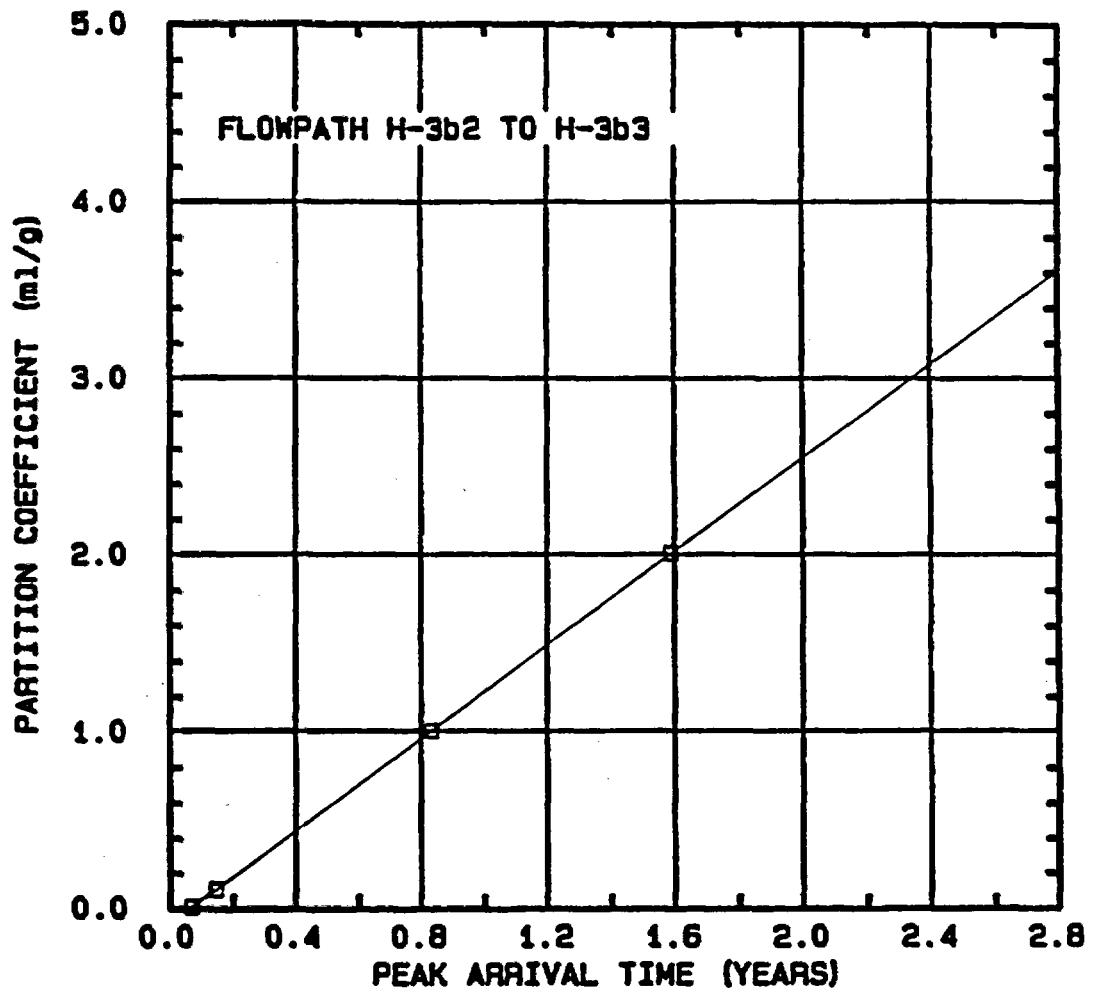
calculated values

Drawn by	Date
Checked by	Date
Revisions	Date

Calculated Peak-Concentration Arrival Times at Pumping Well for Various Assumed Partition Coefficients for the H-3b1 to H-3b3 Flow Path

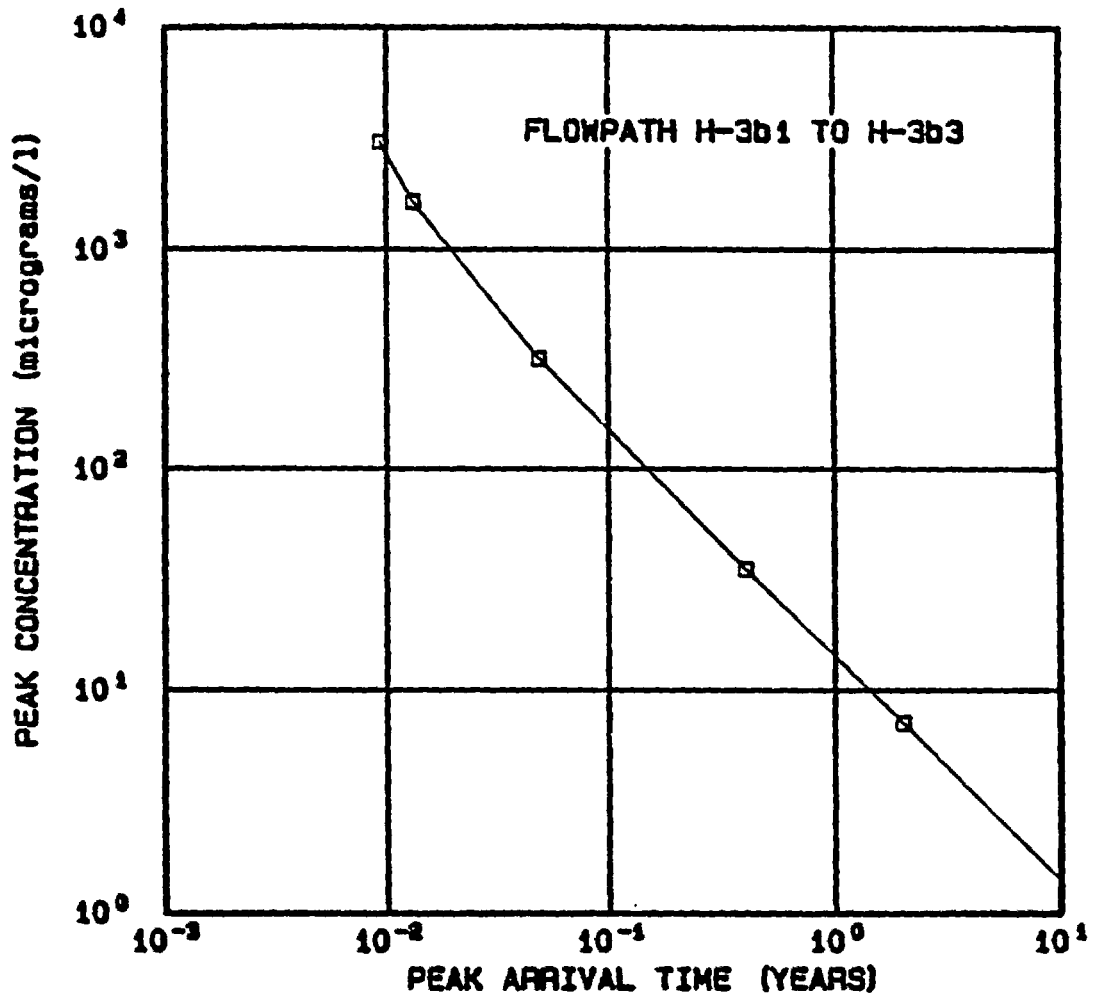
INTERA Technologies

Figure 5.1



□ calculated values

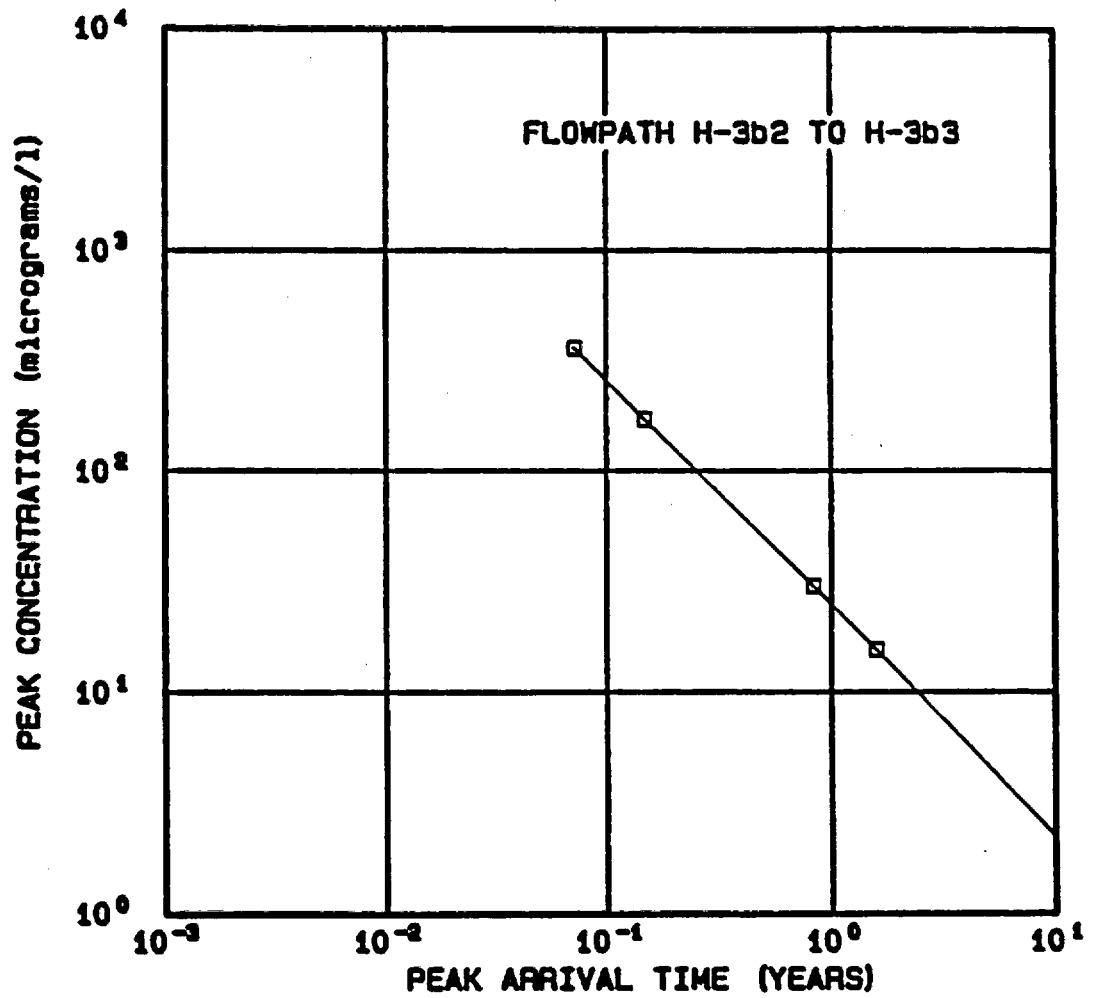
Drawn by	Date	Calculated Peak-Concentration Arrival Times at Pumping Wells for Various Assumed Partition Coefficient for the H-3b2 to H-3b3 Flow Path
Checked by	Date	
Revisions	Date	
INTERA Technologies		Figure 5.2



Note: 1 kg of tracer injected in tracer-addition well
 calculated values

Drawn by	Date
Checked by	Date
Revisions	Date

Peak Concentration Versus Peak-Concentration Arrival Times for the H-3b2 to H-3b3 Flow Path



Note: 1 kg of tracer injected in tracer-addition well

calculated values

Drawn by	Date
Checked by	Date
Revisions	Date

Peak Concentration Versus Peak-Concentration Arrival Times for the H-3b1 to H-3b3 Flow Path

INTERA Technologies

Figure 5.4

Test	Pumping Rate (1/s)	Transmissivity (m ² /s)	Time of First Detection (days)	Time of Peak Concentration (days)
H-2 two-well	1.9 x 10 ⁻²	6 x 10 ⁻⁷	80	234
H-3 convergent	0.19	4 x 10 ⁻⁶	1.0 - 3.8	2.6 - 23
H-4 convergent	1.6 x 10 ⁻² for 167 days 3.3 x 10 ⁻² for 439 days	1 x 10 ⁻⁶	270 - 501	316 - not reached
H-6 convergent	0.50 - 1.3	8 x 10 ⁻⁵	0.02 - 1.6	0.7 - 12.3
H-6 two-well	0.14 - 0.63	8 x 10 ⁻⁵	0.02 - 0.05	0.1 - 2.2

Drawn by	Date
Checked by	Date
Revisions	Date

Relative Transport Rates Determined from the Conservative Tracer Tests

INTERA Technologies

Table 2.1

Hydropad	Hydraulic Charac- terization	Geochemical Charac- terization	Tracer Tests Conducted	Flow Path Location	Opera- tional Period	Overall Suit- ability
H-2	Extensive	Poor	Yes	Suitable	Unsuitable	No
H-3	Extensive	Possible	Yes	Suitable	Suitable	Yes
H-4	Extensive	Possible	Yes	Suitable	Unsuitable	No
H-5	Extensive	Difficult	No	Unsuitable	Unsuitable	No
H-6	Extensive	Poor	Yes	Unsuitable	Suitable	No
H-7	Two Pumping Tests	Poor	No	Suitable?	Suitable	No
H-9	Extensive	Poor	No	Suitable?	Suitable	No
H-11	Extensive	Difficult	No	Suitable	Suitable	No

Drawn by	Date	Summary of Suitability of Multi-Well Hydropad Locations to Site Selection Criteria for the Sorbing Tracer Test
Checked by	Date	
Revisions	Date	
INTERA Technologies		Table 2.2

Parameter	TRACER	
	m-TFMB	PFB
Flow path	H-3b1 to H-3b3	H-3b2 to H-3b3
First reported concentration ($\mu\text{g}/\ell$)	56.0	20.0
Time of first detection (days)	0.92	3.76
Time of arrival of peak concentration (days)	2.59	23.04
Peak concentration ($\mu\text{g}/\ell$) (M/M)	3379 3.3×10^{-6}	444 4.3×10^{-7}
Tracer mass recovered during the test (%)	53	15

Drawn by	Date	Summary of Tracer Arrival Times and Mass Recoveries at the Pumping Well H-3b3
Checked by	Date	
Revisions	Date	
INTERA Technologies		Table 3.1

PARAMETER	SYMBOL		VALUE	
Solute free-water diffusion coefficient (m ² /s)	7.4 x 10 ⁻¹⁰		7.2 x 10 ⁻¹⁰	
Tortuosity	0.15	0.45	0.15	0.45
Matrix block size (m)	1.2	2.1	0.25	0.44
Longitudinal dispersivity (m)	3.0		1.5	
Fracture porosity	1.9 x 10 ⁻³		1.9 x 10 ⁻³	
Matrix porosity	0.2		0.2	

Drawn by	Date	Summary of Best-Fit Parameters for m-TFMB and PFB Breakthrough Curves at the H-3 Hydropad
Checked by	Date	
Revisions	Date	
INTERA Technologies		Table 3.2

Parameter	H-3b1 to H-3b3 Flow Path	H-3b2 to H-3b3 Flow Path
Solute free-water diffusion coefficient (m ² /s)	7.4 x 10 ⁻¹⁰	7.2 x 10 ⁻¹⁰
Tortuosity	0.15	0.15
Longitudinal dispersivity (m)	3.0	1.5
Fracture porosity	1.9 x 10 ⁻³	1.9 x 10 ⁻³
Matrix porosity	0.2	0.2
Matrix block size (m)	1.2	0.25
Pumping rate (l/s)	0.19	0.19
Distance between tracer-addition and pumping well (m)	30.7	26.8
Mass entering aquifer from tracer-addition well (kg)	1.0	1.0
Initial tracer input-zone width (m)	3.4	3.4
Partition coefficients (ml/g)	0.1 1.0 10.0 50.0	0.1 1.0 2.0 10.0

Drawn by	Date	Parameters for the Design Calculations for the Sorbing Tracer Test
Checked by	Date	
Revisions	Date	
INTERA Technologies		Table 3.3

Partition Coefficient (ml/g)	Peak Concentration ⁺		Time to Reach Peak Concentration		Time to Reach 1% of Peak Concentration	
	($\mu\text{g}/\text{l}$)	(M/M)	(days)	(years)	(days)	(years)
(a) H-3b1 to H-3b3 Flow Path						
0.0	3.0×10^3	2.9×10^{-6}	3.5	9.5×10^{-3}	0.5	1.4×10^{-3}
0.1	1.6×10^3	1.6×10^{-6}	4.8	1.3×10^{-2}	0.65	1.8×10^{-3}
1.0	3.2×10^2	3.0×10^{-7}	17.9	4.9×10^{-2}	1.2	3.2×10^{-3}
10.0	3.5×10^1	3.4×10^{-8}	148	0.4	6.1	1.7×10^{-2}
50.0	7.0×10^0	6.8×10^{-9}	732	2.0	28.5	7.8×10^{-2}
(b) H-3B2 TO H-3B3 Flow Path						
0.0	3.6×10^2	3.5×10^{-7}	26.3	7.2×10^{-2}	1.8	5.0×10^{-3}
0.1	1.7×10^2	1.6×10^{-7}	54.0	0.15	3.0	8.3×10^{-4}
1.0	3.0×10^1	2.5×10^{-8}	304	0.83	14.3	3.9×10^{-2}
2.0	1.5×10^1	1.5×10^{-8}	579	1.6	29.7	8.2×10^{-2}
10.0	*	*	*	*	*	*
<p>+ Note: 1 kg of tracer injected at tracer-addition well.</p> <p>* Does not reach peak concentration in 5 year operational period.</p>						
Drawn by	Date	Summary of Tracer Arrival Times and Peak Concentrations Calculated for a Range of Partition Coefficients				
Checked by	Date					
Revisions	Date					
INTERA Technologies					Table 3.4	

Borehole	H-3 (1)		H-3b3 (2)		H-3b3 (3)	
Date Sampled	17-Mar-77		11-Jun-84		4-Feb-85	
pH	7.40		7.30		7.30	
Temp. (C)	24		24		24	
Density (g/ml)	1.04		1.04		1.04	
	mg/l	molality	mg/l	molality	mg/l	molality
Lithium	NA		0.53	7.756E-05	0.4	5.858E-05
Sodium	19000	8.410E-01	17400	7.685E-01	18000	7.957E-01
Potassium	630	1.640E-02	495	1.286E-02	425	1.105E-02
Cesium	NA		NA		<0.007	
Magnesium	670	2.805E-02	828	3.459E-02	780	3.261E-02
Calcium	1500	3.808E-02	1550	3.927E-02	1470	3.727E-02
Strontium	NA		22.3	2.584E-04	30.5	3.538E-04
Manganese	0.12	2.223E-06	0.133	2.458E-06	0.117	2.164E-06
Iron	0.05	9.110E-07	0.573	1.042E-05	0.2	3.640E-06
Sum Cations (meg/kg)		9.896E-01		9.297E-01		9.473E-01
Fluoride	0.5	2.678E-05	2.08	1.112E-04	1.94	1.038E-04
Chloride	29600	8.496E-01	29500	8.449E-01	30300	8.686E-01
Bromide	NA		28.8	3.660E-04	25.8	3.281E-04
Iodide	NA		0.133	1.064E-06	0.138	1.105E-06
Sulfate	5700	6.038E-02	5130	5.423E-02	4823	5.103E-02
Alkalinity (CaCO3)	94	1.911E-03	43.3	8.785E-04	40.3	8.184E-04
Sum Anions (meg/kg)		-9.723E-01		-9.547E-01		-9.719E-01
Silica (SiO2)	1.2	2.032E-05	9.24	1.562E-04	10.56	1.786E-04
Borate (B)	20	1.883E-03	30	2.818E-03	26.3	2.473E-03
Total Iron	84	1.531E-03	NA		NA	
Uranium	0.00009	3.848E-10	NA		0.006	2.562E-08
Total Dissolved Carbonate		1.883E-03		8.348E-04		7.807E-04
log CO2 Partial Pressure (bars)		-2.61		-2.87		-2.90
Dissolved Solids:						
Sum	57272		55163		56041	
Residue	62000					
Difference	-4728					
Percent of sum	-8.3					
Charge Balance (%):		1.77		-2.65		-2.56
Stoichiometric Ionic Strength		1.107		1.071		1.081
NA = not analysed (1) Reported (2) No density (3) No density						
Density = 1.024 or pH reported. reported.						
Drawn by	Date		Chemical Analyses of Water Samples from the Culebra at the H-3 Hydropad.			
Checked by	Date					
Revisions	Date					
INTERA Technologies			Table 4.1			

Borehole:	H-3b3	H-3b2	H-3b2	H-3b3	H-3b3	H-3b2	H-3b2
Depth (ft):	668.3-668.4	682.	689.3	689.3	689.5	700.5	702.9-703.5
Dolomite	4	96	99	81	88	7	--
Gypsum	--	--	--	16	6	--	74
Quartz	23	2	1	1	1	13	7
Mica	11	tr	--	--	--	8	2
K-spar	5	--	--	--	--	tr	--
Bassanite	4	--	--	tr	--	tr	--
Halite	2	--	--	1	5	1	2
Goethite	4	--	--	--	--	--	--
Clay Min.	47	2	<1	1	<1	71	15
<u>Relative Clay Abundance (normalized to 100%)</u>							
Kaolinite	tr	--	--	--		13	12
Chlorite	18	4	4	3		tr	4
Illite	17	16	22	19		29	12
Smectite	--	--	--	tr		--	--
Mixed-Layer							
Chlorite-Smectite:	65	80	74	78		58	72
Source: Core Laboratories, 1986b.							
Drawn by	Date	Whole-Rock Mineral Composition in Weight Percent, of Core Samples from H-3b2 and H-3b3.					
Checked by	Date						
Revisions	Date						
INTERA Technologies						Table 4.2	

Borehole:	H-3	H-3b3	H-3b3
Date Sampled:	17-Mar-77	11-Jun-84	4-Feb-85
	(Alkalinity as reported)	(Alkalinity = mean of '84 and '85 values)	

Saturation Indices:

Calcite	0.38	0.01	-0.06	-0.11
Dolomite*	0.72	-0.01	-0.08	-0.18
2Cal-Dol*	0.04	0.03	-0.04	-0.04
Gypsum	0.11	0.11	0.09	0.04
Celestite	--	--	-0.04	-0.07
Chalcedony	-1.02	-1.02	-0.13	-0.07
Quartz	-0.57	-0.57	0.31	0.37

* $2 \text{ Cal - Dol} = 2 \times \text{SI}_{\text{Calcite}} - \text{SI}_{\text{Dolomite}}$

Drawn by	Date	Saturation Indices Calculated from Analyses of Water Samples from the Culebra at the H-3 Hydropad.
Checked by	Date	
Revisions	Date	
INTERA Technologies		Table 4.3

Date of Collection:	17-Mar-77		11-Jun-84		4-Feb-85	
pH	7.4		7.3		7.3	
	(Eh, volts)	(pE)	(Eh, volts)	(pE)	(Eh, volts)	(pE)
Uraninite	-0.059	-1.003	---	---	0.033	0.562
Goethite	-0.106	-1.800	-0.151	-2.567	-0.124	-2.111
Fe(OH) _{3am}	0.013	0.225	-0.032	-0.542	-0.005	-0.086

Drawn by	Date	Oxidation Potentials Calculated from Equilibrium between H-3 Culebra Waters and Redox-sensitive Minerals.
Checked by	Date	
Revisions	Date	
INTERA Technologies		Table 4.4

Borehole	H-3b3		
Date	Tracer Solution		
pH	7.394	Adjusted for Calcite Saturation	
Eh (volts)	0.00		
Temp. (C)	24		
Density (g/ml)	1.04		
	mg/l	molality	
Lithium	0.465	6.807E-05	Mean of '84 and '85 samples
Sodium	18000	7.953E-01	Adjusted for charge balance
Potassium	460	1.195E-02	Mean of '84 and '85 samples
Magnesium	804	3.360E-02	Mean of '84 and '85 samples
Calcium	1510	3.827E-02	Mean of '84 and '85 samples
Strontium	26.4	3.060E-04	Mean of '84 and '85 samples
Manganese	0.125	2.311E-06	Mean of '84 and '85 samples
Iron	0.3865	7.030E-06	Mean of '84 and '85 samples
Sum Cations (meq/kg)		9.517E-01	
Fluoride	2.01	1.075E-04	Mean of '84 and '85 samples
Chloride	29500	8.452E-01	'84 sample
Bromide	27.3	3.470E-04	Mean of '84 and '85 samples
Iodide	0.1355	1.085E-06	Mean of '84 and '85 samples
Sulfate	4976.5	5.262E-02	Mean of '84 and '85 samples
Akalinity (CaCO ₃)	41.8	8.484E-04	Mean of '84 and '85 samples
Sum Anions (meq/kg)		-9.517E-01	
Silica (SiO ₂)	9.9	1.674E-04	Mean of '84 and '85 samples
Borate (B)	28.15	2.645E-03	Mean of '84 and '85 samples
Uranium	0.006	2.562E-08	'85 samples
Dissolved Solids:			
Sum	55502		
Charge Balance (%)		-0.01	
Stoichiometric Ionic Strength		1.077	

Drawn by	Date	Estimated Composition of Culebra Formation Fluid at the H-3 Hydropad.
Checked by	Date	
Revisions	Date	

Salt	Grams per Liter of Solution
LiCl	0.0028
NaCl	39.6125
KCl	0.8771
MgCl ₂	3.1495
CaCl ₂	4.1814
SrCl ₂	0.0478
NaF	0.0044
NaBr	0.0352
NaI	0.0002
Na ₂ SO ₄	7.3586
NaHCO ₃	0.0702
Na ₂ SiO ₃	0.0201
H ₂ BO ₃	0.1610
Total	55.5208

Drawn by	Date	Masses of Salts to Produce One Liter of Water of the Type Found in the Culebra at the H-3 Hydropad.
Checked by	Date	
Revisions	Date	
INTERA Technologies		Table 5.3

pH:	7.394	7.300
-----	-------	-------

Saturation Indices

Calcite	0.00	-0.08
Dolomite	0.04	-0.13
2Cal-Dol*	-0.04	-0.04
Gypsum	0.06	0.06
Celestite	0.02	0.02
Chalcedony	-0.10	-0.10
Quartz	0.34	0.34
Total Dissolved Carbonate (mol)		
	7.83E-04	8.08E-04
Log CO ₂ Partial Pressure (bars)		
	-2.99	-2.88

* $2\text{Cal-Dol} = 2 \times \text{SI}_{\text{Calcite}} - \text{SI}_{\text{Dolomite}}$

Drawn by	Date	Saturation Indices of Selected Minerals and Parameters of the Carbonate System Calculated for Culebra Formation Water at Two pH Values.
Checked by	Date	
Revisions	Date	
INTERA Technologies		Table 5.2

Solute	Culebra Water (moles per liter solution)	Artificial Solution
Li+	6.700E-05	6.605E-05
Na+	7.830E-01	7.830E-01
K+	1.177E-02	1.177E-02
Mg+2	3.308E-02	3.308E-02
Ca+2	3.767E-02	3.768E-02
Sr+2	3.013E-04	3.015E-04
F-	1.058E-04	1.048E-04
Cl-	8.321E-01	8.317E-01
Br-	3.417E-04	3.421E-04
I-	1.068E-06	1.334E-06
SO ₄ ⁻²	5.181E-02	5.181E-02
Alk	8.353E-04	8.356E-04
SiO ₂	1.648E-04	1.647E-04
B	2.604E-03	2.604E-03

Drawn by	Date	Comparison Between Compositions of Culebra Formation Water at H-3 Hydropad and Artificial Formation Water From Table 5.3
Checked by	Date	
Revisions	Date	
INTERA Technologies		Table 5.4

Isotope	Half-Life (years)	Dominant Dissolved Species	Reference	Estimated Partition Coefficients (ml/g)
Ni-63	9.20E+01	Ni+2 (NiSO4)	(1)	<50
Sr-90	2.81E+01	Sr+2 (SrSO4)	(2)	<2
Cs-137	3.02E+01	Cs+	(3)	<50
Sm-151	9.30E+01	Sm+3	(4)	>c. 10000
Eu-152	1.30E+01	Eu+3	(4)	>c. 10000
Eu-154	1.60E+01			

References:

- (1) By analogy with Fe+2 in Culebra water.
- (2) Calculated for Culebra water.
- (3) By analogy with K+ in Culebra water.
- (4) From Pourbaix (1974) and Baes and Mesmer (1976), considering hydrolysis only.

c. = approximately

NOTE: Estimated partition coefficients are based on distribution coefficients reported in Table 5.8

Drawn by	Date	Properties of Fission Product Nuclides of Possible Importance in Projected WIPP Waste Inventory.
Checked by	Date	
Revisions	Date	
INTERA Technologies		Table 5.5

Isotope	Half-Life (years)	Dominant Dissolved Species	Reference	Estimated Partition Coefficients (ml/g)
U-233	1.62E+05	VI	(1)	<10
Np-237	2.14E+06	V+VI	(2)	<20
Pu-236	2.85E+00	V+VI	(3)	>c. 50
Pu-238	8.60E+01	III	(4)	
Pu-239	2.44E+04			
Pu-240	6.58E+03			
Pu-241	1.32E+01			
Pu-242	3.79E+05			
Am-241	4.58E+02	III	(2)	>c. 50
Am-243	7.37E+03			
Cm-244	1.76E+01	III	(5)	>c. 1000
Cf-252	2.65E+00	?		

References:

- (1) Calculated for Culebra water.
- (2) Cleveland et al. (1985), concordant with Pourbaix (1974).
- (3) Cleveland et al. (1985).
- (4) Pourbaix (1974).
- (5) By analogy with americium.

c. = approximately

NOTE: Estimated partition coefficients are based on distribution coefficients reported in Table 5.8

Drawn by	Date	Properties of Actinide Nuclides of Possible Importance in Projected WIPP Waste Inventory.
Checked by	Date	
Revisions	Date	
INTERA Technologies		Table 5.6

Water Reference	Culebra Water (1)		Brine "A" (2)		Brine "B" (2)		Solution "C" (2)		WIPP (3)		H-3b3 This Report	
pH	7.50		6.50		6.50		7.50		7.90		7.300	
Temp. (C)	25		25		25		25		25		24	
Density (g/ml)	1.00		1.20		1.20		1.00		1.00		1.04	
	mg/l	molality	mg/l	molality	mg/l	molality	mg/l	molality	mg/l	molality	mg/l	molality
Lithium	0	0.000E+00	20	3.214E-03	0	0.000E+00	0	0.000E+00	0	0.000E+00	0.465	6.807E-05
Sodium	2850	1.253E-01	42000	2.037E+00	115000	5.527E+00	100	4.362E-03	6000	2.665E-01	18000	7.954E-01
Potassium	105	2.715E-03	30000	8.555E-01	15	4.239E-04	5	1.283E-04	190	4.962E-03	460	1.195E-02
Cesium	0	0.000E+00	1	8.389E-06	1	8.313E-06	1	7.546E-06	0	0.000E+00	0	0.000E+00
Magnesium	140	5.822E-03	35000	1.606E+00	10	4.546E-04	200	8.253E-03	480	2.016E-02	804	3.360E-02
Calcium	685	1.728E-02	600	1.669E-02	900	2.481E-02	600	1.501E-02	680	1.732E-02	1510	3.827E-02
Strontium	0	0.000E+00	5	6.363E-05	15	1.891E-04	15	1.717E-04	0	0.000E+00	26.4	3.060E-04
Manganese	0.17	3.128E-06	0	0.000E+00	0	0.000E+00	0	0.000E+00	0.1	1.859E-06	0.000E+00	0.000E+00
Iron	0.065	1.176E-06	2	3.993E-05	2	3.957E-05	1	1.796E-05	0.15	2.742E-06	0.000E+00	0.000E+00
Sum Cations (meq/kg)		1.742E-01		6.141E+00		5.578E+00		5.141E-02		3.464E-01		9.517E-01
Fluoride	1.8	9.577E-05	0	0.000E+00	0	0.000E+00	0	0.000E+00	1.8	9.674E-05	2.01	1.075E-04
Chloride	3750	1.069E-01	190000	5.976E+00	175000	5.453E+00	200	5.658E-03	8200	2.362E-01	29500	8.452E-01
Bromide	0	0.000E+00	400	5.582E-03	400	5.531E-03	0	0.000E+00	0	0.000E+00	27.3	3.470E-04
Iodide	0	0.000E+00	10	8.786E-05	10	8.706E-05	0	0.000E+00	0	0.000E+00	0.1355	1.085E-06
Sulfate	3100	3.262E-02	3500	4.063E-02	3500	4.026E-02	1750	1.827E-02	5000	5.315E-02	4976.5	5.262E-02
Alkalinity-CaCO3	48.8	9.857E-04	574	1.279E-02	8.2	1.810E-04	82	1.643E-03	59	1.204E-03	41.8	8.484E-04
Sum Anions (meq/kg)		-1.732E-01		-6.075E+00		-5.540E+00		-4.384E-02		-3.438E-01		-9.517E-01
Silica (SiO2)	2.6	4.374E-05	0	0.000E+00	0	0.000E+00	0	0.000E+00	11	1.869E-04	9.9	1.674E-04
Borate (B)	1.79	1.674E-04	221	2.280E-02	1.8	1.840E-04	0	0.000E+00	0	0.000E+00	28.15	2.645E-03
Total Dissolved Carbonate		1.015E-03						1.710E-03		1.171E-03		8.075E-04
log CO2 Partial Pressure (bars)	-2.84						-2.57		-3.22			-2.88
Sum Dissolved Solids:	10674		303137		294868		2921		20598		55504	
Ion Balance (%)		0.57		1.07		0.69		15.89		0.77		0.00
Stoichiometric Ionic Strength		0.459		15.542		11.249		0.179		0.871		2.153
Saturation Indices:												
Calcite	0.06		--		--		0.40		0.42			-0.08
Dolomite	-0.28		--		--		0.59		0.98			-0.13
XCal-Dol	0.40		--		--		0.20		-0.14			-0.04
Gypsum	-0.01		--		--		-0.06		-0.01			0.06
Celestite	--		--		--		0.06		--			0.02

References:

- (1) Lynch and Dosch (1980, Tab 1, pH=8.4); Dosch (1981, Tab 1, pH=7.5).
- (2) Setne (1977, Tab I); Dosch and Lynch (1978, Tab 2); Dosch (1981, Tab 1).
- (3) Cleveland et al. (1985, Tab I).

Drawn by	Date	Composition of Waters Used for Measurements of Sorption Coefficients and Actinide Speciation with Culebra Core Material.
Checked by	Date	
Revisions	Date	
INTERA Technologies		Table 5.7

Element	Ref- er- ence	Distribution Coefficient (Kd), in ml/g			
		Culebra Water (1)	Brine "A" (2)	Brine "B" (2)	Solution "C" (2)
Water Reference					
	Cesium (3)		<1	1-2	7-10
	(4)	9.0-68.3		0.2-2.4	11-16
	(6)				
Strontium	(3)		<1	1-2	4-5
	(4)	0.3-0.6		0.0-1.7	0.0-2.4
	(6)				
Iodide	(3)		<1	<1	<1
Europium	(3)		>1E+04	>1E+04	>1E+04
	(4)	0.9-1.2E+04			
Uranium	(5)	1.1-7.4	0.9-1.6	2.6-27	13-69
	(6)			0.0-1.5	0-13
Neptunium	(6)			10.0-12.6	5.7-10.5
Plutonium	(3)			2.1E+03	7.3E+03
	(4)	1.1-4.5E+03		0.5-2.3E+02	0.04-2.2E+03
	(6)				
Americium	(3)			2.6E+03	2.2E+04
	(4)	4.8-7.7E+03		0.3-1.2E+03	2.6-2.9E+03
	(6)				
Curium	(3)			1.2E+04	1.1E+05
	(6)			0.0-12.4E+03	1.6-2.2E+03

References:
(1) Lynch and Dosch (1980, Tab 1); Dosch (1981, Tab 1).
(2) Serne et al. (1977, Tab I); Dosch and Lynch (1978, Tab 2); Dosch (1981, Tab 1).
(3) Dosch and Lynch (1978, Tab 7).
(4) Lynch and Dosch (1980, Tab IIIB dolomites).
(5) Dosch (1981, Tab 5 dolomites).
(6) Serne et al. (1977, Tab 12d, 13b).

Drawn by	Date	Distribution Coefficient (Kd) Values Measured on Culebra Core Material.
Checked by	Date	
Revisions	Date	

INTERA Technologies	Table 5.8
----------------------------	-----------

Divalent Cation (Ion Size, AU)	Total Moles of Divalent Cations (molality)	%	Free Ion (molality)	%	Complex with SO ₄ O (molality)	%
Mg (0.65)	3.4E-02	100	2.9E-02	85	4.6E-03	15
Iron (0.76)	7.0E-06	100	6.3E-06	90	7.0E-07	10
Calcium (0.99)	3.8E-02	100	3.3E-02	87	5.0E-03	13
Strontium (1.13)	3.1E-04	100	2.7E-04	87	3.7E-05	13

Notes:

AU - Angstrom Units

Drawn by	Date	Speciation of Divalent Cations in H-3 Culebra Water.
Checked by	Date	
Revisions	Date	
INTERA Technologies		Table 5.9

Element	Estimated Solubility (Molality)	Ref-er-ence	Waste and Possible Tracer Isotopes	Half-life (years)	Injection Amount for Peak Concentration of 100 pCi/l at Two years		
					Total Mass (Curies)	(moles)	Volume at Sat-uration (liters)
Nickel	7E-06	(1)	Ni- 63	9.20E+01	1.02E-02	2.61E-06	3.73E-01
Cobalt proxy for nickel	7E-06	(1)	Co- 58	1.95E-01	1.21E+01	6.63E-06	9.47E-01
	7E-06		Co- 60	5.26E+00	1.30E-02	1.91E-07	2.74E-02
Strontium	3E-04	(2)	Sr- 85	1.75E-01	2.73E+01	1.34E-05	4.46E-02
	3E-04		Sr- 89	1.42E-01	1.69E+02	6.74E-05	2.25E-01
	3E-04		Sr- 90	2.81E+01	1.05E-02	8.26E-07	2.75E-03
Cesium	8E-06	(6)	Cs- 134	2.05E+00	1.97E-02	1.13E-07	1.41E-02
	8E-06		Cs- 137	3.02E+01	1.05E-02	8.85E-07	1.11E-01
Uranium	3E-09	(3)	U- 230	5.69E-02	3.73E+08	5.95E+01	1.98E+10
	3E-09		U- 232	7.36E+01	1.02E-02	2.10E-06	6.99E+02
	3E-09		U- 233	1.62E+05	1.00E-02	4.53E-03	1.51E+06
Neptunium	3E-10	(4)	Np- 235	1.12E+00	3.44E-02	1.08E-07	3.60E+02
	3E-10		Np- 237	2.14E+06	1.00E-02	5.99E-02	2.00E+08
Plutonium	4E-10	(5)	Pu- 236	2.85E+00	1.63E-02	1.30E-07	3.24E+02
	4E-10		Pu- 237	1.25E-01	6.64E+02	2.32E-04	5.80E+05
	4E-10		Pu- 238	8.60E+01	1.02E-02	2.44E-06	6.11E+03
	4E-10		Pu- 240	6.85E+03	1.00E-02	1.92E-04	4.79E+05
	4E-10		Pu- 241	1.32E+01	1.11E-02	4.10E-07	1.03E+03

References:

- (1) Mean analysed iron concentration in 1984 and 1985 samples (Table 4.1). Cobalt and nickel solubility should be higher (Pourbaix, 1974; Baes and Mesmer, 1976).
- (2) Calculated for H-3 Culebra water at celestite saturation (Table 4.1).
- (3) Calculated for uraninite saturation in H-3 Culebra waters at Eh = 0.0 volts; equals one-tenth uranium concentration analyzed in 1985 sample (Table 4.1).
- (4) Pourbaix (1974); Cleveland et al. (1985), suggest c. 8E-09.
- (5) Cleveland et al. (1985), with element in (V+VI) oxidation state. At Eh and pH of H-3 Culebra water, Pourbaix (1974) shows element in (III) state with solubility c. 3E-14.
- (6) Corresponds to 1 mg/l as used in laboratory measurements leading to Kd values summarized in Table 5.8.

Drawn by	Date	Possible Sorbing Tracer Isotopes and Input Concentrations Required for Peak Concentrations of 100 pCi/l at Pumping Well if Breakthrough Peak is at Two Years.
Checked by	Date	
Revisions	Date	

INTERA Technologies

Table 5.10

Conser- vative Tracer Isotopes	Half- Life (days)	Injection Amount for Peak Breakthrough of 100 pCi/l Total Mass		Molality in Culebra Water
		(milli- curies)	(milli- moles)	

H-3b1 to H-3b3 Flow Path
3.5 day Peak Arrival Time

H- 3	4.48E+03	3.30E-02	4.14E-04	1.10E+02
Br- 82	1.48E+00	1.70E-01	7.04E-07	3.47E-04
I- 131	8.07E+00	4.46E-02	1.01E-06	1.08E-06

H-3b2 to H-3b3 Flow Path
26.3 day Peak Arrival Time

H- 3	4.48E+03	2.91E-01	3.65E-03	5.50E+01
Br- 82	1.48E+00	6.53E+04	2.70E-01	3.47E-04
I- 131	8.07E+00	2.78E+00	6.27E-05	1.08E-06

Drawn by	Date
Checked by	Date
Revisions	Date

Possible Conservative Tracer Isotopes with
Input Concentrations Required for Peak
Concentrations of 100 pCi/l at Pumping Well.

INTERA Technologies

Table 5.11

APPENDIX

THERMOCHEMICAL DATA BASE

APPENDIX: THERMOCHEMICAL DATA BASE

Intera Technologies, Inc.
6850 Austin Center Blvd. Suite 300
Austin, TX 78731

List of Figures and Tables

Table:

- 1 Values of parameters in activity coefficient equations for individual ions. Truesdell-Jones coefficients from Truesdell and Jones (1974). WATEQ coefficients calculated for this data set (see text).
- 2 Values for stability constants for carbonate and sulfate ion pairs of divalent cations.
- 3 Values of stability constants for aluminum hydrolysis species and gibbsite.
- 4 Thermodynamic data for aqueous species.
- 5 Thermodynamic data for minerals.

Figure:

- 1 GRAPH OF CALCULATED AND MEAN-SALT VALUES FOR THE ACTIVITY COEFFICIENT OF Ca^{+2} WITH IONIC STRENGTH.
- 2 GRAPH OF CALCULATED AND MEAN-SALT VALUES FOR THE ACTIVITY COEFFICIENT OF SO_4^{-2} WITH IONIC STRENGTH.
- 3 GRAPH OF CARBONATE ION PAIR PROPERTIES AGAINST CARBONATE MINERAL PROPERTIES.
- 4 GRAPH OF SULFATE ION PAIR PROPERTIES AGAINST SULFATE MINERAL PROPERTIES.

A.1. INTRODUCTION

This text describes the thermodynamic data base used to make geochemical calculations in support of this report. The explanatory text begins with a discussion of the principles underlying the selection of the data. This is followed by discussions of the data for individual minerals and for selected solute species. Finally, complete citations to the sources of all data are given.

Although thermodynamic data are independent of any particular geochemical computer model, the fact that these data were to be used principally with PHREEQE (Parkhurst, and others, 1980, INTERA, 1983a) influenced the structure of the data base. For example, PHREEQE treats redox reactions using the concept of operational valence (OPV), so the value of the OPV for each species is given. Likewise, PHREEQE uses logarithms of equilibrium constants (logK) to characterize reactions rather than Gibbs energies of phases and aqueous species. Thus, logK values are stressed in the data base and experimentally determined logK values are taken as the preferred sources of data from which other thermodynamic properties are calculated.

These data could be equally well be used with a number of other geochemical codes which employ the ion-pair model of solution behavior. Such codes include, for example, codes in the WATEQ series (Truesdell and Jones, 1974, Plummer and others, 1976, Ball, and others, 1980), MINEQL (Schweingruber, 1983), and EQ3/EQ6 (Wolery, 1983, INTERA, 1983b). The same results as given in the body of this report should be obtained with any of these or similar codes if used with this data set (INTERA, 1983c).

A.2. DESCRIPTION OF DATA

A.2.1 Aqueous Species

Thermodynamic data for aqueous species are given in Table A-4. The first thirty species are the "master species" of PHREEQE (Parkhurst and others, 1980) or the "basis species" of EQ3/EQ6 (Wolery, 1983). They are the species in terms of which the association reactions of all subsequent species are written.

First Line:

Species number, chemical formula, and sources of data chosen. Numbered references to the sources of data for each species and mineral are given. The full reference corresponding to each number is given in Section A.5.1, below. The letter and symbol codes have the following meanings:

C: Source gives coefficients for $\log K(T)$ expression.

K: Source gives value for $\log K(25)$.

Gr,Hr,Sr: Source gives Gibbs energy, enthalpy or entropy of reaction data, respectively.

G,H,S: Source gives Gibbs energy, enthalpy or entropy of formation data, respectively.

"=": The data sources give the same values.

",,": Data from both sources are combined to reach the value given.

Second line:

Gibbs energy (ΔG°_f), enthalpy (ΔH°_f) and entropy (ΔS°_f) of formation of the species in its standard state at 25°C and 1 bar, in kilojoules/mol, kilojoules/mol and joules/mol/K, respectively. Entropies of formation are discussed in Section A.3.3, below.

Gibbs energy (ΔG°_r), enthalpy (ΔH°_r) and entropy (ΔS°_r) of the association reaction for the species in its standard state at 25°C and 1 bar, in the same units as above.

Third Line:

Thor (operational valence or OPV of PHREEQE) of each species. The operational valence is the valence of any species which can be oxidized or reduced under natural conditions. It is required for the conservation of electron equations used in PHREEQE for calculations of redox reactions, and is described in detail in the documentation for that code (Parkhurst and others, 1980, p. 6-11).

Charge of species.

Debye-Hückel a° value, discussed in section A.3.5.

Value of logK of the association reaction at 25°C.

Left Side, Fourth, Fifth, Sixth and Subsequent Lines:

These lines contain the headings and data describing the association reaction for the aqueous species. The stoichiometric coefficient, chemical formula, and number (in this data base) of each component species of the reaction forming the species appear in the sixth and subsequent lines. The Gibbs energy, enthalpy and entropy of reaction and the logK values are for this reaction.

Right side, Fourth through Eighth Lines:

These lines contain coefficients A through E for the expression:

$$\log K(T) = A + B \cdot T + C/T + D \cdot T^2 + E/T^2 \quad (1)$$

This is the expression used in WATEQ and PHREEQE. Other expressions, as used in EQ3/EQ6 or more consistent with the Maier-Kelly heat capacity equation, might be more appropriate for other geochemical models.

A.2.2 Mineral and Redox Pairs

Data for minerals are given in Table A-5. The form of the entries in this table is the same as that for the aqueous species and described in the preceding section. Note that the mineral reactions are written as dissociation reactions, rather than as association reactions as are those for the dissolved species. The method for developing the reactions for calculation of oxidation potential is described in Section A.3.4, below.

A.3 DISCUSSION

A.3.1 Sources of Data

A number of previous compilations of thermodynamic data were drawn upon to develop this data base.

CODATA (1978, 1980) values of ΔH°_f and S° were used whenever available for elements and aqueous species. Few CODATA values have been published for minerals included in this data base.

Data sets accompanying the PHREEQE program (Parkhurst and others, 1980) and several of the predecessor WATEQ programs (Ball, and others, 1980; Plummer and others, 1976; and Truesdell and Jones, 1974) are the sources of the $\log K(25)$ and ΔH°_r values for many of the aqueous ion pairs. These sources were also considered in choosing mineral data.

Data from what is referred to here as the Perkins/Berman data set accompany the version of PATH running at the University of Bern, Switzerland. With few exceptions, these data are identical to those published by Helgeson and others (1978, 1981). The Perkins/Berman data set includes ΔH°_f and S° values from which the $\log K(25)$ and ΔH°_r values discussed below were calculated.

Data published by the National Bureau of Standards (Wagman, and others, 1982) includes ΔG°_f , ΔH°_f and S° data for many aqueous species and minerals. Values of $\log K(25)$ and ΔH°_r discussed below were calculated from the ΔG°_f and ΔH°_f given.

The U. S. Geological Survey data base (Robie and others, 1978, 1979) was also used. As with the NBS data, the $\log K(25)$ and ΔH°_r values discussed below were calculated from the ΔG°_f and ΔH°_f values in this data set.

Data used by the Swiss Federal Institute for Reactor Research (EIR) have also been considered (Schweingruber, 1983, 1984; Wanner, 1986).

References to the sources of data are given for most species and minerals. Data for those entries for which no references are given are from the data set accompanying the original release of PHREEQE (Parkhurst and others, 1980). The PHREEQE data were, in turn, taken from the WATEQ2 data set (Ball and others, 1980) and the original WATEQ data set (Truesdell and Jones, 1974).

Sources of the Debye-Hückel a° values are discussed in section A.3.5.

A.3.2 Internal Consistency of Data

The data for any species or mineral are internally consistent, and obey the appropriate thermodynamic equalities such as:

$$\Delta G^\circ = \Delta H^\circ - T \Delta S^\circ. \quad (2)$$

$$\Delta G^\circ_r = -RT \ln K(25) \quad (3)$$

$$\Delta H^\circ_r = R T^2 d(\log K(T))/dT \quad (4)$$

This consistency is maintained by calculating all values from the "highest" data available. The data rank from "highest" to "lowest" as follows:

Coefficients for the equation for $\log K(T)$ as a function of temperature, such as values of A through E in equation (1);

$\log K(25)$;

ΔG , H, and S° of reaction;

ΔG , H, and S° of formation.

For example, if values for some or all of the coefficients of the $\log K$ expression are available, the values which appear in the table are calculated from them as follows:

Evaluate equation (1) at $T = 298.15K$ to find $\log K(25)$;

Calculate ΔG°_r using equation (3);

Calculate ΔH°_r using equation (4) at $T = 298.15K$.
For equation (1) for $\log K(T)$, this expression is:

$$\Delta H^\circ_r = 2.303 * 0.00813 * 298.15^2 * (B - C/298.15^2 + 2 * D * 298.15 - 2 * E / 298.15^3) \quad (5)$$

Calculate ΔS°_r using:

$$\Delta S^\circ_r = (\Delta H^\circ_r - \Delta G^\circ_r) / 298.15 \quad (6)$$

Calculate ΔG , H and S°_f from the ΔG , H, and S°_r values just found and the ΔG , H, and S°_f values of the reactant species (in the case of the association reactions of dissolved species) or product species (in the case of mineral dissolution reactions).

For many species and minerals, only values $\log K(25)$ and the standard enthalpy of reaction (ΔH°_r) are available. For these substances the coefficients of equation 1 are set to zero and the Gibbs energy and entropy of reaction are calculated from the available values of $\log K(25)$ and enthalpy of reaction. Gibbs energies, enthalpies, and entropy of formation are found from the reaction values and the Gibbs energy, enthalpy, and entropy values of formation of the species reacting to form the dissolved species or produced by dissolving minerals.

Many compilations of thermodynamic data, including those of the CODATA group (1978, 1980) and Wagman et al. (1982) give only the enthalpies (ΔH°_f) absolute entropies (S°_f) and in some cases Gibbs energies (ΔG°_f) of formation of species and minerals. Direct comparison of properties of formation from one compilation to another can be misleading unless all are first normalized to a common set of properties for the elementary species in terms of which all reactions are written. Those elementary species are the basis species of EQ3/EQ6 (INTERA, 1983b; Wolery, 1983) or the master species PHREEQE (INTERA, 1983a; Parkhurst et al., 1980).

To assure that values given in this data base would be internally consistent regardless of their source, the following procedure was followed:

From the (presumably) internally consistent values of the properties of formation of species and minerals given in data compilations such as those mentioned above, values of $\log K(25)$ and of reaction enthalpies were calculated. These values were then compared with those from other sources and the selected ones entered into this data base. Properties of formation were then calculated as described above. The values of the properties of formation of the species or minerals in this data base will be the same as those in the referenced source compilation only if the properties of the elementary species in this and the source compilation are the same.

A.3.3 Entropy Values

The entropies given are not the usual absolute entropies S°_f , but are the entropies of formation of the species or minerals from their component elements at 25°C and 1 bar, ΔS°_f . This facilitates the use of equation (6) relating ΔG° to ΔH° and ΔS° .

Wagman and others (1982, p.2-16) point out that the "best" values for ΔH°_f and ΔG°_f of ions are often derived from solution data, while "best" values for absolute entro-

pies are usually taken from "thermal" data and are independent of solution processes. Thus, compilations of "best" data on dissolved species may not rigorously obey equation (2). To make this data base rigorously consistent internally, the following convention was adopted:

When the original source of data included both ΔH_f° and ΔG_f° , ΔS_f° for the species was calculated using equation (2).

When only ΔH_f° and absolute entropies were available, ΔS_f° values were first calculated using:

$$\Delta S_f^\circ = S_{f,ion}^\circ - \sum S_{f,elements}^\circ + (n/2) S_{f,H_2(g)}^\circ$$

where n = charge of the ion (Wagman and others, 1982, p.2-22). Then ΔG_f° values were calculated using equation (2).

A.3.4 Calculation of Oxidation Potentials

If concentrations of both members of an oxidation-reduction couple are available, the PE value corresponding to that couple can be calculated in a manner similar to that used to calculate mineral saturation indices (SI's). The reaction for the oxidation of R to O can be written (Garrels and Christ, 1965, Chapter 7):



with equilibrium constant:

$$\log K(T) = \log a_O + n \log a_{H^+} + m \log a_{e^-} - \log a_R. \quad (8)$$

By definition, $PE = -\log a_{e^-}$, so the $\log K(T)$ expression can be rewritten:

$$PE = -\log K(T)/m + (\log a_O + n \log a_{H^+} - \log a_R)/m. \quad (9)$$

The saturation index, SI is written:

$$SI = \log IAP - \log K(T) \quad (9a)$$

where IAP is the value of the ion activity product in the solution of interest. Equation (9a) has the same form as the PE expression (9). Thus, if reaction (7) is written for the transfer of one-electron, $\underline{a. q.}$, so that m in (7), (8) and (9) equals one, the SI calculated for it in the usual manner will equal its PE.

The reactions such as (7) used to calculate PE values are association reactions forming "minerals" which are single

electrons. The delta G, delta H and delta S of formation of the electron is zero, and is so entered in the data base. The delta G, delta H, delta S and logK(25) values for the reactions are then determined by the properties only of the reactant species. The use of the saturation index routine of PHREEQE to calculate PE values is described in the documentation for that program (Parkhurst, and others, 1980, p.59).

Field data are frequently reported as Eh values rather than as PE's. The two are related by the expression:

$$Eh = (\ln 10 R^*T/F)*PE \quad (10)$$

where: $\ln 10$ = natural log of 10
 R = gas constant
 F = Faraday's constant
 T = Absolute temperature

For EH in volts and temperature in Celsius equation (10) becomes:

$$PE = Eh*5040.07/(273.15 + temperature) \quad (11)$$

A.3.5 Activity Coefficients of Solute Species

Activity coefficients of dissolved species in solutions of ionic strengths of less than a few tenths molal can be calculated using the extended Debye-Hückel equation:

$$\log \gamma_i = - \frac{A*z_i^2*I^{0.5}}{1 + B*a_o*I^{0.5}}$$

in which: A and B are temperature-dependent functions of the density and dielectric constant of water. Values of A and B are calculated in WATEQ, and PHREEQE and they also appear in tables in many standard texts (e.g., Nordstrom and Munoz, 1985, Table 7-3). At 25°C, A = 0.5092 and B = 0.3283;

z_i is the charge of ion i;

I is the ionic strength of the solution given by $I = 1/2 \sum M_i Z_i^2$; and

a_o is the Debye-Hückel ion-size parameter.

Values of a_o in this data base are taken from Table 24 of Whitfield (1979), except as follows:

Values for Ca^{+2} and Sr^{+2} and by analogy for Mg^{+2} and Ba^{+2} , and for the carbonate species and their complexes are from Plummer and Busenberg (1982) and Busenberg and others (1984).

Values for Al^{+3} and its complexes are those used by Roberson and Hem (1969) and Smith and Hem (1972).

Values not given in these sources were estimated based on the similarity of the unknown species to other, listed species. The errors introduced by this procedure are thought to be less than those which would have come about by calculating activity coefficients using the Davies equation (Plummer and Busenberg, 1982).

In more concentrated solutions, activity coefficients calculated using the extended Debye-Hückel equation are likely to be seriously in error. Thus the WATEQ Debye-Hückel equation, which is useful up to ionic strengths of several molal, was employed for the calculations described in the body of this report. This semi-empirical equation was developed by Truesdell and Jones (1974) for use in their original WATEQ program for aqueous speciation calculations, and it has been included in the subsequent versions of WATEQ and is present in PHREEQE as an option for calculating activity coefficients. This equation is also discussed by Nordstrom and Munoz (1985, Sect. 7-6) who refer to it as the Truesdell-Jones equation

The WATEQ Debye-Hückel equation is written:

$$\log \gamma_i = - \frac{A \cdot z_i^2 \cdot I^{0.5}}{1 + B \cdot a_w \cdot I^{0.5}} + b_w \cdot I$$

where: A, B, z_i and I have the same meanings as in the extended Debye-Hückel equation described above, and

a_w and b_w are the WATEQ Debye-Hückel individual ion activity coefficient parameters. These are determined by fitting the WATEQ Debye-Hückel equation to experimental mean-salt activity coefficient data as described by Truesdell and Jones (1974).

Values for WATEQ Debye-Hückel coefficients are not included in this data base, but are included in the PHREEQE data set derived from these data and used for the calculations described in the body of the report. Table 1 gives values for

the WATEQ Debye-Hückel coefficients and for the a_0 parameter required for the extended Debye-Hückel equation. The columns labeled Truesdell-Jones Coefficients include the a_w and b_w values originally given by those authors (1974, Table 2; see also, Nordstrom and Munoz, 1985, Table 7-6). The columns labeled WATEQ D-H Fitted Coefficients include newly fitted values for a_w and b_w . These values were determined by a least-squares fit of the WATEQ Debye-Hückel equation to experimental ion activities calculated from mean-salt data given by Robinson and Stokes (1959) using the conventions described and adopted by Truesdell and Jones (1974). It was necessary to calculate the coefficients for Sr^{+2} and UO_2^{+2} , for this work and for consistency, values for the remaining ions were recalculated.

The new values were fit to data in the range of ionic strengths of 0 to 3 molal, and they agree well with the original Truesdell and Jones values. Figures 1 and 2 illustrate how well activity coefficients calculated for Ca^{+2} and SO_4^{-2} using the two equations and sets of parameters reproduce the mean-salt data.

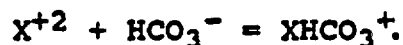
A.4 SELECTION OF DATA

A.4.1 Aqueous Species

Divalent Cation - Carbonate Ion Pairs: Values for $\log K(25)$ and ΔH_r for the carbonate (XCO_3^0) and bicarbonate ($XHCO_3^+$) ion pairs with the cations Mg^{+2} , Ca^{+2} , Sr^{+2} , Ba^{+2} , Mn^{+2} , and Fe^{+2} are given in Table 2. Two columns appear for the bicarbonate species: The first is for the reaction:



which is the way the ion association reaction is written in the data base. The second column is for the reaction:



The value in the second column equals that of the first minus 10.33 for $\log K(25)$ and minus -14.90 for ΔH_r . The values subtracted are those for the reaction:



Data for the Ca^{+2} and Sr^{+2} pairs are those given by Plummer and Busenberg (1982) and by Busenberg and others (1984), respectively. The data selected for the minerals calcite ($CaCO_3$) and strontianite ($SrCO_3$) are taken

from the same work and so are internally consistent with the ion pair data.

Data for the Mg^{+2} pairs and $MnHCO_3^+$ are taken from the PHREEQE data base and its predecessor WATEQ data bases.

No measured values for the Ba^{+2} pairs were found so the data in the table were estimated. Figure 3 shows plots of the $\log K(25)$ and ΔH_r values of the ion pairs against equivalent values for the carbonate minerals of the cations. The Mg^{+2} values are not included because $MgCO_3$ does not have the same crystal structure as the carbonate minerals of the other divalent ions. As the figure shows, the $\log K(25)$ values for the CO_3^0 pairs of Mn^{+2} , Sr^{+2} , and Ca^{+2} correlate well with the $\log K(25)$ values of their carbonate minerals and a value for the $BaCO_3^0$ pair is readily assumed. $\log K(25)$ values are available only for the $CaHCO_3^+$ and $SrHCO_3^+$ pairs so the $\log K(25)$ value for $BaHCO_3^+$ was estimated from them.

ΔH_r values for the Ba^{+2} pairs were estimated the same way. As Figure 3 shows, ΔH_r of $MnCO_3^+$ does not group well with the values for Ca^{+2} and Sr^{+2} and was not used in estimating the Ba^{+2} values.

Divalent Cation - Sulfate Ion Pairs: Values for $\log K(25)$ and ΔH_r for the sulfate ion pairs and sulfate minerals of the divalent cations are also given in Table 2. Literature values are available for all XSO_4^0 pairs except $BaSO_4^0$. Values for this pair used in the data base were estimated from correlation with the values of the sulfate minerals, as was done for the carbonate ion pairs. As Table 2 shows, the $\log K(25)$ values for all XSO_4^0 pairs are so similar, that the $\log K(25)$ value for $BaSO_4^0$ can be estimated with little error. As Figure 4 shows, the correlation among the several values for ΔH_r is poor, and the ΔH_r value for $BaSO_4^0$, which was based on extrapolation from the values for $CaSO_4^0$ and $SrSO_4^0$, may be significantly in error.

Aluminum Hydroxide Solution Complexes: The formation of these entities can be written:



Values of $\log K(25)$ and ΔH_r for this reaction from a number of sources are given in Table 3.

The $\log K(25)$ values for gibbsite from Hemingway and others (1978), May and others (1979) and the Perkins/Berman data set are the same within the errors quoted. The Perkins/Berman, Wagman and others (1982) and Hem-

ingway and others (1978) values of ΔH°_r also are in good agreement.

The $\log K(25)$ values for the aluminum species given by May and others (1979) are an internally consistent set based on experimental solubility data. Total dissolved aluminum concentrations calculated from them (May and others, 1979, figure 3) are virtually the same as those given by the data of Baes and Mesmer (1976, figure 6.4c) if the $\text{Al}(\text{OH})_3^0$ species is left out. The $\log K(25)$ data of May and others (1979) were selected.

The ΔH°_r value of Wagman and others (1982) for $\text{Al}(\text{OH})_4^-$ and of Baes and Mesmer (1976) for $\text{Al}(\text{OH})^{+2}$ were chosen. A value of 90 kilojoules/mole was estimated for $\text{Al}(\text{OH})_2^+$ by interpolation between the values for the other two species.

A.4.2 Minerals

Calcite CaCO_3 : The values chosen are based on the equation for $\log K(T)$ given by Plummer and Busenberg (1982). They compare with the other data considered as follows:

	<u>$\log K(25)$</u>	<u>ΔH°_r</u>
Data chosen:	-8.48	-9.61
Original PHREEQE:	-8.48	-10.80
Perkins/Berman:	-8.52	-11.78
Wanner (1986):	-8.36	-13.18
Wagman and		
others (1982):	-8.304	-13.05
Robie and		
others (1979):	-8.305	-12.60

The Plummer and Busenberg (1982) data are consistent with the data adopted for the ion pairs of calcium and the carbonate species in this data base.

Dolomite $\text{CaMg}(\text{CO}_3)_2$: The values chosen are those from the original PHREEQE data set. They compare with the other values considered as follows:

	<u>logK(25)</u>	<u>delta H^o_r</u>
Data chosen: Perkins/Berman	-17.00	-34.685
Disordered dolomite:	-16.52	-46.36
Ordered dolomite:	-18.06	-34.12
Wanner (1986):	-17.00	-34.98
Wagman and Others (1982):	-17.41	-37.66
Robie and Others (1979):	-17.09	-39.48

These values range from those representative of high-temperature, well-ordered dolomites to disordered sedimentary dolomites (see Helgeson and others, 1978). Waters from three dolomitic aquifers, the karstic Malm and the Schilfsandstein/Gansinger Dolomite in northern Switzerland and the Edwards aquifer in Texas, appear to be in equilibrium with a dolomite with $\log K(25) = -17.0$ (Pearson and Lolcama, in preparation; Pearson and Rettman, 1976). However, waters from a fourth dolomitic aquifer, the Muschelkalk of northern Switzerland, are more consistent with a value of -16.8. This difference may be a result of slight differences in composition or crystallinity between the dolomites of the several formations.

Strontianite SrCO_3 : The values chosen are as given by the equation for $\log K(T)$ of Busenberg and others, (1984). They compare with the other data considered as follows:

	<u>logK(25)</u>	<u>delta H^o_r</u>
Data chosen:	-9.27	-1.67
Original PHREEQE:	-9.25	-2.89
Wanner (1986):	-9.03	-0.42
Wagman and Others (1982):	-9.25	-2.84
Robie and others (1978):	-8.81	-4.26

The data chosen are consistent with the data in this data base for the ion pairs of strontium and the carbonate solution species and with the calcite data.

Witherite BaCO_3 : The data chosen are from the WATEQ2 data set (Ball and others, 1980). They compare with values derived from the other data sets examined as follows:

	<u>logK(25)</u>	<u>delta H^o_r</u>
Data chosen:	-8.58	1.51
Wagman and Others (1982):	-8.59	1.52
Robie and others (1978):	-7.63	-3.93

Rhodochrosite MnCO_3 : The values selected for logK(25) and delta H^o_r are derived from delta G^o_f and delta H^o_r values of Robie and others (1979). They compare with the values for the other data sets considered as follows:

	<u>logK(25)</u>	<u>delta H^o_r</u>
Data chosen:	-10.54	-8.57
Perkins/Berman:	-10.53	-8.61
Wanner (1986):	-10.52	-8.66
Stumm and Morgan (1981):	-10.53	-8.5
Ball and others (1980):	-10.41	-8.70
Wagman and others (1982):	-10.65	-3.79

The values chosen are virtually identical with those in the Perkins/Berman and Wanner (1986) data sets but differ from those in the WATEQ2 and NBS sets.

Siderite FeCO_3 : The values chosen are from the original PHREEQE data set. They compare with values derived from the other data sets considered as follows:

	<u>logK(25)</u>	<u>delta H^o_r</u>
Data chosen:	-10.55	-22.29
Wanner (1986):	-10.69	-21.13
Perkins/Berman:	-12.73	-16.67
Stumm and Morgan (1981):	-10.50	-29.2
Wagman and Others (1982):	-10.50	-25.67
Robie and others (1978):	-10.50	-29.26

Gypsum $\text{CaSO}_4 \cdot 2\text{H}_2\text{O}$: Values derived from the equation for logK(T) of Langmuir and Melchior (1985, eqn. 3) were chosen. They compare with values derived from the other data sets examined as follows:

	<u>logK(25)</u>	<u>delta H^o_r</u>
Data chosen:	-4.580	-0.45
Original PHREEQE:	-4.848	1.09
Wanner (1986):	-4.86	0.92
Wagman and Others (1982):	-4.36	-1.13
Robie and others (1978):	-4.34	-1.13

The logK(25) value selected is virtually identical with that in the original PHREEQE data base. Waters from two gypsiferous aquifers, the Muschelkalk in northern Switzerland (Pearson and Lolcama, in preparation) and the Edwards of central Texas (Pearson and Rettman, 1976), appear to be in equilibrium with gypsum of logK(25) = -4.6, supporting the choice made. The data for the other sulfate minerals, anhydrite, celestite and barite, were also selected from Langmuir and Melchior (1985) and are consistent with the value chosen for gypsum.

Anhydrite CaSO₄: Langmuir and Melchior (1985) present three expressions (equations 4, 5 and 9) which give similar values for logK(T) of anhydrite. Eqn. 4, which best fits the experimental data below 56°C is tentatively accepted until such time as validation analyses permit a choice between them. This data compares with the values derived from the other data sets examined as follows:

	<u>logK(25)</u>	<u>delta H^o_r</u>
Data chosen:	-4.239	-19.954
Perkins/Berman:	-4.14	-18.01
Wanner (1985):	-4.65	-15.69
Wagman and Others (1982):	-4.15	-17.99
Robie and others (1978):	-4.12	-17.99

Celestite SrSO₄: Values derived from the equation for logK(T) of Langmuir and Melchior (1985, eqn. 10) have been chosen. They are significantly different from the values in the original PHREEQE data set:

	<u>logK(25)</u>	<u>delta H^o_r</u>
Data chosen:	-6.633	2.52
Original PHREEQE:	-6.465	-1.97
Wanner (1985):	-6.50	2.09
Wagman and Others (1982):	-6.46	-1.97
Robie and others (1978):	-6.46	-1.90

Waters from two celestite-bearing aquifers, the Muschelkalk in northern Switzerland (Pearson and Lolcama, in preparation) and the Edwards of central Texas (Pearson and Rettman, 1976), appear to be in equilibrium with celestite with logK(25) values more consistent with those of Langmuir and Melchior (1985) than with those of the other data sets.

Barite BaSO₄: Data from Langmuir and Melchior (1985, eqn. 2) and from all the other data bases examined are virtually identical.

	<u>logK(25)</u>	<u>delta H⁰_r</u>
Data chosen:	-9.97	26.57
Original PHREEQE:	-9.976	26.28
Wagman and Others (1982):	-9.97	26.29
Robie and others (1978):	-9.95	26.28

Data from Langmuir and Melchior were chosen for consistency with the other sulfate minerals. There is a great deal of scatter associated with the barium analyses of the waters from the Muschelkalk which were used to validate the data chosen for the other alkaline-earth sulfate minerals (Schmassmann and others, 1984). Thus, these samples cannot be used to validate the barite values chosen.

Fluorite CaF₂: The values chosen are from the WATEQ2 data set (Ball and others, 1978). They compare with values from the other data sets examined as follows:

	<u>logK(25)</u>	<u>delta H⁰_r</u>
Data chosen:	-10.96	19.71
Perkins/Berman:	-10.93	17.88
Wanner (1986):	-10.41	15.90
Wagman and Others (1982):	-9.84	11.51
Robie and others (1978):	-10.51	15.73

Portlandite Ca(OH)₂: The values chosen are derived from the data of Wagman and others (1982) for the Gibbs energy and enthalpy of formation for crystalline Ca(OH)₂. These values compare with the values from the other data sets examined as follows:

	<u>logK(25)</u>	<u>delta H^o_r</u>
Data chosen:	22.66	-128.40
Wanner (1986):	22.80	-129.70
Robie and others (1978):	22.67	-128.40

The resulting logK(T) is consistent with the analysis of water from a zone in a Swiss borehole which was apparently influenced by cement (Pearson and Lolcama, in preparation, Sect. 4.3.4).

Chalcedony SiO₂: and

Quartz SiO₂: Fournier (1981) gives equations for the variation with temperature of the solubility of several silica phases important as controls on the dissolved silica content of ground waters. His values for both quartz and chalcedony have been adopted. The chalcedony values are essentially the same as those from the original PHREEQE data set. The several sets of quartz data available agree well:

	<u>logK(25)</u>	<u>delta H^o_r</u>
Data chosen:	-3.979	25.06
Original PHREEQE:	-4.006	26.02
Perkins/Berman:	-4.033	26.08

Pyrolusite MnO₂: The values for logK(25) and delta H^o_r are derived from delta G^o_f and delta H^o_f data of Robie and others (1979). They compare with values from the other data sets examined as follows:

	<u>logK(25)</u>	<u>delta H^o_r</u>
Data chosen:	41.55	-272.33
Stumm and Morgan (1981):	41.57	-272.36
Ball and others (1980):	41.37	-229.87
Wagman and others (1982):	41.56	-272.38

The values chosen are virtually identical with those derived from the NBS data set, but differ from those of WATEQ2.

Manganite MnOOH: The WATEQ2 value for logK(25) has been chosen.

	<u>logK(25)</u>	<u>delta H^o_r</u>
Data chosen:	25.27	- -
Stumm and Morgan (1981):	25.34	- -
Ball and others (1980):	25.27	- -

Magnetite Fe₃O₄: The values chosen are derived from data of Robie and others (1979). They compare with values from the other data sets considered as follows:

	<u>logK(25)</u>	<u>delta H^o_r</u>
Data chosen:	-8.80	-173.09
Schweingruber (1984):	-6.59	-168.66
Perkins/Berman:	-12.59	-170.76
Stumm and Morgan (1981):	-8.77	-173.12
Wagman and others (1982):	-9.25	-170.42

Hematite Fe₂O₃: The values chosen are derived from the data of Robie and others (1979). They compare with values from the other data sets considered as follows:

	<u>logK(25)</u>	<u>delta H^o_r</u>
Data chosen:	-3.86	-129.85
Perkins/Berman:	-4.32	-127.31
Schweingruber (1984):	-1.9	-129.70
Stumm and Morgan (1981):	-3.85	-129.9
Wagman and others (1982):	-3.75	-130.29

Goethite FeOOH: The logK(25) value chosen is that of Baes and Mesmer (1976), and is consistent with the stability constants used for iron hydroxide solution species. The same logK(25) value appears in the original PHREEQE and in the Schweingruber (1984) data bases. The delta H^o_r value selected is from the original PHREEQE data base. These values compare with those from the other data sets considered as follows:

	<u>logK(25)</u>	<u>delta H^o_r</u>
Data chosen:	0.5	-60.58
Schweingruber (1984):	0.5	-59.83
Stumm and Morgan (1981):	-1.69	-60.9
Robie and others (1978):	-1.69	-60.83

Ferric Hydroxide $\text{Fe}(\text{OH})_3$: The $\log K(25)$ value chosen is that of Baes and Mesmer (1976), and is consistent with the stability constants used for iron hydroxide solution species. The same $\log K(25)$ value appears in the Schweingruber (1984) data base. The ΔH°_r value selected is from the Schweingruber (1984) data base. These values compare with those from the other data sets considered as follows:

	<u>$\log K(25)$</u>	<u>ΔH°_r</u>
Data chosen:	2.5	-81.58
Original PHREEQE:	4.891	- -
Stumm and Morgan (1981):	3.00	- -
Wagman and others (1982):	3.43	-82.99

A.5 REFERENCES

A.5.1 Numbered References in Data Base

The numbered data sources in the data base refer to the following publications or other sources:

- 1) Wagman and others, 1982.
- 2) CODATA, 1978, 1980.
- 3) Perkins/Berman PATH data. This as yet undocumented data set is used with the version of PATH presently (May, 1986) running at the University, Bern. These data are derived primarily from the work of Helgeson and his colleagues as published formally (see references below) and in the SUPCRIT data base.
- 4) Helgeson and others, 1981.
- 5) By definition.
- 6) Estimated. See text.
- 7) Baes and Mesmer, 1976.
- 8) Plummer and Busenberg, 1982.
- 9) Busenberg and others, 1984.
- 10) Langmuir and Melchior, 1985.
- 11) Helgeson and others, 1978.
- 12) Nordstrom and others, 1984.
- 13) Fournier, 1981.
- 14) May and others, 1979.
- 15) Original PHREEQE data: See below.
- 16) Schweingruber, 1984, and Wanner, 1986.
- 17) Schweingruber, 1983, Data Base A. Only those aqueous species which are stable enough to appear prominently in Schweingruber's figures 6 and 7 are included.
- 18) Helgeson, 1969.

No numbered references are given for many of the aqueous species in the data base. Un-numbered data are from the data set supplied with PHREEQE (Parkhurst and others, 1980), which were derived from WATEQ2 (Ball and others, 1980) and(or) original WATEQ data (Truesdell and Jones, 1974).

A.5.2 References Cited

Baes, C. F. and Mesmer, R. E., 1976, The Hydrolysis of Cations: John Wiley and Sons, New York, 489p.

Ball, J. W., Nordstrom, D. K. and Jenne, E. A., 1980, Additional and Revised Thermochemical Data and Computer Code for WATEQ2--A Computerized Model for Trace and Major Element Speciation and Mineral Equilibria of Natural

Waters: U. S. Geological Survey Water Resources Investigations WRI-78-116, 109p.

Busenberg, Eurybiades, Plummer, L. N., and Parker, V. B., 1984, The solubility of strontianite (SrCO_3) in $\text{CO}_2\text{-H}_2\text{O}$ solutions between 2 and 91°C , the association constants of $\text{SrHCO}_3^+(\text{aq})$ and $\text{SrCO}_3^0(\text{aq})$ between 5 and 80°C , and an evaluation of the thermodynamic properties of $\text{Sr}^{+2}(\text{aq})$ and $\text{SrCO}_3(\text{cr})$ at 25°C and 1 atm total pressure: *Geochimica et Cosmochimica Acta*, v.48, p. 2021-2035.

CODATA Task Group on key values for thermodynamics, 1978, CODATA recommended key values for thermodynamics, 1977: *Journal of Chemical Thermodynamics*, v. 10, p. 903-906.

CODATA Task Group on key values for thermodynamics, 1980, Tentative set of key values for thermodynamics. Part VIII. CODATA Special Report, April, 1980.

Fournier, R. O., 1981, Application of water chemistry to geothermal exploration and reservoir engineering: in Rybach, L. and Muffler, L. J. P., eds., *Geothermal Systems: Principles and Case Histories*, John Wiley and Sons, Chichester, p. 109-143.

Garrels, R. M. and Christ, C. L., 1965, *Solutions, Minerals, and Equilibria*: Harper & Row, New York, 450 p.

Helgeson, H. C., 1969, Thermodynamics of hydrothermal systems at elevated temperatures and pressures: *American Journal of Science*, v. 267, p. 729-804.

Helgeson, H. C., Delany, J. M., Nesbitt, H. W., and Bird, D. K., 1978, Summary and critique of the thermodynamic properties of rock-forming minerals: *American Journal of Science*, v. 278-A, 229p.

Helgeson, H. C., Kirkham, D. H. and Flowers, G. C., 1981, Theoretical prediction of the thermodynamic behavior of aqueous electrolytes at high pressures and temperatures: IV. Calculation of activity coefficients, osmotic coefficients, and apparent molal and standard and relative partial molal properties to 600°C and 5 kb: *American Journal of Science*, v. 281, p. 1249-1516.

Hemingway, B. S., Robie, R. A. and Kittrick, J. A., 1978, Revised values for the Gibbs free energy of formation of $[\text{Al}(\text{OH})_4^-]_{\text{aq}}$, diaspore, boehmite and bayerite at 298.15 K and 1 bar, the thermodynamic properties of kaolinite to 800 K and 1 bar, and the heats of solution of several

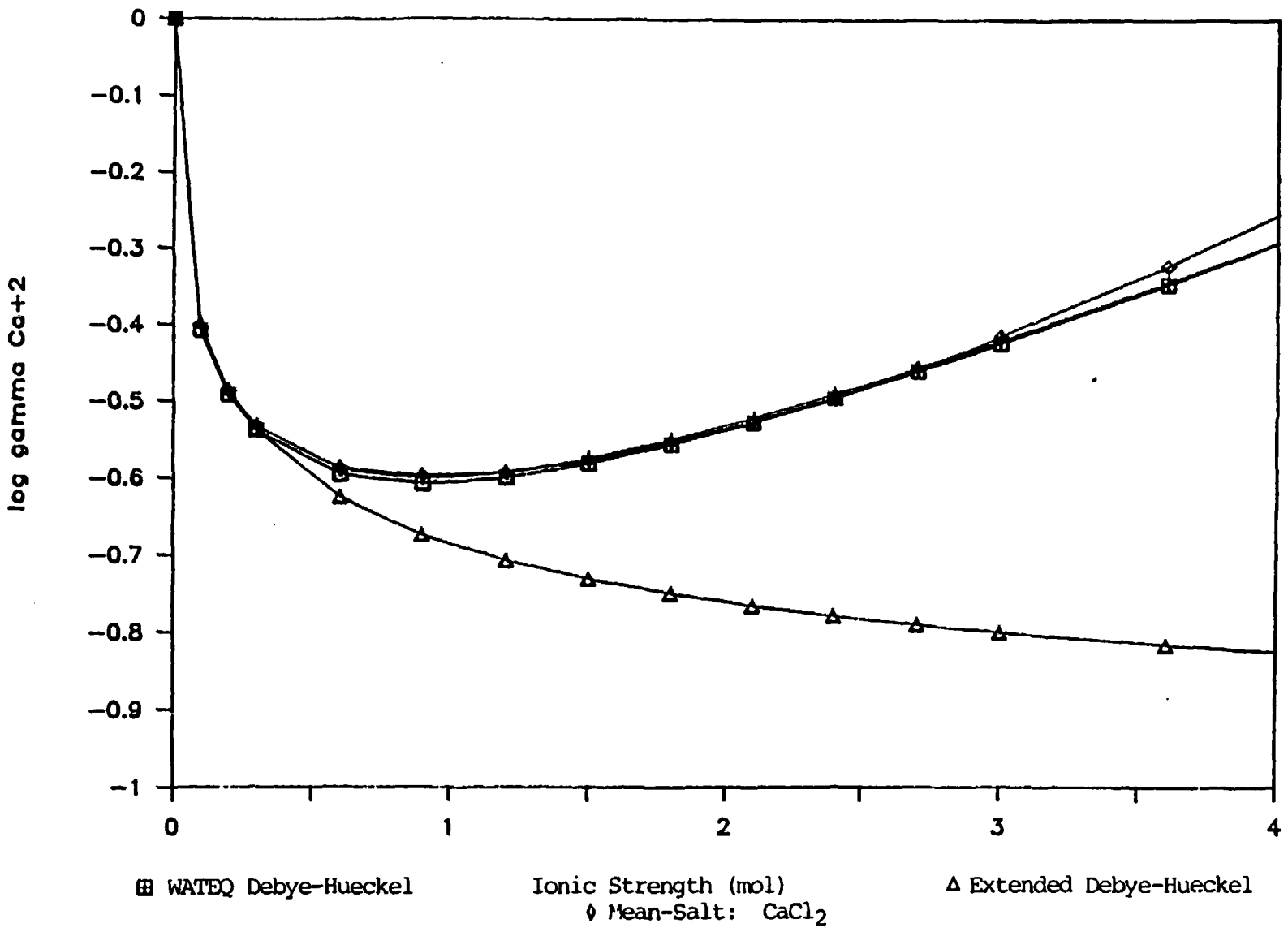
gibbsite samples: *Geochimica et Cosmochimica Acta*, v.42, p.1533-1543.

- INTERA Environmental Consultants, Inc., 1983a, PHREEQE: A Geochemical Speciation and Mass Transfer Code Suitable for Nuclear Waste Performance Assessment: ONWI-435, prepared for Battelle Memorial Institute, Office of Nuclear Waste Isolation, Columbus, OH, 304 p.
- INTERA Environmental Consultants, Inc., 1983b, EQ3/EQ6: A Geochemical Speciation and Reaction Path Code Package Suitable for Nuclear Waste Performance Assessment: ONWI-472, prepared for Battelle Memorial Institute, Office of Nuclear Waste Isolation, Columbus, OH, 712 p.
- INTERA Environmental Consultants, Inc., 1983c, Geochemical Models Suitable for Performance Assessment of Nuclear Waste Storage: Comparison of PHREEQE and EQ3/EQ6: ONWI-473, prepared for Battelle Memorial Institute, Office of Nuclear Waste Isolation, Columbus, OH, 114 p.
- Langmuir, Donald and Melchior, Daniel, 1985, The geochemistry of Ca, Sr, Ba and Ra sulfates in some deep brines from the Palo Duro Basin, Texas: *Geochimica et Cosmochimica Acta*, v. 49, p. 2423-2432.
- May, H. M., Helmke, P. A. and Jackson, M. L., 1979, Gibbsite solubility and thermodynamic properties of hydroxy-aluminum ions in aqueous solution at 25°C: *Geochimica et Cosmochimica Acta*, v. 43, p.861-868.
- Nordstrom, D.K. and Munoz, J.L., 1985, *Geochemical Thermodynamics*. The Benjamin/Cummings Publishing Co., Inc., Menlo Park, CA, 447p.
- Nordstrom, D. K., Valentine, S. D., Ball, J. W., Plummer, L. N., and Jones, B. F., 1984, Partial Compilation and Revision of Basic Data in the WATEQ Programs: U. S. Geological Survey Water-Resources Investigations Report 84-4186, 19p.
- Parkhurst, D. L., Thorstenson, D. C. and Plummer, L. N., 1980, PHREEQE - A computer program for geochemical calculations: U. S. Geological Survey Water- Resources Investigations 80-96, 210pp.
- Pearson, F. J., Jr. and Lolcama, J. L., in preparation, Chemistry of Ground Waters in the Boettstein, Weiach, Riniken, Schafisheim, Kaisten and Leuggern Boreholes: A Hydrochemically Consistent Data Set: Nagra, Baden, Switzerland, Technischer Bericht NTB 86-19

- Pearson, F. J. Jr. and Rettman, P.L., 1976, Geochemical and Isotopic Analyses of Waters Associated with the Edwards Limestone Aquifer, Central Texas: U. S. Geological Survey Report published by Edwards Underground Water District, San Antonio, TX, 35 p.
- Plummer, L. N. and Busenberg, Eurybiades, 1982, The solubilities of calcite, aragonite and vaterite in $\text{CO}_2\text{-H}_2\text{O}$ solutions between 0 and 90°C , and an evaluation of the aqueous model for the system $\text{CaCO}_3\text{-CO}_2\text{-H}_2\text{O}$: *Geochimica et Cosmochimica Acta*, v. 46, p. 1011-1040.
- Plummer, L. N., Jones, B. F. and Truesdell, A. H., 1976, WATEQF - A computer program for calculating chemical equilibrium of natural waters: U. S. Geological Survey Water-Investigations 76-13, 61p.
- Reardon, E. J., 1983, Determination of SrSO_4° ion pair formation using conductimetric and ion exchange techniques: *Geochimica et Cosmochimica Acta*, v. 47, p.1971-1922.
- Roberson, C. E. and Hem, J. D., 1969, Solubility of aluminum in the presence of hydroxide, fluoride, and sulfate: U. S. Geological Survey Water-Supply Paper 1827-C, p.C1-C37.
- Robie, R. A., Hemingway, B. S., Fisher, J. R., 1978, Thermodynamic Properties of Minerals and Related Substances at 198.15 K and 1 Bar (10^5 Pascals) Pressure and at Higher Temperatures: U. S. Geological Survey Bulletin 1452, 456 p. Reprinted with corrections 1979
- Robinson, R. A. and Stokes, R. H., 1959, Electrolyte Solutions, Second Edition (Revised): Butterworths, London, 571 p.
- Schmassmann, H., Balderer, W., Kanz, W. and Pekdeger, A., 1984, Beschaffenheit der Tiefengrundwässer in der zentralen Nordschweiz und angrenzenden Gebieten: Nagra, Baden, Switzerland, Technischer Bericht 84-21, 335p.
- Schweingruber, M., 1983, Actinide solubility in deep groundwaters - Estimates for upper limits based on chemical equilibrium calculations: Nagra, Baden, Switzerland, Technischer Bericht 83-24, 63p.
- Schweingruber, M., 1984, On probable in-situ pH, PCO_2 and redox conditions for waters sampled at 400, 600, and 1300 m depth in borehole KRISTAL I, Boettstein: Eidgenössisches Institut für Reactorforschung, Würenlingen, Switzerland, TM-45-84-20, 21p.

- Smith, R. W. and Hem, J. D., 1972, Effect of aging on aluminum hydroxide complexes in dilute aqueous solutions: U. S. Geological Survey Water-Supply Paper 1827-D, p.D1-D51.
- Stumm, Werner, and Morgan, J. J., 1981, Aquatic Chemistry, 2nd ed: John Wiley & Sons, New York, 780 p.
- Truesdell, A. H. and Jones, B. F., 1974, WATEQ, A computer program for calculating chemical equilibria of natural waters: U. S. Geological Survey Journal of Research, v.2, p.233-248.
- Wagman, D. D., Evans, W. H., Parker, V. B., Schumm, R. H., Halow, Iva, Bailey, S. M., Churney, K. L., and Nuttall, R. L., 1982, The NBS tables of chemical thermodynamic properties: Journal of Physical and Chemical Reference Data, v. 11, suppl. 2, 392 p.
- Wanner, H., 1986, Modeling Interaction of Deep Groundwaters with Bentonite and Radionuclide Speciation: Eidgenössisches Institut für Reactorforschung, Würenlingen, Switzerland, EIR-Bericht 589, 103p.
- Whitfield, M., 1979, Activity coefficients in natural waters in: Pytkowicz, R. M., ed., Activity Coefficients in Electrolyte Solutions: CRC Press, Boca Raton, FL, vol. II, p. 154-299.
- Wolery, T. J., 1983, EQ3NR A Computer Program for Geochemical Aqueous Speciation-Solubility Calculations: User's Guide and Documentation: Lawrence Livermore Laboratory, Livermore, CA, UCRL-53414, 191p.

Figure 1 Graph of Calculated and Mean-Salt Values for the Activity Coefficient of Ca²⁺ With Ionic Strength



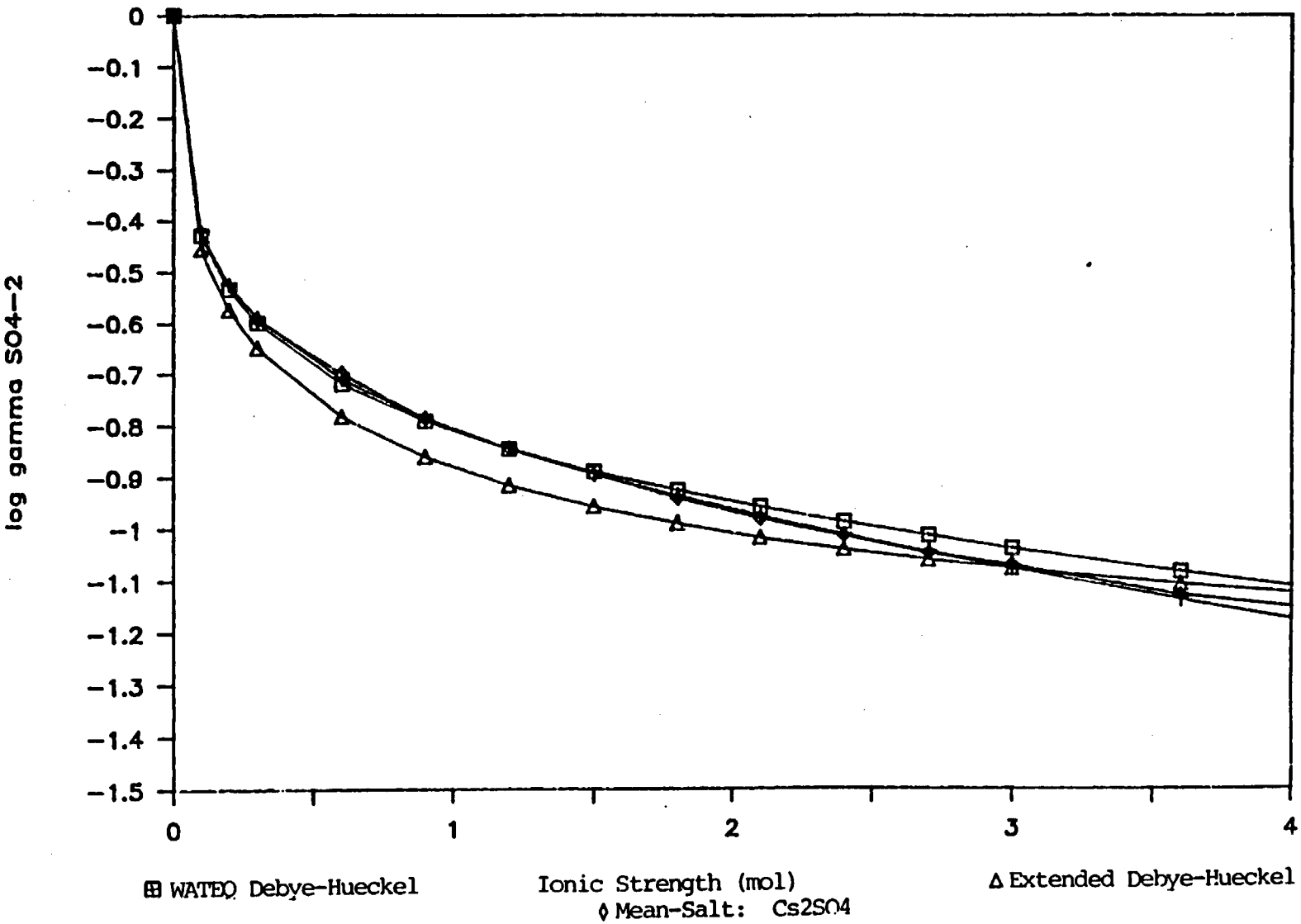


Figure 2 Graph of Calculated and Mean-Salt Values for the Activity Coefficient of SO_4^{2-} with Ionic Strength

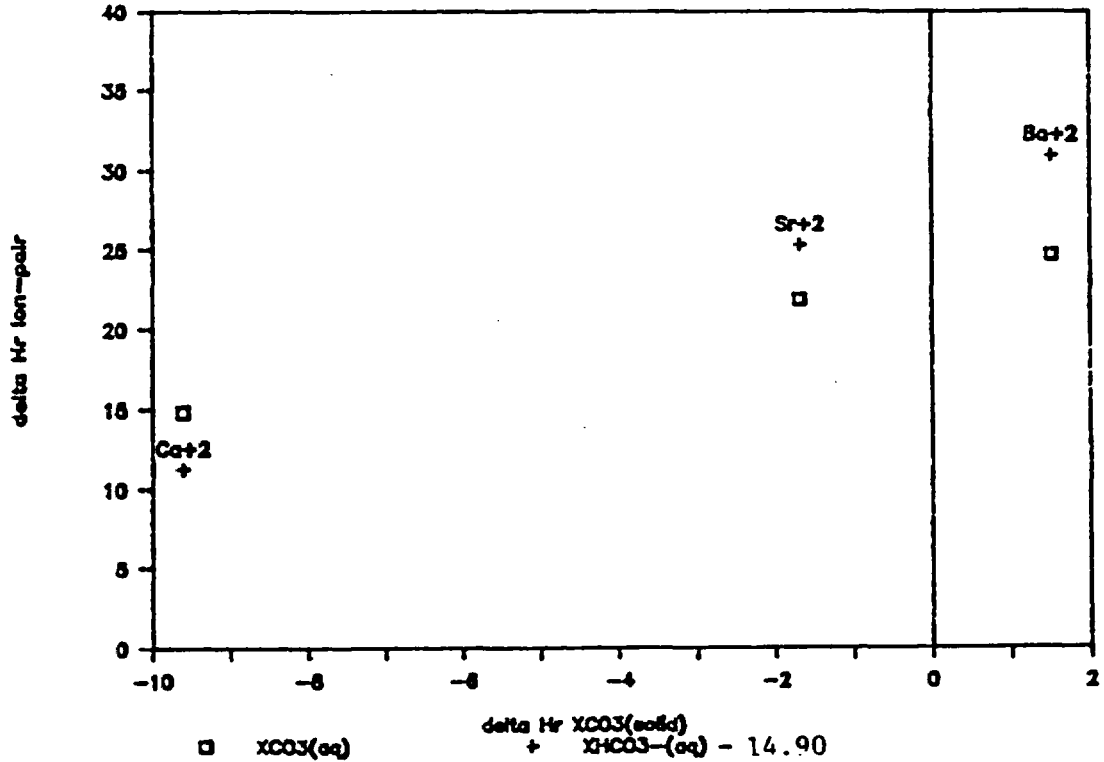
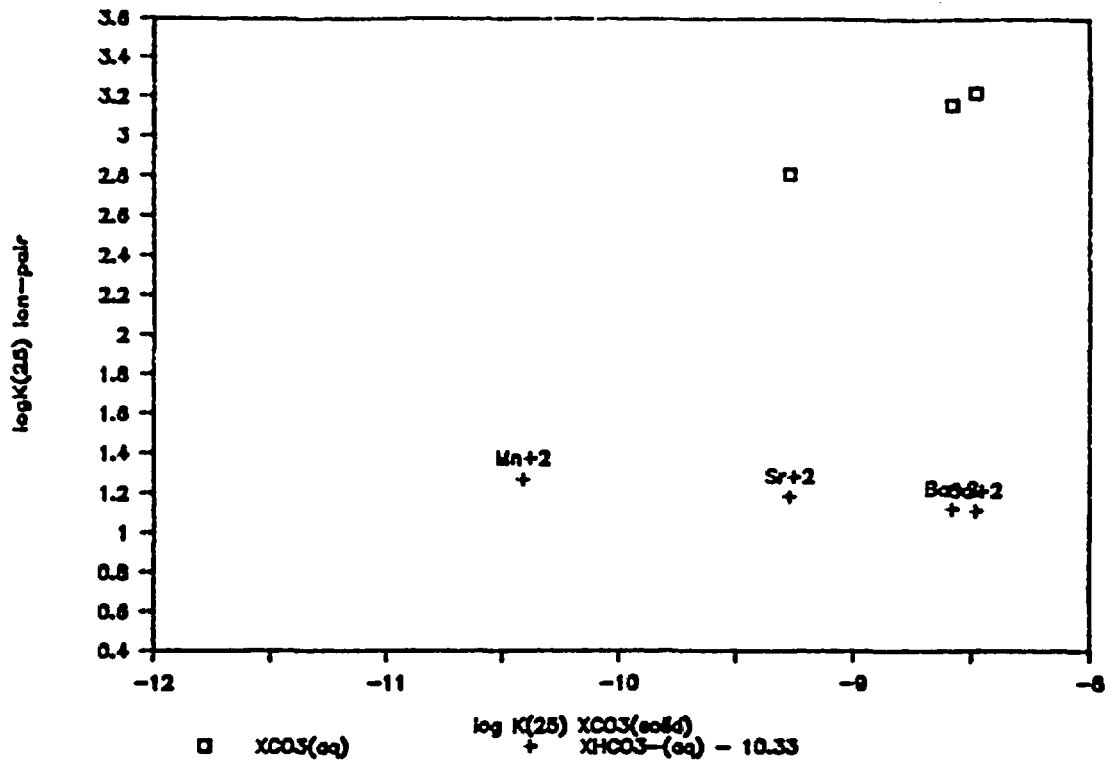


Figure 3 Graph of Carbonate Ion Pair Properties Against Carbonate Mineral Properties.

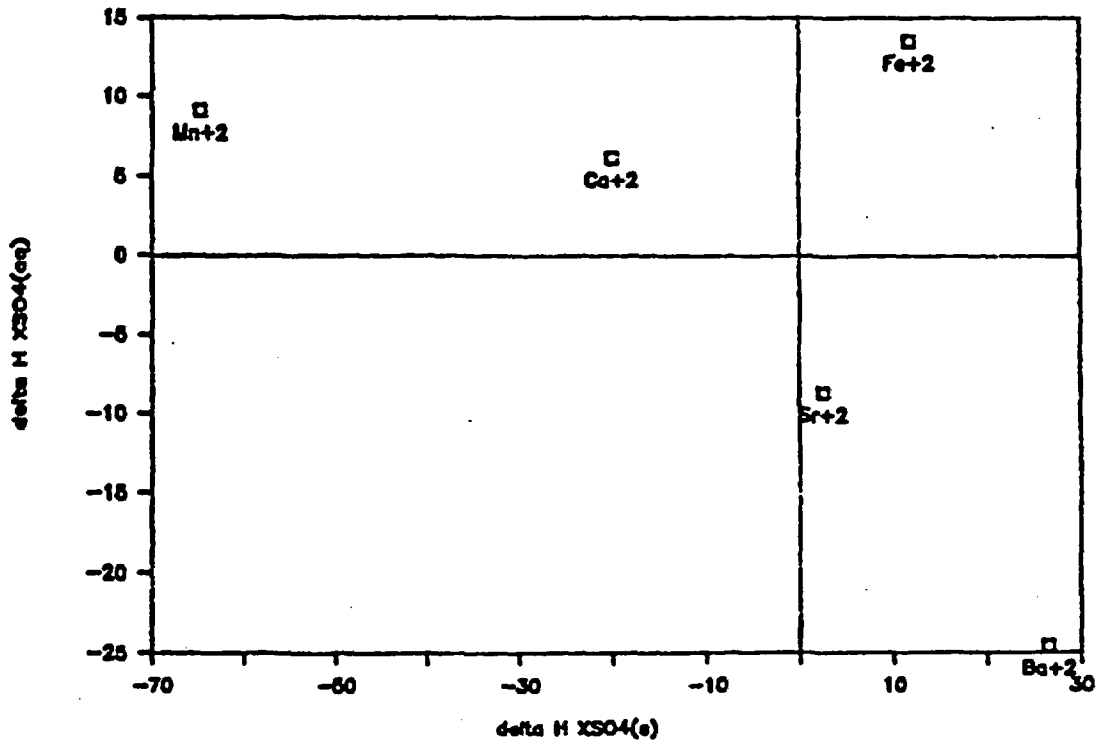
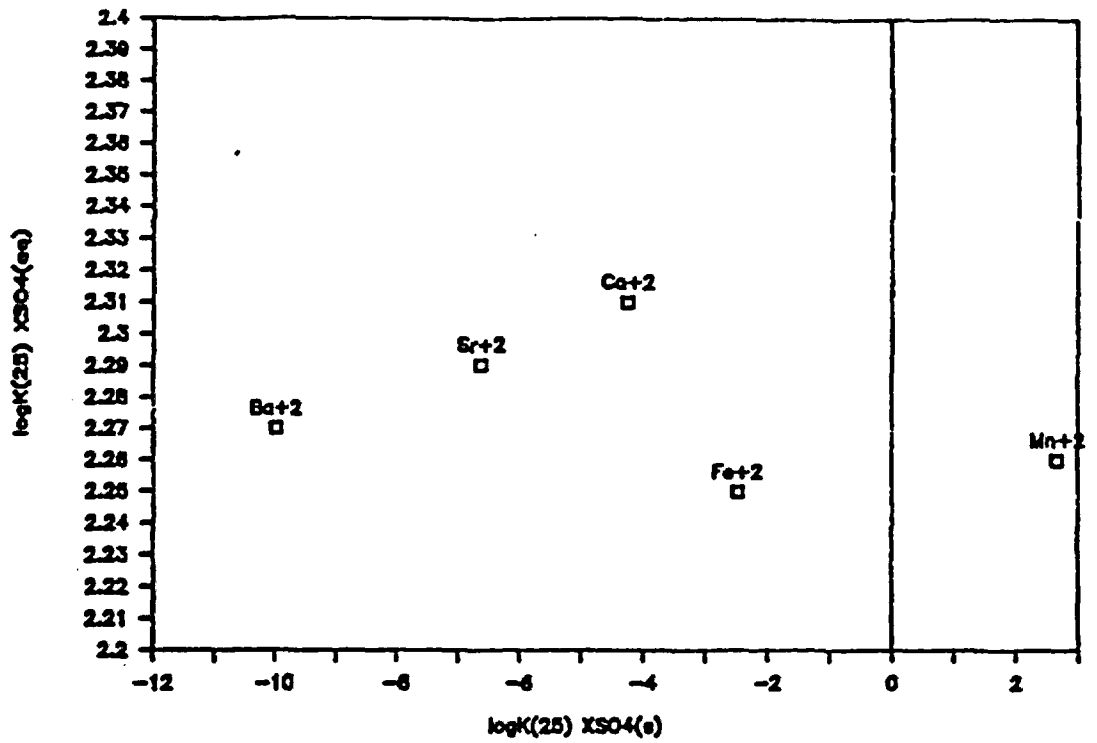


Figure 4 Graph of Sulfate Ion Pair Properties Against Sulfate Mineral Data.

ION	Truesdell-Jones		WATEQ	
	a_w	b_w	a_w	b_w
Na ⁺	4.0	0.075	3.85	0.078
K ⁺	3.5	0.015	3.54	0.016
Mg ⁺²	5.5	0.20	5.29	0.208
Ca ⁺²	5.0	0.165	5.12	0.161
Sr ⁺²			5.16	0.127
UO ₂ ⁺²			5.88	0.223
Cl ⁻	3.5	0.015	3.54	0.016
SO ₄ ⁻²	5.0	-0.04	5.35	-0.068
HCO ₃ ⁻	5.4	0	5.4	0
CO ₃ ⁻²	5.4	0	5.4	0

TABLE A-1: Values of parameters in activity coefficient equations for individual ions. Truesdell-Jones coefficients from Truesdell and Jones (1974). WATEQ coefficients calculated for this data set (see text).

Values of logK(25) for association of ion pairs
and for dissolution of minerals

X	XOH-	Ref	XHCO3+			XCO3s	Ref	XSO4O	XSO4s	Ref
			XCO3O	XHCO3+	-10.33					
Mg+2	-11.44	1	2.98	11.39	1.06		4	2.25	-2.14	6,a
Ca+2	-12.85	1	3.22	11.44	1.11	-8.48	2	2.31	-4.24	5,7
Sr+2	-13.29	1	2.81	11.51	1.18	-9.27	3	2.29	-6.63	8,7
Ba+2	-13.47	1	3.16	11.45	1.12	-8.58	E,6	2.27	-9.98	E,7
Mn+2	-10.59	1		11.6	1.27	-10.41	5	2.26	2.67	6
Fe+2	-9.5	1				-10.55	5	2.25	-2.47	6,a

Values of delta H for association of ion pairs
and for dissolution of minerals

X	XOH-	Ref	XHCO3+			XCO3s	Ref	XSO4O	XSO4s	Ref
			XCO3O	XHCO3+	+14.90					
Mg+2	64.51	5	11.35	-10.58	4.32		4	5.85	11.97	6,a
Ca+2	60.81	5	14.83	-3.64	11.26	-9.61	2	6.15	-19.95	6,7
Sr+2	60.65	5	21.83	10.4	25.3	-1.68	3	-8.7	2.52	8,7
Ba+2	63.16	5	24.65	16.05	30.95	1.51	E,6	-24.6	26.57	E,7
Mn+2	60.25	1		-15.1	-0.2	-8.7	6	9.08	-64.77	6
Fe+2	55.2	1				-22.29	5	13.51	11.8	6,a

References and Notes

- | | |
|--------------------------------|--------------------------------|
| a/ Solid is XSO4.7H2O | 1/ Baes and Mesmer, 1976 |
| 2/ Plummer and Busenberg, 1982 | 3/ Busenberg and others, 1984 |
| 4/ Plummer and others, 1976 | 5/ Parkhurst and others, 1980 |
| 6/ Ball and others, 1980 | 7/ Langmuir and Melchoir, 1985 |
| 8/ Reardon, 1983 | |

Table A-2: Values for stability constants for carbonate and sulfate ion pairs of divalent cations

dir a:

Values of logK(25) of association of solution species
and of dissociation of the solid

SPECIES:	(1)	(2)	(3)	(4)	(5)	(6)
Al(OH) ⁺²	-4.91	-4.97±0.02	- -	-4.74	-4.99	-5.0±0.3
Al(OH) ₂ ⁺	- -	-9.3	-8.7±0.4	- -	-10.1	-10.2±0.3
Al(OH) ₃ ⁰	- -	-15.0	- -	- -	-16.0	- -
Al(OH) ₄ ⁻	-22.5	-23.0±0.3	-23.3±0.3	-23.25	-23.0	-22.2±0.3
Al(OH) ₃ (cr)	-7.23	-8.5±0.1	-8.0±0.3	-7.25	-8.77	-8.1±0.3

Perkins/Berman logK(gibbsite): = -7.90

Values of delta H_r of association of solution species
and of dissociation of the solid

SPECIES:	(1)	(2)	(3)	(4)	(5)	(6)
Al(OH) ⁺²	- -	50±2	- -	64.12	49.8	- -
Al(OH) ₂ ⁺	- -	- -	- -	- -	0.0	- -
Al(OH) ₃ ⁰	- -	- -	- -	- -	0.0	- -
Al(OH) ₄ ⁻	171.42	- -	- -	180.20	184.35	- -
Al(OH) ₃ (cr)	95.155	- -	95.16	95.67	95.4	- -

Perkins/Berman delta H^o_r(gibbsite): 95.06

References

- (1) Wagman and others, (1982)
- (2) Baes and Mesmer, (1976)
- (3) Hemingway and others, (1978)
- (4) Perkins/Berman PATH
- (5) PHREEQE (Parkhurst and others, 1980) and
WATEQ2 (Ball and others, 1980)
- (6) May and others, (1979).

Table A-3: Values of stability constants for aluminum hydrolysis
species and gibbsite.

	Gibbs Energy kJ/mol	Enthalpy kJ/mol	Entropy J/mol/K	Gibbs Energy kJ/mol	Enthalpy kJ/mol	Entropy J/mol/K
1: H+				Data Sources: G:5 H:5 S:5		
Form:	.000	.000	.000	Rean: .000	.000	.000
Thor:	.0	Charge:	1.0	D-H a0: 9.0	logK(25): .0000	
	Reactant Species			logK(T)=	.000000	
Coef.	Name	No.		+	.000000	*T
1.00	H+	1				
2: e-				Data Sources: Definition		
Form:	.000	.000	.000	Rean: .000	.000	.000
Thor:	-1.0	Charge:	-1.0	D-H a0: .0	logK(25): .0000	
	Reactant Species			logK(T)=	.000000	
Coef.	Name	No.		+	.000000	*T
1.00	e-	2				
3: H2O				Data Sources: G:1=3 H:1=2=3		
Form:	-237.129	-285.830	-163.344	Rean: .000	.000	.000
Thor:	.0	Charge:	.0	D-H a0: .0	logK(25): .0000	
	Reactant Species			logK(T)=	.000000	
Coef.	Name	No.		+	.000000	*T
1.00	H2O	3				
4: LI+				Data Sources: G:2=3=4 H:2=3=4		
Form:	-292.630	-278.455	47.543	Rean: .000	.000	.000
Thor:	.0	Charge:	1.0	D-H a0: 6.0	logK(25): .0000	
	Reactant Species			logK(T)=	.000000	
Coef.	Name	No.		+	.000000	*T
1.00	LI+	4				
5: NA+				Data Sources: G:1=2=3=4 H:2=3=4		
Form:	-261.930	-240.300	72.547	Rean: .000	.000	.000
Thor:	.0	Charge:	1.0	D-H a0: 4.0	logK(25): .0000	
	Reactant Species			logK(T)=	.000000	
Coef.	Name	No.		+	.000000	*T
1.00	NA+	5				
6: K+				Data Sources: G:4 H:2=4		
Form:	-282.740	-252.170	102.532	Rean: .000	.000	.000
Thor:	.0	Charge:	1.0	D-H a0: 3.0	logK(25): .0000	
	Reactant Species			logK(T)=	.000000	
Coef.	Name	No.		+	.000000	*T
1.00	K+	6				
7: MG+2				Data Sources: G:1=3=4 H:1=3=4		
Form:	-454.800	-466.800	-40.248	Rean: .000	.000	.000
Thor:	.0	Charge:	2.0	D-H a0: 8.0	logK(25): .0000	
	Reactant Species			logK(T)=	.000000	
Coef.	Name	No.		+	.000000	*T
1.00	MG+2	7				
8: CA+2				Data Sources: G:4 H:2=4		
Form:	-552.940	-543.100	33.004	Rean: .000	.000	.000
Thor:	.0	Charge:	2.0	D-H a0: 6.0	logK(25): .0000	
	Reactant Species			logK(T)=	.000000	
Coef.	Name	No.		+	.000000	*T
1.00	CA+2	8				

Table A-4: Thermodynamic data for aqueous species.

	Gibbs Energy kJ/mol	Enthalpy kJ/mol	Entropy J/mol/K	Gibbs Energy kJ/mol	Enthalpy kJ/mol	Entropy J/mol/K
9: SR+2				Data Sources: G:1=3=4 H:1=3=4		
Form:	-559.460	-545.820	45.749	Rean: .000	.000	.000
	Thor: .0	Charge: 2.0	D-H a0: 5.0	logK(25): .0000		
	Reactant Species			logK(T)= .000000		
	Coef.	Name	No.	+	.000000	*T
	1.00	SR+2	9			
10: BA+2				Data Sources: G:1=3=4 H:1=3=4		
Form:	-560.760	-537.640	77.545	Rean: .000	.000	.000
	Thor: .0	Charge: 2.0	D-H a0: 5.0	logK(25): .0000		
	Reactant Species			logK(T)= .000000		
	Coef.	Name	No.	+	.000000	*T
	1.00	BA+2	10			
11: Mn+2				Data Sources: G: 1=4 H: 1=4		
Form:	-228.100	-220.750	24.652	Rean: .000	.000	.000
	Thor: 2.0	Charge: 2.0	D-H a0: 6.0	logK(25): .0000		
	Reactant Species			logK(T)= .000000		
	Coef.	Name	No.	+	.000000	*T
	1.00	Mn+2	11			
12: Fe+2				Data Sources: G: H: 12		
Form:	-85.350	-87.400	-6.876	Rean: .000	.000	.000
	Thor: 2.0	Charge: 2.0	D-H a0: 6.0	logK(25): .0000		
	Reactant Species			logK(T)= .000000		
	Coef.	Name	No.	+	.000000	*T
	1.00	Fe+2	12			
14: H3BO3				Data Sources: G:1 H:1		
Form:	-968.750	-1072.320	-347.375	Rean: .000	.000	.000
	Thor: .0	Charge: .0	D-H a0: .0	logK(25): .0000		
	Reactant Species			logK(T)= .000000		
	Coef.	Name	No.	+	.000000	*T
	1.00	H3BO3	14			
15: Al+3				Data Sources: G:4=14 H:3=4		
Form:	-489.400	-531.380	-140.802	Rean: .000	.000	.000
	Thor: .0	Charge: 3.0	D-H a0: 9.0	logK(25): .0000		
	Reactant Species			logK(T)= .000000		
	Coef.	Name	No.	+	.000000	*T
	1.00	Al+3	15			
16: CO3-2				Data Sources: G:1=3 H:1=3		
Form:	-527.810	-677.140	-500.855	Rean: .000	.000	.000
	Thor: 4.0	Charge: -2.0	D-H a0: 5.4	logK(25): .0000		
	Reactant Species			logK(T)= .000000		
	Coef.	Name	No.	+	.000000	*T
	1.00	CO3-2	16			
17: H4SiO4				Data Sources: G:3 H:3		
Form:	-1307.600	-1456.280	-498.675	Rean: .000	.000	.000
	Thor: .0	Charge: .0	D-H a0: .0	logK(25): .0000		
	Reactant Species			logK(T)= .000000		
	Coef.	Name	No.	+	.000000	*T
	1.00	H4SiO4	17			

Table A-4 (Continued): Thermodynamic data for aqueous species.

	Gibbs Energy kJ/mol	Enthalpy kJ/mol	Entropy J/mol/K	Gibbs Energy kJ/mol	Enthalpy kJ/mol	Entropy J/mol/K
18: PO4-3				Data Sources: G:1 H:1		
Form:	-1018.700	-1277.400	-867.684	Rean: .000	.000	.000
Thor:	.0	Charge: -3.0	D-H a0: 4.0	logK(25): .0000		
	Reactant Species			logK(T)= .000000		
Coef.	Name	No.		+	.000000	*T
1.00	PO4-3	18				
19: H3AsO3				Data Sources: G:1 H:1		
Form:	-639.800	-742.200	-343.451	Rean: .000	.000	.000
Thor:	3.0	Charge: .0	D-H a0: .0	logK(25): .0000		
	Reactant Species			logK(T)= .000000		
Coef.	Name	No.		+	.000000	*T
1.00	H3AsO3	19				
20: SO4-2				Data Sources: G:1 H:1		
Form:	-744.530	-909.270	-552.541	Rean: .000	.000	.000
Thor:	6.0	Charge: -2.0	D-H a0: 4.0	logK(25): .0000		
	Reactant Species			logK(T)= .000000		
Coef.	Name	No.		+	.000000	*T
1.00	SO4-2	20				
21: F-				Data Sources: G:2=4 H:2=4		
Form:	-281.710	-335.350	-179.910	Rean: .000	.000	.000
Thor:	.0	Charge: -1.0	D-H a0: 3.5	logK(25): .0000		
	Reactant Species			logK(T)= .000000		
Coef.	Name	No.		+	.000000	*T
1.00	F-	21				
22: CL-				Data Sources: G:2=3=4 H:2=3=4		
Form:	-131.291	-167.080	-120.037	Rean: .000	.000	.000
Thor:	.0	Charge: -1.0	D-H a0: 3.0	logK(25): .0000		
	Reactant Species			logK(T)= .000000		
Coef.	Name	No.		+	.000000	*T
1.00	CL-	22				
23: BR-				Data Sources: G:2=3=4 H:2=3=4		
Form:	-104.040	-121.500	-58.561	Rean: .000	.000	.000
Thor:	.0	Charge: -1.0	D-H a0: 3.0	logK(25): .0000		
	Reactant Species			logK(T)= .000000		
Coef.	Name	No.		+	.000000	*T
1.00	BR-	23				
24: U4+				Data Sources: G:1 H:1		
Form:	-531.000	-591.200	-201.912	Rean: .000	.000	.000
Thor:	4.0	Charge: 4.0	D-H a0: 11.0	logK(25): .0000		
	Reactant Species			logK(T)= .000000		
Coef.	Name	No.		+	.000000	*T
1.00	U4+	24				
25: O2 AQ				Data Sources: G:1 H:1		
Form:	16.400	-11.700	-94.248	Rean: .000	.000	.000
Thor:	4.0	Charge: .0	D-H a0: .0	logK(25): .0000		
	Reactant Species			logK(T)= .000000		
Coef.	Name	No.		+	.000000	*T
1.00	O2 AQ	25				

Table A-4 (Continued): Thermodynamic data for aqueous species.

	Gibbs Energy kJ/mol	Enthalpy kJ/mol	Entropy J/mol/K	Gibbs Energy kJ/mol	Enthalpy kJ/mol	Entropy J/mol/K
26: CH4 AQ				Data Sources: G:1 H:1		
Form:	-34.330	-89.040	-183.498	Rean: .000	.000	.000
Thor:	-4.0	Charge:	.0	D-H a0: .0	logK(25): .0000	
	Reactant Species			logK(T) =	.000000	
Coef.	Name	No.		+	.000000	*T
1.00	CH4 AQ	26				
27: ASO4-3				Data Sources: G:1 H:1		
Form:	-648.410	-888.140	-804.058	Rean: .000	.000	.000
Thor:	5.0	Charge:	-3.0	D-H a0: 4.0	logK(25): .0000	
	Reactant Species			logK(T) =	.000000	
Coef.	Name	No.		+	.000000	*T
1.00	ASO4-3	27				
28: H2S AQ				Data Sources: G:1 H:1		
Form:	-27.830	-39.700	-39.812	Rean: .000	.000	.000
Thor:	-2.0	Charge:	.0	D-H a0: .0	logK(25): .0000	
	Reactant Species			logK(T) =	.000000	
Coef.	Name	No.		+	.000000	*T
1.00	H2S AQ	28				
31: OH-				Data Sources:		
Form:	-157.230	-229.994	-244.053	Rean: 79.899	55.836	-80.709
Thor:	.0	Charge:	-1.0	D-H a0: 3.5	logK(25): -13.9980	
	Reactant Species			logK(T) =	.000000	
Coef.	Name	No.		+	.000000	*T
1.00	H2O	3		+	.000000	/T
-1.00	H+	1		+	.000000	*T^2
				+	.000000	/T^2
32: NACO3-				Data Sources:		
Form:	-796.978	-880.156	-278.982	Rean: -7.238	37.284	149.326
Thor:	4.0	Charge:	-1.0	D-H a0: 4.0	logK(25): 1.2680	
	Reactant Species			logK(T) =	.000000	
Coef.	Name	No.		+	.000000	*T
1.00	NA+	5		+	.000000	/T
1.00	CO3-2	16		+	.000000	*T^2
				+	.000000	/T^2
33: NAHCO3				Data Sources:		
Form:	-847.276	-932.519	-285.907	Rean: -57.536	-15.079	142.400
Thor:	4.0	Charge:	.0	D-H a0: .0	logK(25): 10.0800	
	Reactant Species			logK(T) =	.000000	
Coef.	Name	No.		+	.000000	*T
1.00	NA+	5		+	.000000	/T
1.00	H+	1		+	.000000	*T^2
1.00	CO3-2	16		+	.000000	/T^2
34: NASO4-				Data Sources:		
Form:	-1010.456	-1144.884	-450.875	Rean: -3.996	4.686	29.118
Thor:	6.0	Charge:	-1.0	D-H a0: 4.0	logK(25): .7000	
	Reactant Species			logK(T) =	.000000	
Coef.	Name	No.		+	.000000	*T
1.00	NA+	5		+	.000000	/T
1.00	SO4-2	20		+	.000000	*T^2
				+	.000000	/T^2

Table A-4 (Continued): Thermodynamic data for aqueous species.

	Gibbs Energy kJ/mol	Enthalpy kJ/mol	Entropy J/mol/K	Gibbs Energy kJ/mol	Enthalpy kJ/mol	Entropy J/mol/K
35: KSO4-						
Form:	-1032.122	-1152.030	-402.174	Rean: -4.852	9.410	47.834
Thor:	6.0	Charge: -1.0	D-H a0: 4.0	logK(25): .8500		
	Reactant Species			logK(T)=	.000000	
Coef.	Name	No.		+	.000000	*T
1.00	K+	6		+	.000000	/T
1.00	SO4-2	20		+	.000000	*T^2
				+	.000000	/T^2
36: MgOH+						
Form:	-626.631	-688.120	-206.237	Rean: 65.298	64.510	-2.645
Thor:	.0	Charge: 1.0	D-H a0: 4.0	logK(25): -11.4400		
	Reactant Species			logK(T)=	.000000	
Coef.	Name	No.		+	.000000	*T
1.00	Mg+2	7		+	.000000	/T
1.00	H2O	3		+	.000000	*T^2
-1.00	H+	1		+	.000000	/T^2
37: MgCO3						
Form:	-999.618	-1132.589	-445.988	Rean: -17.008	11.351	95.116
Thor:	4.0	Charge: .0	D-H a0: .0	logK(25): 2.9797		
	Reactant Species			logK(T)=	.991000	
Coef.	Name	No.		+	.667000E-02	*T
1.00	Mg+2	7		+	.000000	/T
1.00	CO3-2	16		+	.000000	*T^2
				+	.000000	/T^2
38: MGHCO3+						
Form:	-1047.646	-1154.520	-358.457	Rean: -65.036	-10.580	182.647
Thor:	4.0	Charge: 1.0	D-H a0: 5.4	logK(25): 11.3940		
	Reactant Species			logK(T)=	-4.17900	
Coef.	Name	No.		+	.127300E-01	*T
1.00	Mg+2	7		+	2902.39	/T
1.00	H+	1		+	.229810E-04	*T^2
1.00	CO3-2	16		+	.000000	/T^2
39: MgSO40						
Form:	-1212.173	-1370.210	-530.059	Rean: -12.843	5.860	62.729
Thor:	6.0	Charge: .0	D-H a0: .0	logK(25): 2.2500		
	Reactant Species			logK(T)=	.000000	
Coef.	Name	No.		+	.000000	*T
1.00	Mg+2	7		+	.000000	/T
1.00	SO4-2	20		+	.000000	*T^2
				+	.000000	/T^2
40: MGF+						
Form:	-746.898	-782.594	-119.724	Rean: -10.388	19.556	100.434
Thor:	.0	Charge: 1.0	D-H a0: 4.0	logK(25): 1.8200		
	Reactant Species			logK(T)=	.000000	
Coef.	Name	No.		+	.000000	*T
1.00	Mg+2	7		+	.000000	/T
1.00	F-	21		+	.000000	*T^2
				+	.000000	/T^2

Table A-4 (Continued): Thermodynamic data for aqueous species.

	Gibbs Energy kJ/mol	Enthalpy kJ/mol	Entropy J/mol/K	Gibbs Energy kJ/mol	Enthalpy kJ/mol	Entropy J/mol/K
41: CaOH+				Data Sources: K: 7 H: 15		
Form:	-716.722	-768.120	-172.388	Rean: 73.347	60.810	-42.048
Thor:	.0	Charge:	1.0	D-H a0: 4.0	logK(25): -12.8500	
	Reactant Species			logK(T)=	.000000	
Coef.	Name	No.		+	.000000	*T
1.00	CA+2	8		+	.000000	/T
1.00	H2O	3		+	.000000	*T^2
-1.00	H+	1		+	.000000	/T^2
42: CaCO3				Data Sources: C:8		
Form:	-1099.154	-1205.408	-356.379	Rean: -18.404	14.832	111.472
Thor:	4.0	Charge:	.0	D-H a0: .0	logK(25): 3.2243	
	Reactant Species			logK(T)=	-16.4029	
Coef.	Name	No.		+	.149383	*T
1.00	CA+2	8		+	-8438.30	/T
1.00	CO3-2	16		+	-.178474E-03	*T^2
				+	.171173E+07	/T^2
43: CaHCO3+				Data Sources: C:8		
Form:	-1146.017	-1223.878	-261.147	Rean: -65.267	-3.638	206.705
Thor:	4.0	Charge:	1.0	D-H a0: 5.4	logK(25): 11.4345	
	Reactant Species			logK(T)=	25.0996	
Coef.	Name	No.		+	-.132820	*T
1.00	CA+2	8		+	6919.18	/T
1.00	CO3-2	16		+	.190189E-03	*T^2
1.00	H+	1		+	-.126037E+07	/T^2
44: CASO4				Data Sources: K: 15 H: 19		
Form:	-1310.650	-1446.220	-454.705	Rean: -13.180	6.150	64.832
Thor:	6.0	Charge:	.0	D-H a0: .0	logK(25): 2.3090	
	Reactant Species			logK(T)=	.000000	
Coef.	Name	No.		+	.000000	*T
1.00	CA+2	8		+	.000000	/T
1.00	SO4-2	20		+	.000000	*T^2
				+	.000000	/T^2
45: CAF+				Data Sources: K: 15 H: 19		
Form:	-840.015	-862.559	-75.612	Rean: -5.365	15.891	71.294
Thor:	.0	Charge:	1.0	D-H a0: 4.0	logK(25): .9400	
	Reactant Species			logK(T)=	.000000	
Coef.	Name	No.		+	.000000	*T
1.00	CA+2	8		+	.000000	/T
1.00	F-	21		+	.000000	*T^2
				+	.000000	/T^2
46: SrOH+				Data Sources: K: 7 H: 15		
Form:	-720.731	-771.000	-168.603	Rean: 75.858	60.650	-51.008
Thor:	.0	Charge:	1.0	D-H a0: 4.0	logK(25): -13.2900	
	Reactant Species			logK(T)=	.000000	
Coef.	Name	No.		+	.000000	*T
1.00	SR+2	9		+	.000000	/T
1.00	H2O	3		+	.000000	*T^2
-1.00	H+	1		+	.000000	/T^2

Table A-4 (Continued): Thermodynamic data for aqueous species.

	Gibbs Energy kJ/mol	Enthalpy kJ/mol	Entropy J/mol/K	Gibbs Energy kJ/mol	Enthalpy kJ/mol	Entropy J/mol/K
47: SrCO3						
Form:	-1103.281	-1201.133	-328.195	Rean: -16.011	21.827	126.911
Thor:	4.0	Charge:	.0	D-H a0:	.0	logK(25): 2.8051
	Reactant Species			logK(T) = -1.01900		
Coef.	Name	No.				
1.00	SR+2	9		+	.128260E-01	*T
1.00	CO3-2	16		+	.000000	/T
				+	.000000	*T^2
				+	.000000	/T^2
48: SrHCO3+						
Form:	-1152.988	-1212.560	-199.805	Rean: -65.718	10.400	255.301
Thor:	4.0	Charge:	1.0	D-H a0:	5.4	logK(25): 11.5135
	Reactant Species			logK(T) = 7.50265		
Coef.	Name	No.				
1.00	SR+2	9		+	.114338E-01	*T
1.00	CO3-2	16		+	-1630.26	/T
1.00	H+	1		+	.143000E-04	*T^2
				+	426564.	/T^2
49: SRSO4						
Form:	-1317.061	-1448.940	-442.324	Rean: -13.071	6.150	64.468
Thor:	6.0	Charge:	.0	D-H a0:	.0	logK(25): 2.2900
	Reactant Species			logK(T) = .000000		
Coef.	Name	No.				
1.00	SR+2	9		+	.000000	*T
1.00	SO4-2	20		+	.000000	/T
				+	.000000	*T^2
				+	.000000	/T^2
50: SRF+						
Form:	-846.022	-864.170	-60.870	Rean: -4.852	17.000	73.291
Thor:	.0	Charge:	1.0	D-H a0:	4.0	logK(25): .8500
	Reactant Species			logK(T) = .000000		
Coef.	Name	No.				
1.00	SR+2	9		+	.000000	*T
1.00	F-	21		+	.000000	/T
				+	.000000	*T^2
				+	.000000	/T^2
51: BaOH+						
Form:	-721.004	-760.310	-131.835	Rean: 76.885	63.160	-46.035
Thor:	.0	Charge:	1.0	D-H a0:	4.0	logK(25): -13.4700
	Reactant Species			logK(T) = .000000		
Coef.	Name	No.				
1.00	BA+2	10		+	.000000	*T
1.00	H2O	3		+	.000000	/T
-1.00	H+	1		+	.000000	*T^2
				+	.000000	/T^2
52: BACO3						
Form:	-1106.607	-1197.948	-306.359	Rean: -18.037	16.832	116.951
Thor:	4.0	Charge:	.0	D-H a0:	.0	logK(25): 3.1600
	Reactant Species			logK(T) = .000000		
Coef.	Name	No.				
1.00	BA+2	10		+	.000000	*T
1.00	CO3-2	16		+	.000000	/T
				+	.000000	*T^2
				+	.000000	/T^2

Table A-4 (Continued): Thermodynamic data for aqueous species.

	Gibbs Energy kJ/mol	Enthalpy kJ/mol	Entropy J/mol/K	Gibbs Energy kJ/mol	Enthalpy kJ/mol	Entropy J/mol/K
53: BAHCO3+						
Form:	-1156.209	-1207.214	-171.073	Rean: -67.639	7.566	252.238
Thor:	4.0	Charge:	1.0	D-H a0: 5.4	logK(25): 11.8500	
	Reactant Species			logK(T)=	.000000	
Coef.	Name	No.		+	.000000	*T
1.00	BA+2	10		+	.000000	/T
1.00	CO3-2	16		+	.000000	*T^2
1.00	H+	1		+	.000000	/T^2
54: BASO4						
Form:	-1318.304	-1440.760	-410.719	Rean: -13.014	6.150	64.276
Thor:	6.0	Charge:	.0	D-H a0: .0	logK(25): 2.2800	
	Reactant Species			logK(T)=	.000000	
Coef.	Name	No.		+	.000000	*T
1.00	BA+2	10		+	.000000	/T
1.00	SO4-2	20		+	.000000	*T^2
				+	.000000	/T^2
55: BAF+						
Form:	-847.265	-855.990	-29.265	Rean: -4.795	17.000	73.100
Thor:	.0	Charge:	1.0	D-H a0: 4.0	logK(25): .8400	
	Reactant Species			logK(T)=	.000000	
Coef.	Name	No.		+	.000000	*T
1.00	BA+2	10		+	.000000	/T
1.00	F-	21		+	.000000	*T^2
				+	.000000	/T^2
56: MnOH+						
Form:	-404.782	-446.330	-139.352	Rean: 60.447	60.250	-.660
Thor:	2.0	Charge:	1.0	D-H a0: 4.0	logK(25): -10.5900	
	Reactant Species			logK(T)=	.000000	
Coef.	Name	No.		+	.000000	*T
1.00	Mn+2	11		+	.000000	/T
1.00	H2O	3		+	.000000	*T^2
-1.00	H+	1		+	.000000	/T^2
57: Mn(OH)3-						
Form:	-879.041	.000	.000	Rean: 198.635	.000	.000
Thor:	2.0	Charge:	-1.0	D-H a0: 4.0	logK(25): -34.8000	
	Reactant Species			logK(T)=	.000000	
Coef.	Name	No.		+	.000000	*T
1.00	Mn+2	11		+	.000000	/T
3.00	H2O	3		+	.000000	*T^2
-3.00	H+	1		+	.000000	/T^2
58: Mn2(OH)3+						
Form:	-1107.141	.000	.000	Rean: 136.419	.000	.000
Thor:	4.0	Charge:	1.0	D-H a0: 4.0	logK(25): -23.9000	
	Reactant Species			logK(T)=	.000000	
Coef.	Name	No.		+	.000000	*T
2.00	Mn+2	11		+	.000000	/T
3.00	H2O	3		+	.000000	*T^2
-3.00	H+	1		+	.000000	/T^2

Table A-4 (Continued): Thermodynamic data for aqueous species.

	Gibbs Energy kJ/mol	Enthalpy kJ/mol	Entropy J/mol/K		Gibbs Energy kJ/mol	Enthalpy kJ/mol	Entropy J/mol/K
59: MnSO40				Data Sources: K: H: 19=16			
Form:	-985.530	-1121.120	-454.772	Rean:	-12.900	8.900	73.117
	Thor: 8.0	Charge:	.0	D-H a0:	.0	logK(25):	2.2600
	Reactant Species				logK(T)=		
Coef.	Name	No.					
1.00	Mn+2	11			+	.000000	*T
1.00	SO4-2	20			+	.000000	/T
					+	.000000	*T^2
					+	.000000	/T^2
60: MnCl+				Data Sources: K: 19 H:=0.0			
Form:	-372.291	.000	.000	Rean:	-3.465	.000	.000
	Thor: 2.0	Charge:	1.0	D-H a0:	4.0	logK(25):	.6070
	Reactant Species				logK(T)=		
Coef.	Name	No.					
1.00	Mn+2	11			+	.000000	*T
1.00	CL-	22			+	.000000	/T
					+	.000000	*T^2
					+	.000000	/T^2
61: MnCl20				Data Sources: K: 19 H:=0.0			
Form:	-503.582	.000	.000	Rean:	-.234	.000	.000
	Thor: 2.0	Charge:	.0	D-H a0:	.0	logK(25):	.0410
	Reactant Species				logK(T)=		
Coef.	Name	No.					
1.00	Mn+2	11			+	.000000	*T
2.00	CL-	22			+	.000000	/T
					+	.000000	*T^2
					+	.000000	/T^2
62: MnCl3-				Data Sources: K: 19 H:=0.0			
Form:	-634.873	.000	.000	Rean:	1.741	.000	.000
	Thor: 2.0	Charge:	-1.0	D-H a0:	4.0	logK(25):	-.3050
	Reactant Species				logK(T)=		
Coef.	Name	No.					
1.00	Mn+2	11			+	.000000	*T
3.00	CL-	22			+	.000000	/T
					+	.000000	*T^2
					+	.000000	/T^2
63: MnHCO3+				Data Sources: K:15(#16) H:15			
Form:	-822.122	-912.990	-304.774	Rean:	-66.212	-15.100	171.430
	Thor: 6.0	Charge:	1.0	D-H a0:	5.4	logK(25):	11.6000
	Reactant Species				logK(T)=		
Coef.	Name	No.					
1.00	Mn+2	11			+	.000000	*T
1.00	CO3-2	16			+	.000000	/T
1.00	H+	1			+	.000000	*T^2
					+	.000000	/T^2
64: FeOH+				Data Sources: K: H: 7=15=16			
Form:	-268.254	-318.030	-166.950	Rean:	54.225	55.200	3.270
	Thor: 2.0	Charge:	1.0	D-H a0:	4.0	logK(25):	-9.5000
	Reactant Species				logK(T)=		
Coef.	Name	No.					
1.00	Fe+2	12			+	.000000	*T
1.00	H2O	3			+	.000000	/T
-1.00	H+	1			+	.000000	*T^2
					+	.000000	/T^2

Table A-4 (Continued): Thermodynamic data for aqueous species.

	Gibbs Energy kJ/mol	Enthalpy kJ/mol	Entropy J/mol/K	Gibbs Energy kJ/mol	Enthalpy kJ/mol	Entropy J/mol/K
65: Fe(OH)20				Data Sources: K: H: 7=19		
Form:	-442.025	-539.560	-327.134	Rean: 117.583	119.500	6.430
Thor:	2.0	Charge:	.0	D-H a0: .0	logK(25): -20.6000	
	Reactant Species			logK(T)=	.000000	
Coef.	Name	No.		+	.000000	*T
1.00	Fe+2	12		+	.000000	/T
2.00	H2O	3		+	.000000	*T^2
-2.00	H+	1		+	.000000	/T^2
66: Fe(OH)3-				Data Sources: K: H: 7=19		
Form:	-619.792	-818.090	-665.095	Rean: 176.945	126.800	-168.188
Thor:	2.0	Charge:	-1.0	D-H a0: 4.0	logK(25): -31.0000	
	Reactant Species			logK(T)=	.000000	
Coef.	Name	No.		+	.000000	*T
1.00	Fe+2	12		+	.000000	/T
3.00	H2O	3		+	.000000	*T^2
-3.00	H+	1		+	.000000	/T^2
67: FeSO40				Data Sources: K: 19=16 H: 16		
Form:	-842.723	-989.970	-493.869	Rean: -12.843	6.700	65.547
Thor:	8.0	Charge:	.0	D-H a0: .0	logK(25): 2.2500	
	Reactant Species			logK(T)=	.000000	
Coef.	Name	No.		+	.000000	*T
1.00	Fe+2	12		+	.000000	/T
1.00	SO4-2	20		+	.000000	*T^2
				+	.000000	/T^2
68: Fe+3				Data Sources: K: H: 15		
Form:	-10.976	-45.560	-115.995	Rean: 74.374	41.840	-109.120
Thor:	3.0	Charge:	3.0	D-H a0: 9.0	logK(25): -13.0300	
	Reactant Species			logK(T)=	.000000	
Coef.	Name	No.		+	.000000	*T
1.00	Fe+2	12		+	.000000	/T
-1.00	e-	2		+	.000000	*T^2
				+	.000000	/T^2
69: FeOH+2				Data Sources: K: H: 7=15		
Form:	-235.605	-287.890	-175.366	Rean: 86.874	85.340	-5.146
Thor:	3.0	Charge:	2.0	D-H a0: 4.0	logK(25): -15.2200	
	Reactant Species			logK(T)=	.000000	
Coef.	Name	No.		+	.000000	*T
1.00	Fe+2	12		+	.000000	/T
1.00	H2O	3		+	.000000	*T^2
-1.00	e-	2		+	.000000	/T^2
-1.00	H+	1				
70: Fe(OH)2+				Data Sources: K: 7=19 H=0.0		
Form:	-452.870	-617.220	-551.232	Rean: 106.738	41.840	-217.659
Thor:	3.0	Charge:	1.0	D-H a0: 4.0	logK(25): -18.7000	
	Reactant Species			logK(T)=	.000000	
Coef.	Name	No.		+	.000000	*T
1.00	Fe+2	12		+	.000000	/T
2.00	H2O	3		+	.000000	*T^2
-1.00	e-	2		+	.000000	/T^2
-2.00	H+	1				

Table A-4 (Continued): Thermodynamic data for aqueous species.

	Gibbs Energy kJ/mol	Enthalpy kJ/mol	Entropy J/mol/K	Gibbs Energy kJ/mol	Enthalpy kJ/mol	Entropy J/mol/K
71: Fe(OH)30				Data Sources: K: 7=19 H=0.0		
Form:	-644.679	-903.050	-866.583	Rean: 152.059	41.840	-369.675
Thor:	3.0	Charge:	.0	D-H a0:	.0	logK(25): -26.6400
	Reactant Species			logK(T)=	.000000	
Coef.	Name	No.		+	.000000	*T
1.00	Fe+2	12		+	.000000	/T
3.00	H2O	3		+	.000000	*T^2
-1.00	e-	2		+	.000000	/T^2
-3.00	H+	1				
72: Fe(OH)4-				Data Sources: K: 5=15 H=0.0		
Form:	-836.202	-1188.880	-1182.891	Rean: 197.665	41.840	-522.639
Thor:	3.0	Charge:	-1.0	D-H a0:	4.0	logK(25): -34.6300
	Reactant Species			logK(T)=	.000000	
Coef.	Name	No.		+	.000000	*T
1.00	Fe+2	12		+	.000000	/T
4.00	H2O	3		+	.000000	*T^2
-1.00	e-	2		+	.000000	/T^2
-4.00	H+	1				
73: FeSO4+				Data Sources: K: H: 19		
Form:	-777.881	-938.470	-538.618	Rean: 51.999	58.200	20.798
Thor:	9.0	Charge:	1.0	D-H a0:	4.0	logK(25): -9.1100
	Reactant Species			logK(T)=	.000000	
Coef.	Name	No.		+	.000000	*T
1.00	Fe+2	12		+	.000000	/T
1.00	SO4-2	20		+	.000000	*T^2
-1.00	e-	2		+	.000000	/T^2
74: Fe(SO4)2				Data Sources: K: H: 19		
Form:	-1530.973	-1844.850	-1052.749	Rean: 43.437	61.090	59.208
Thor:	15.0	Charge:	-1.0	D-H a0:	4.0	logK(25): -7.6100
	Reactant Species			logK(T)=	.000000	
Coef.	Name	No.		+	.000000	*T
1.00	Fe+2	12		+	.000000	/T
2.00	SO4-2	20		+	.000000	*T^2
-1.00	e-	2		+	.000000	/T^2
75: FeCl+2				Data Sources: K: H: 15=18		
Form:	-150.715	-179.540	-96.681	Rean: 65.926	74.940	30.232
Thor:	3.0	Charge:	2.0	D-H a0:	4.0	logK(25): -11.5500
	Reactant Species			logK(T)=	.000000	
Coef.	Name	No.		+	.000000	*T
1.00	Fe+2	12		+	.000000	/T
1.00	CL-	22		+	.000000	*T^2
-1.00	e-	2		+	.000000	/T^2
76: FeCl2+				Data Sources: K:15=18 H:18		
Form:	-285.716	-346.370	-203.435	Rean: 62.216	75.190	43.514
Thor:	3.0	Charge:	1.0	D-H a0:	4.0	logK(25): -10.9000
	Reactant Species			logK(T)=	.000000	
Coef.	Name	No.		+	.000000	*T
1.00	Fe+2	12		+	.000000	/T
2.00	CL-	22		+	.000000	*T^2
-1.00	e-	2		+	.000000	/T^2

Table A-4 (Continued): Thermodynamic data for aqueous species.

	Gibbs Energy kJ/mol	Enthalpy kJ/mol	Entropy J/mol/K	Gibbs Energy kJ/mol	Enthalpy kJ/mol	Entropy J/mol/K
77: FeCl30				Data Sources: K:15=18 H:18		
Form:	-411.299	-503.750	-310.083	Rean: 67.924	84.890	56.904
Thor:	3.0	Charge:	.0	D-H a0: .0	logK(25): -11.9000	
	Reactant Species			logK(T)=		
Coef.	Name	No.				
1.00	Fe+2	12		+	.000000	*T
3.00	CL-	22		+	.000000	/T
-1.00	e-	2		+	.000000	*T^2
						/T^2
78: FeCl4-				Data Sources: K: H: 18		
Form:	-531.688	-655.890	-416.576	Rean: 78.826	99.830	70.447
Thor:	3.0	Charge:	-1.0	D-H a0: 4.0	logK(25): -13.8100	
	Reactant Species			logK(T)=		
Coef.	Name	No.				
1.00	Fe+2	12		+	.000000	*T
4.00	CL-	22		+	.000000	/T
-1.00	e-	2		+	.000000	*T^2
						/T^2
79: H2BO3-				Data Sources:		
Form:	-916.009	-1058.831	-479.027	Rean: 52.741	13.489	-131.652
Thor:	.0	Charge:	-1.0	D-H a0: 4.0	logK(25): -9.2400	
	Reactant Species			logK(T)=		
Coef.	Name	No.				
1.00	H3BO3	14		+	.000000	*T
-1.00	H+	1		+	.000000	/T
						*T^2
						/T^2
80: H2AsO3-				Data Sources: G:1 H:1		
Form:	-587.130	-714.790	-428.174	Rean: 52.670	27.410	-84.723
Thor:	3.0	Charge:	-1.0	D-H a0: 4.0	logK(25): -9.2276	
	Reactant Species			logK(T)=		
Coef.	Name	No.				
1.00	H3AsO3	19		+	.000000	*T
-1.00	H+	1		+	.000000	/T
						*T^2
						/T^2
81: Al(OH)+2				Data Sources: K:14 H:7		
Form:	-697.990	-767.210	-232.167	Rean: 28.539	50.000	71.979
Thor:	.0	Charge:	2.0	D-H a0: 5.0	logK(25): -5.0000	
	Reactant Species			logK(T)=		
Coef.	Name	No.				
1.00	Al+3	15		+	.000000	*T
1.00	H2O	3		+	.000000	/T
-1.00	H+	1		+	.000000	*T^2
						/T^2
82: Al(OH)2+				Data Sources: K:14 H:6		
Form:	-905.438	-1013.040	-360.901	Rean: 58.221	90.000	106.589
Thor:	.0	Charge:	1.0	D-H a0: 4.0	logK(25): -10.2000	
	Reactant Species			logK(T)=		
Coef.	Name	No.				
1.00	Al+3	15		+	.000000	*T
2.00	H2O	3		+	.000000	/T
-2.00	H+	1		+	.000000	*T^2
						/T^2

Table A-4 (Continued): Thermodynamic data for aqueous species.

	Gibbs Energy kJ/mol	Enthalpy kJ/mol	Entropy J/mol/K	Gibbs Energy kJ/mol	Enthalpy kJ/mol	Entropy J/mol/K
83: Al(OH)4-						
Form:	-1311.201	-1503.280	-644.237	Rean: 126.715	171.420	149.941
Thor:	.0	Charge: -1.0	D-H a0: 4.0	logK(25): -22.2000		
	Reactant Species			logK(T)=	.000000	
Coef.	Name	No.		+	.000000	*T
1.00	Al+3	15		+	.000000	/T
4.00	H2O	3		+	.000000	*T^2
-4.00	H+	1		+	.000000	/T^2
84: ALF+2						
Form:	-644.394	.000	.000	Rean: -40.012	.000	.000
Thor:	.0	Charge: 2.0	D-H a0: 5.0	logK(25): 7.0100		
	Reactant Species			logK(T)=	.000000	
Coef.	Name	No.		+	.000000	*T
1.00	Al+3	15		+	.000000	/T
1.00	F-	21		+	.000000	*T^2
				+	.000000	/T^2
85: ALF2+						
Form:	-1125.596	-1118.380	24.202	Rean: -72.776	83.700	524.822
Thor:	.0	Charge: 1.0	D-H a0: 4.0	logK(25): 12.7500		
	Reactant Species			logK(T)=	.000000	
Coef.	Name	No.		+	.000000	*T
1.00	Al+3	15		+	.000000	/T
2.00	F-	21		+	.000000	*T^2
				+	.000000	/T^2
86: ALF3						
Form:	-1431.679	-1526.970	-319.609	Rean: -97.149	10.460	360.921
Thor:	.0	Charge: .0	D-H a0: .0	logK(25): 17.0200		
	Reactant Species			logK(T)=	.000000	
Coef.	Name	No.		+	.000000	*T
1.00	Al+3	15		+	.000000	/T
3.00	F-	21		+	.000000	*T^2
				+	.000000	/T^2
87: ALF4-						
Form:	-1713.389	.000	.000	Rean: -112.560	.000	.000
Thor:	.0	Charge: -1.0	D-H a0: 4.0	logK(25): 19.7200		
	Reactant Species			logK(T)=	.000000	
Coef.	Name	No.		+	.000000	*T
1.00	Al+3	15		+	.000000	/T
4.00	F-	21		+	.000000	*T^2
				+	.000000	/T^2
88: HCO3-						
Form:	-586.766	-692.041	-353.091	Rean: -58.957	-14.901	147.764
Thor:	4.0	Charge: -1.0	D-H a0: 5.5	logK(25): 10.3289		
	Reactant Species			logK(T)=	10.7507	
Coef.	Name	No.		+	-.343322E-02	*T
1.00	CO3-2	16		+	-1630.26	/T
1.00	H+	1		+	.143000E-04	*T^2
				+	426564.	/T^2

Table A-4 (Continued): Thermodynamic data for aqueous species.

	Gibbs Energy kJ/mol	Enthalpy kJ/mol	Entropy J/mol/K		Gibbs Energy kJ/mol	Enthalpy kJ/mol	Entropy J/mol/K
89: H2CO3				Data Sources: C:8			
Form:	-623.174	-700.845	-260.509	Rean:	-95.364	-23.705	240.346
Thor:	4.0	Charge:	.0	D-H a0:	.0	logK(25):	16.7074
	Reactant Species				logK(T) = 50.5538		
Coef.	Name	No.					
1.00	CO3-2	16			+ .596900E-01	*T	
2.00	H+	1			+ -11990.2	/T	
					+ .611947E-04	*T^2	
					+ .166459E+07	/T^2	
90: H3SiO4-				Data Sources:			
Form:	-1250.926	-1418.894	-563.367	Rean:	56.674	37.386	-64.691
Thor:	.0	Charge:	-1.0	D-H a0:	4.0	logK(25):	-9.9290
	Reactant Species				logK(T) = 6.36800		
Coef.	Name	No.					
1.00	H4SiO4	17			+ -.163460E-01	*T	
-1.00	H+	1			+ -3405.90	/T	
					+ .000000	*T^2	
					+ .000000	/T^2	
91: HPO4-2				Data Sources:			
Form:	-1089.170	-1291.170	-677.512	Rean:	-70.470	-13.770	190.172
Thor:	.0	Charge:	-2.0	D-H a0:	4.0	logK(25):	12.3460
	Reactant Species				logK(T) = .000000		
Coef.	Name	No.					
1.00	PO4-3	18			+ .000000	*T	
1.00	H+	1			+ .000000	/T	
					+ .000000	*T^2	
					+ .000000	/T^2	
92: H2PO4-				Data Sources:			
Form:	-1130.307	-1296.310	-556.778	Rean:	-111.607	-18.910	310.906
Thor:	.0	Charge:	-1.0	D-H a0:	4.5	logK(25):	19.5530
	Reactant Species				logK(T) = .000000		
Coef.	Name	No.					
1.00	PO4-3	18			+ .000000	*T	
2.00	H+	1			+ .000000	/T	
					+ .000000	*T^2	
					+ .000000	/T^2	
93: HAsO4-2				Data Sources: G:1 H:1			
Form:	-714.600	-906.340	-643.099	Rean:	-66.190	-18.200	160.959
Thor:	5.0	Charge:	-2.0	D-H a0:	4.0	logK(25):	11.5962
	Reactant Species				logK(T) = .000000		
Coef.	Name	No.					
1.00	ASO4-3	27			+ .000000	*T	
1.00	H+	1			+ .000000	/T	
					+ .000000	*T^2	
					+ .000000	/T^2	
94: H2AsO4-				Data Sources: G:1 H:1			
Form:	-753.170	-909.560	-524.535	Rean:	-104.760	-21.420	279.523
Thor:	5.0	Charge:	-1.0	D-H a0:	4.5	logK(25):	18.3535
	Reactant Species				logK(T) = .000000		
Coef.	Name	No.					
1.00	ASO4-3	27			+ .000000	*T	
2.00	H+	1			+ .000000	/T	
					+ .000000	*T^2	
					+ .000000	/T^2	

Table A-4 (Continued): Thermodynamic data for aqueous species.

	Gibbs Energy kJ/mol	Enthalpy kJ/mol	Entropy J/mol/K	Gibbs Energy kJ/mol	Enthalpy kJ/mol	Entropy J/mol/K
95: U(OH)4				Data Sources: K:17 H:17		
Form:	-1430.999	-1630.760	-670.003	Rean: 48.517	103.760	185.285
Thor:	4.0	Charge:	.0	D-H a0: .0	logK(25): -8.5000	
	Reactant Species			logK(T)=	.000000	
Coef.	Name	No.		+	.000000	*T
1.00	U4+	24		+	.000000	/T
4.00	H2O	3		+	.000000	*T^2
-4.00	H+	1		+	.000000	/T^2
96: U(OH)5-				Data Sources: K:17 H:17		
Form:	-1641.587	-1904.870	-883.059	Rean: 75.059	115.480	135.573
Thor:	4.0	Charge:	-1.0	D-H a0: 4.0	logK(25): -13.1500	
	Reactant Species			logK(T)=	.000000	
Coef.	Name	No.		+	.000000	*T
1.00	U4+	24		+	.000000	/T
5.00	H2O	3		+	.000000	*T^2
-5.00	H+	1		+	.000000	/T^2
97: UO2+				Data Sources: K:17 H:17		
Form:	-968.545	-1032.610	-214.876	Rean: 36.713	130.250	313.724
Thor:	5.0	Charge:	1.0	D-H a0: 4.0	logK(25): -6.4320	
	Reactant Species			logK(T)=	.000000	
Coef.	Name	No.		+	.000000	*T
1.00	U4+	24		+	.000000	/T
2.00	H2O	3		+	.000000	*T^2
-4.00	H+	1		+	.000000	/T^2
-1.00	e-	2				
98: UL=UO2+2				Data Sources: K:17 H:17		
Form:	-952.746	-1018.511	-220.577	Rean: 52.513	144.350	308.024
Thor:	6.0	Charge:	2.0	D-H a0: 5.0	logK(25): -9.2000	
	Reactant Species			logK(T)=	.000000	
Coef.	Name	No.		+	.000000	*T
1.00	U4+	24		+	.000000	/T
2.00	H2O	3		+	.000000	*T^2
-4.00	H+	1		+	.000000	/T^2
-2.00	e-	2				
99: ULCO3				Data Sources: K:17 H:17		
Form:	-1537.920	-1707.371	-568.339	Rean: -4.852	132.630	461.116
Thor:	10.0	Charge:	.0	D-H a0: .0	logK(25): .8500	
	Reactant Species			logK(T)=	.000000	
Coef.	Name	No.		+	.000000	*T
1.00	U4+	24		+	.000000	/T
2.00	H2O	3		+	.000000	*T^2
1.00	CO3-2	16		+	.000000	/T^2
-4.00	H+	1				
-2.00	e-	2				

Table A-4 (Continued): Thermodynamic data for aqueous species.

	Gibbs Energy kJ/mol	Enthalpy kJ/mol	Entropy J/mol/K	Gibbs Energy kJ/mol	Enthalpy kJ/mol	Entropy J/mol/K
100: ULCO32-2				Data Sources: K:17 H:17		
Form:	-2105.400	-2357.731	-846.321	Rean: -44.522	159.410	683.990
	Thor: 14.0	Charge: -2.0	D-H a0: 4.0	logK(25): 7.8000		
	Reactant Species			logK(T)=	.000000	
Coef.	Name	No.		+	.000000	*T
1.00	U4+	24		+	.000000	/T
2.00	H2O	3		+	.000000	*T^2
2.00	CO3-2	16		+	.000000	/T^2
-4.00	H+	1				
-2.00	e-	2				
101: ULCO33-4				Data Sources: K:17 H:17		
Form:	-2658.325	-3090.521	-1449.592	Rean: -69.636	103.760	581.575
	Thor: 18.0	Charge: -4.0	D-H a0: 6.0	logK(25): 12.2000		
	Reactant Species			logK(T)=	.000000	
Coef.	Name	No.		+	.000000	*T
1.00	U4+	24		+	.000000	/T
2.00	H2O	3		+	.000000	*T^2
3.00	CO3-2	16		+	.000000	/T^2
-4.00	H+	1				
-2.00	e-	2				
102: ULOH+				Data Sources: K:17 H:17		
Form:	-1156.769	-1258.321	-340.606	Rean: 85.619	190.370	351.338
	Thor: 6.0	Charge: 1.0	D-H a0: 4.5	logK(25): -15.0000		
	Reactant Species			logK(T)=	.000000	
Coef.	Name	No.		+	.000000	*T
1.00	U4+	24		+	.000000	/T
3.00	H2O	3		+	.000000	*T^2
-5.00	H+	1		+	.000000	/T^2
-2.00	e-	2				
103: UL(OH)2				Data Sources: K:17 H:17		
Form:	-1358.509	-1517.371	-532.825	Rean: 121.008	217.150	322.463
	Thor: 6.0	Charge: .0	D-H a0: .0	logK(25): -21.2000		
	Reactant Species			logK(T)=	.000000	
Coef.	Name	No.		+	.000000	*T
1.00	U4+	24		+	.000000	/T
4.00	H2O	3		+	.000000	*T^2
-6.00	H+	1		+	.000000	/T^2
-2.00	e-	2				
104: S-2				Data Sources:		
Form:	85.809	116.780	103.878	Rean: 113.639	156.480	143.690
	Thor: -2.0	Charge: -2.0	D-H a0: 5.0	logK(25): -19.9090		
	Reactant Species			logK(T)=	.000000	
Coef.	Name	No.		+	.000000	*T
1.00	H2S AQ	28		+	.000000	/T
-2.00	H+	1		+	.000000	*T^2
				+	.000000	/T^2

Table A-4 (Continued): Thermodynamic data for aqueous species.

	Gibbs Energy kJ/mol	Enthalpy kJ/mol	Entropy J/mol/K	Gibbs Energy kJ/mol	Enthalpy kJ/mol	Entropy J/mol/K
105: HS-						
Form:	12.080	66.160	181.386	39.910	105.860	221.199
	Thor: -2.0	Charge: -1.0	D-H a0: 3.5	logK(25): -6.9920		
	Reactant Species			logK(T)=	.000000	
Coef.	Name	No.		+	.000000	*T
1.00	H2S AQ	28		+	.000000	/T
-1.00	H+	1		+	.000000	*T^2
				+	.000000	/T^2

Table A-4 (Continued): Thermodynamic data for aqueous species.

	Gibbs Energy kJ/mol	Enthalpy kJ/mol	Entropy J/mol/K	Gibbs Energy kJ/mol	Enthalpy kJ/mol	Entropy J/mol/K
1: Calcite						
	Data Sources: C:8					
Thor:	4.0	logK(25):	-8.480			
Form:	-1129.152	-1210.631	-273.282	Rean: 48.402	-9.609	-194.570
	Reactant Species			logK(T)=	6.75444	
Coef.	Name	No.		+		
1.00	CO3-2	16		+	-.118494E-01	*T
1.00	CA+2	8		+	-3637.75	/T
				+	-.263017E-04	*T^2
				+	252258.	/T^2
2: Dolomite						
	Data Sources:					
Thor:	8.0	logK(25):	-17.000			
Form:	-2160.394	-2329.495	-567.166	Rean: 97.034	-34.685	-441.789
	Reactant Species			logK(T)=	.000000	
Coef.	Name	No.		+		
1.00	CA+2	8		+	.000000	*T
1.00	MG+2	7		+	.000000	/T
2.00	CO3-2	16		+	.000000	*T^2
				+	.000000	/T^2
3: Strontianite						
	Data Sources: C:9					
Thor:	4.0	logK(25):	-9.271			
Form:	-1140.185	-1221.285	-272.010	Rean: 52.915	-1.675	-183.096
	Reactant Species			logK(T)=	13.8232	
Coef.	Name	No.		+		
1.00	SR+2	9		+	-.522789E-01	*T
1.00	CO3-2	16		+	-2120.44	/T
				+	.207889E-04	*T^2
				+	-199367.	/T^2
4: Witherite						
	Data Sources: K, H: 15					
Thor:	4.0	logK(25):	-8.580			
Form:	-1137.544	-1216.290	-264.116	Rean: 48.974	1.510	-159.195
	Reactant Species			logK(T)=	.000000	
Coef.	Name	No.		+		
1.00	BA+2	10		+	.000000	*T
1.00	CO3-2	16		+	.000000	/T
				+	.000000	*T^2
				+	.000000	/T^2
5: Rhodochrosite						
	Data Sources: K, H: 19					
Thor:	6.0	logK(25):	-10.540			
Form:	-816.071	-889.320	-243.677	Rean: 60.161	-8.570	-230.526
	Reactant Species			logK(T)=	.000000	
Coef.	Name	No.		+		
1.00	Mn+2	11		+	.000000	*T
1.00	CO3-2	16		+	.000000	/T
				+	.000000	*T^2
				+	.000000	/T^2
6: Siderite						
	Data Sources: K, H: 15					
Thor:	6.0	logK(25):	-10.550			
Form:	-673.378	-742.250	-230.996	Rean: 60.218	-22.290	-276.735
	Reactant Species			logK(T)=	.000000	
Coef.	Name	No.		+		
1.00	Fe+2	12		+	.000000	*T
1.00	CO3-2	16		+	.000000	/T
				+	.000000	*T^2
				+	.000000	/T^2

Table A-5 : Thermodynamic data for minerals .

	Gibbs Energy kJ/mol	Enthalpy kJ/mol	Entropy J/mol/K	Gibbs Energy kJ/mol	Enthalpy kJ/mol	Entropy J/mol/K
7: Gypsum						
	Thor: 6.0 logK(25): -4.581			Data Sources: C:10(eq4)		
Form:	-1797.875	-2023.576	-757.002	Rean: 26.147	-0.454	-89.222
	Reactant Species			logK(T)= 5.69760		
Coef.	Name	No.				
1.00	CA+2	8		+	-.231542E-01	*T
1.00	SO4-2	20		+	-954.120	/T
2.00	H2O	3		+	.920711E-05	*T^2
				+	-88306.9	/T^2
8: Anhydrite						
	Thor: 6.0 logK(25): -4.239			Data Sources: C:10(eq4)		
Form:	-1321.668	-1432.417	-371.453	Rean: 24.198	-19.954	-148.085
	Reactant Species			logK(T)= 5.83989		
Coef.	Name	No.				
1.00	CA+2	8		+	-.303452E-01	*T
1.00	SO4-2	20		+	-239.299	/T
				+	.120667E-04	*T^2
				+	-115728.	/T^2
9: Celestite						
	Thor: 6.0 logK(25): -6.633			Data Sources: C:10(eq10)		
Form:	-1341.853	-1457.612	-388.259	Rean: 37.863	2.522	-118.532
	Reactant Species			logK(T)= 14.2330		
Coef.	Name	No.				
1.00	SR+2	9		+	-.456563E-01	*T
1.00	SO4-2	20		+	-2059.93	/T
				+	.181551E-04	*T^2
				+	-174121.	/T^2
10: Barite						
	Thor: 6.0 logK(25): -9.970			Data Sources: C:10(eq2)		
Form:	-1362.200	-1473.484	-373.250	Rean: 56.910	26.574	-101.746
	Reactant Species			logK(T)= 14.7689		
Coef.	Name	No.				
1.00	BA+2	10		+	-.448943E-01	*T
1.00	SO4-2	20		+	-3284.06	/T
				+	.178518E-04	*T^2
				+	-171224.	/T^2
11: Fluorite						
	Thor: .0 logK(25): -10.500			Data Sources:		
Form:	-1176.293	-1233.510	-191.907	Rean: 59.933	19.710	-134.909
	Reactant Species			logK(T)= .000000		
Coef.	Name	No.				
1.00	CA+2	8		+	.000000	*T
2.00	F-	21		+	.000000	/T
				+	.000000	*T^2
				+	.000000	/T^2
12: Portlandite						
	Thor: .0 logK(25): 22.549			Data Sources: G:1 H:1		
Form:	-898.490	-986.090	-293.812	Rean: -128.708	-128.670	.127
	Reactant Species			logK(T)= .000000		
Coef.	Name	No.				
1.00	CA+2	8		+	.000000	*T
2.00	H2O	3		+	.000000	/T
-2.00	H+	1		+	.000000	*T^2
				+	.000000	/T^2

Table A-5 (continued): Thermodynamic data for minerals.

	Gibbs Energy kJ/mol	Enthalpy kJ/mol	Entropy J/mol/K		Gibbs Energy kJ/mol	Enthalpy kJ/mol	Entropy J/mol/K
13: Chalcedony Data Sources: C:13							
Thor:	.0	logK(25):	-3.550				
Form:	-1090.736	-1190.207	-333.628	Rean:	20.265	19.757	-1.704
	Reactant Species				logK(T)=	-.890000E-01	
Coef.	Name	No.			+	.000000	*T
1.00	H4SiO4	17			+	-1032.00	/T
-1.00	H2O	3			+	.000000	*T^2
					+	.000000	/T^2
14: Quartz Data Sources: C:13							
Thor:	.0	logK(25):	-3.979				
Form:	-856.056	-909.680	-179.856	Rean:	22.714	25.060	7.868
	Reactant Species				logK(T)=	.411000	
Coef.	Name	No.			+	.000000	*T
1.00	H4SiO4	17			+	-1309.00	/T
-2.00	H2O	3			+	.000000	*T^2
					+	.000000	/T^2
15: Uraninite Data Sources: K:17 H:17							
Thor:	4.0	logK(25):	-4.600				
Form:	-1031.515	-1084.620	-178.117	Rean:	26.256	-78.240	-350.483
	Reactant Species				logK(T)=	.000000	
Coef.	Name	No.			+	.000000	*T
1.00	U4+	24			+	.000000	/T
2.00	H2O	3			+	.000000	*T^2
-4.00	H+	1			+	.000000	/T^2
16: Pyrolusite Data Sources: K, H: 19							
Thor:	4.0	logK(25):	41.550				
Form:	-465.195	-520.081	-184.087	Rean:	-237.163	-272.330	-117.949
	Reactant Species				logK(T)=	.000000	
Coef.	Name	No.			+	.000000	*T
1.00	Mn+2	11			+	.000000	/T
2.00	H2O	3			+	.000000	*T^2
-2.00	e-	2			+	.000000	/T^2
-4.00	H+	1					
17: Manganite Data Sources: K: 15							
Thor:	3.0	logK(25):	25.270				
Form:	-558.120	-792.411	-785.816	Rean:	-144.239	.000	483.780
	Reactant Species				logK(T)=	.000000	
Coef.	Name	No.			+	.000000	*T
1.00	Mn+2	11			+	.000000	/T
2.00	H2O	3			+	.000000	*T^2
-1.00	e-	2			+	.000000	/T^2
-3.00	H+	1					

Table A-5 (continued): Thermodynamic data for minerals.

	Gibbs Energy kJ/mol	Enthalpy kJ/mol	Entropy J/mol/K	Gibbs Energy kJ/mol	Enthalpy kJ/mol	Entropy J/mol/K
18: Magnetite						
	Data Sources: K, H: 19					
	Thor: 8.0	logK(25): -8.800				
Form:	-1031.675	-1106.911	-252.345	Rean: 50.230	-173.090	-749.018
	Reactant Species			logK(T)=	.000000	
Coef.	Name	No.		+	.000000	*T
3.00	Fe+3	68		+	.000000	/T
4.00	H2O	3		+	.000000	*T^2
1.00	e-	2		+	.000000	/T^2
-8.00	H+	1				
19: Hematite						
	Data Sources: K, H: 19					
	Thor: 6.0	logK(25): -3.860				
Form:	-755.520	-818.741	-212.043	Rean: 22.032	-129.850	-509.417
	Reactant Species			logK(T)=	.000000	
Coef.	Name	No.		+	.000000	*T
2.00	Fe+3	68		+	.000000	/T
3.00	H2O	3		+	.000000	*T^2
-6.00	H+	1		+	.000000	/T^2
20: Goethite						
	Data Sources: K: 7, H: 16					
	Thor: 3.0	logK(25): .500				
Form:	-482.454	-556.630	-248.788	Rean: -2.854	-60.580	-193.614
	Reactant Species			logK(T)=	.000000	
Coef.	Name	No.		+	.000000	*T
1.00	Fe+3	68		+	.000000	/T
2.00	H2O	3		+	.000000	*T^2
-3.00	H+	1		+	.000000	/T^2
21: Fe(OH)3(am)						
	Data Sources: K: 7, H: 16					
	Thor: 3.0	logK(25): 2.500				
Form:	-708.167	-821.460	-379.986	Rean: -14.270	-81.580	-225.760
	Reactant Species			logK(T)=	.000000	
Coef.	Name	No.		+	.000000	*T
1.00	Fe+3	68		+	.000000	/T
3.00	H2O	3		+	.000000	*T^2
-3.00	H+	1		+	.000000	/T^2
22: P CO2						
	Data Sources: C:8					
	Thor: 4.0	logK(25): -1.468				
Form:	-394.423	-395.031	-2.038	Rean: 8.378	-19.984	-95.127
	Reactant Species			logK(T)=	7.44232	
Coef.	Name	No.		+	-.175208E-01	*T
1.00	H2CO3	89		+	-3259.97	/T
-1.00	H2O	3		+	.148607E-04	*T^2
				+	526840.	/T^2

Table A-5 (continued): Thermodynamic data for minerals.

DISTRIBUTION:

US Department of Energy (5)
Office of Civilian Radioactive Waste Management
Office of Geologic Repositories
Attn: Associate Director
W. J. Purcell, RW-20
Director, Repository Coordination Div.
T. H. Isaacs, RW-22
Director, Engineering & Licensing
R. Stein, RW-23
Director, Geosciences & Technology
R. Stein, Actg., RW-24
Director, Siting Division
E. Burton, RW-25
Forrestal Building
Washington, DC 20585

US Department of Energy (3)
Albuquerque Operations
Attn: R. G. Romatowski
D. L. Krenz
D. G. Jackson, Director, Public Affairs Division
PO Box 5400
Albuquerque, NM 87185

US Department of Energy (6)
Attn: J. Tillman
WIPP Project Office (Carlsbad) (2)
G. Pappas, WPO (Carlsbad)
A. Hunt, WPO (Carlsbad)
R. Eastmond, WPO (Carlsbad) (2)
PO Box 3090
Carlsbad, NM 88221

US Department of Energy, SRPO (4)
Office of Nuclear Waste Isolation
Attn: J. O. Neff
R. Wunderlich
G. Appel
J. Sherwin
505 King Avenue
Columbus, OH 43201

US Department of Energy (2)
Idaho Operations Office
Nuclear Fuel Cycle Division
Attn: R. M. Nelson
J. Whitsett
550 Second Street
Idaho Falls, ID 83401

US Department of Energy (2)
Savannah River Operations Office
Waste Management Project Office
Attn: S. Cowan
W. J. Brumley
PO Box A
Aiken, SC 29801

US Department of Energy (3)
Office of Defense Waste and
Transportation Management
Attn: J. E. Dieckhoner, DP-122
L. H. Harmon, DP-121
A. Follett, DP-121
Washington, DC 20545

US Department of Energy
Research & Technical Support Division
Attn: D. E. Large
PO Box E
Oak Ridge, TN 37830

US Department of the Interior
Attn: E. Roedder
959 National Center
Geological Survey
Reston, VA 22092

US Nuclear Regulatory Commission (2)
Division of Waste Management
Attn: M. Bell
H. Miller
Mail Stop 623SS
Washington, DC 20555

US Geological Survey
Special Projects
Attn: R. Snyder
MS954, Box 25046
Denver Federal Center
Denver, CO 80255

US Geological Survey
Conservation Division
Attn: W. Melton
PO Box 1857
Roswell, NM 88201

US Geological Survey (2)
Water Resources Division
Attn: H. L. Case
P. Davies
Western Bank Bldg.
505 Marquette NW, #720
Albuquerque, NM 87102

State of New Mexico (3)
Environmental Evaluation Group
Attn: R. H. Neill, Director
320 Marcy Street
PO Box 968
Santa Fe, NM 87503

NM Department of Energy & Minerals
Attn: K. LaPlante, Librarian
PO Box 2770
Santa Fe, NM 87501

New Mexico Bureau of Mines and Mineral
Resources (2)
Attn: F. E. Kottolowski, Director
J. Hawley
Socorro, NM 87801

Battelle Pacific Northwest Laboratories
Attn: D. J. Bradley
Battelle Boulevard
Richland, WA 99352

Battelle Memorial Institute (13)
Project Management Division
Attn: W. Carbiener, General Manager (3)
J. Treadwell
T. Naymik
J. Kirchner
V. Adams
O. Swanson
A. Razem
S. Gupta
W. Newcomb
A. LaSala
ONWI Library
505 King Avenue
Columbus, OH 43201

Bechtel Inc. (2)
Attn: E. Weber
M. Bethard
PO Box 3965
45-11-B34
San Francisco, CA 94119

IT Corporation (2)
Attn: W. E. Coons
J. E. Zurkoff
2340 Alamo, SE
Suite 306
Albuquerque, NM 87106

IT Corporation (5)
Attn: W. Patrick
R. McKinney
D. Deal
D. Winstanley
D. W. Uhland
PO Box 2078
Carlsbad, NM 88221
INTERA Technologies, Inc. (20)
Attn: G. E. Grisak
J. F. Pickens (5)
G. J. Saulnier
V. A. Kelley (5)
A. Haug
M. Reeves
R. W. Andrews
G. A. Freeze
INTERA Library
F. J. Pearson (5)
6850 Austin Center Blvd., #300
Austin, TX 78731

INTERA Technologies, Inc.
Attn: W. Stensrud
PO Box 2123
Carlsbad, NM 88221

Martin Marietta Energy Systems, Inc.
Oak Ridge National Laboratory
Attn: J. A. Carter
Box Y
Oak Ridge, TN 37830

Martin Marietta Energy Systems, Inc.
Oak Ridge National Laboratory
Environmental Science
Attn: E. Bondiatti
X10 Area, Bldg. 1505, Rm. 322
Oak Ridge, TN 37831

RE/SPEC Inc.
Attn: P. Gnirk
PO 725
Rapid City, SD 57701

RE/SPEC Inc.
Attn: S. W. Key
PO Box 14984
Albuquerque, NM 87191

Rockwell International
Atomics International Division
Rockwell Hanford Operations
Attn: W. W. Schultz
PO Box 800
Richland, WA 99352

Serata Geomechanics
Attn: S. Serata
4124 Lakeside Drive
Richmond, CA 94806-1941

G. O. Bachman
Star Route Box 1028
Corrales, NM 87048

Leonard Minerals Co.
Attn: B. Donegan
3202 Candelaria NE
Albuquerque, NM 87107

Peters Technology Transfer
Attn: L. Lantz
PO Box 216
Swarthmore, PA 19081

Stanford University
Department of Geology
Attn: K. B. Krauskopf
Stanford, CA 94305

Vanderbilt University
Department of Environmental and
Water Resources Engineering
Attn: F. L. Parker
Nashville, TN 37235

Oak Ridge National Laboratory
Attn: J. O. Blomeke
PO Box X
Oak Ridge, TN 37830

US Geological Survey
Water Resources Division
Attn: J. D. Bredehoeft
Western Region Hydrologist
345 Middlefield Road
Menlo Park, CA 94025

K. P. Cohen
928 N. California Avenue
Palo Alto, CA 94303

F. M. Ernsberger
1325 NW 10th Avenue
Gainesville, FL 32601

Johns Hopkins University
Department of Earth Sciences
Attn: H. P. Eugster
Baltimore, MD 21218

University of New Mexico
Department of Geology
Attn: R. C. Ewing
Albuquerque, NM 87131

University of Minnesota
Department of Geological Sciences
Attn: C. Fairhurst
Minneapolis, MN 55455

University of Texas at Austin
Department of Geological Sciences
Attn: W. R. Muehlberger
Austin, TX 78712

D. A. Shock
233 Virginia
Ponca City, OK 74601

National Academy of Sciences
Committee on Radioactive Waste Management
Attn: P. Meyers
2101 Constitution Avenue, NW
Washington, DC 20418

New Mexico Junior College
Pannell Library
Attn: R. Hill
Lovington Highway
Hobbs, NM 88240

New Mexico Tech
Martin Speere Memorial Library
Campus Street
Socorro, NM 87810

New Mexico Tech (3)
Department of Geoscience
Attn: J. Wilson
D. Stephens
C. S. Chen
Socorro, NM 87801

New Mexico State Library
Attn: I. Vollenhofer
PO Box 1629
Santa Fe, NM 87503

US Geological Survey (2)
Water Resources Division
Attn: P. Hsieh and A.F. Moench
345 Middlefield Rd.
Menlo Park, CA 94025

University of New Mexico
Zimmerman Library
Attn: Z. Vivian
Albuquerque, NM 87131

Atomic Museum
WIPP Public Reading Room
Attn: G. Schreiner
Kirtland East AFB
Albuquerque, NM 87185

Carlsbad Municipal Library
WIPP Public Reading Room
Attn: L. Hubbard, Head Librarian
101 S. Hallagueno St.
Carlsbad, NM 88220

Thomas Brannigan Library
Attn: D. Dresp, Head Librarian
106 W. Hadley St.
Las Cruces, NM, 88001

Roswell Public Library
Attn: N. Langston
301 N. Pennsylvania Avenue
Roswell, NM 88201

University of Minnesota
Dept. of Energy and Materials Science
Attn: R. Oriani
151 Amundson Hall
421 Washington Ave SE
Minneapolis, MN 55455

Texas A&M University
Center of Tectonophysics
Attn: J. Handin
College Station, TX 77840

Texas A&M University
Department of Geology
Attn: P. A. Domenico
College Station, TX 77843

University of British Columbia
Department of Geological Sciences
Attn: R. A. Freeze
Vancouver, British Columbia V6T 1W5
CANADA

University of Arizona (2)
Department of Nuclear Engineering
Attn: J. G. McCray
J. J. K. Daemen
Tucson, AZ 85721

University of Arizona
Department of Hydrology
Attn: S. P. Neuman
Tucson, AZ 85721

University of New Mexico (2)
Geology Department
Attn: D. G. Brookins
Library
Albuquerque, NM 87131

University of Texas at El Paso
Department of Geological Sciences
Attn: D. W. Powers
El Paso, TX 79968

Princeton University
Department of Civil Engineering
Attn: G. Pinder
Princeton, NJ 08504

Scientific Software-Intercomp
Attn: A. C. Gringarten
1801 California, 3rd Floor
Denver, CO 80202

University of California (2)
Lawrence W. Berkeley Laboratory
Attn: J. Long
S. M. Benson
Berkeley, CA 94720

Netherlands Energy Research Foundation ECN (2)
Attn: T. Deboer, Mgr.
L. H. Vons
3 Westerduinweg
PO Box 1
1755 ZG Petten
THE NETHERLANDS

Nationale Genossenschaft für die Lagerung
Radioaktiver Abfälle (3)
Attn: P. Hufschmied
C. McCombie
M. Thury
Parkstrasse 23
CH5401 Baden
SWITZERLAND

University of Wisconsin-Madison
Department of Geology and Geophysics
Attn: M. P. Anderson
1215 W. Dayton St.
Madison, WI 53706

1540 W. C. Luth
1543 W. H. Casey
6000 D. L. Hartley
6300 R W. Lynch
6310 T. O. Hunter
6311 L. W. Scully
6312 F. W. Bingham
6314 J. R. Tillerson
6330 W. D. Weart
6330 Sandia WIPP Central Files (700H IND) (2)
6331 A. R. Lappin
6331 R. L. Beauheim (2)
6331 D. J. Borns
6331 M. M. Gonzales
6331 A. L. Jensen
6331 S. J. Lambert
6331 K. L. Robinson
6331 C. L. Stein
6331 D. Tomasko
6332 L. D. Tyler
6332 F. G. Yost
6334 D. R. Anderson
6334 L. H. Brush
6431 P. A. Davis
6431 K. Brinster
6431 M. D. Siegel
6431 C. D. Updegraff
7100 C. D. Broyles
7120 M. J. Navratil
7125 R. L. Rutter
7130 J. D. Kennedy
7133 R. D. Statler
7133 J. W. Mercer
7135 P. D. Seward
8024 P. W. Dean
3141 S. A. Landenberger (5)
3151 W. L. Garner (3)
3154-1 C. H. Dalin (28)
For DOE/OSTI (Unlimited Release)